AD-A160 329 PHOTODISSOCIATION DYNAMICS OF SMALL MOLECULES(U) HOWARD 1/2
UNIV WASHINGTON DC LASER CHEMISTRY DIV
W M JACKSON ET AL. 04 OCT 85 ONR-TR-19 N00014-80-C-0305
UNCLASSIFIED F/G 7/5 NL

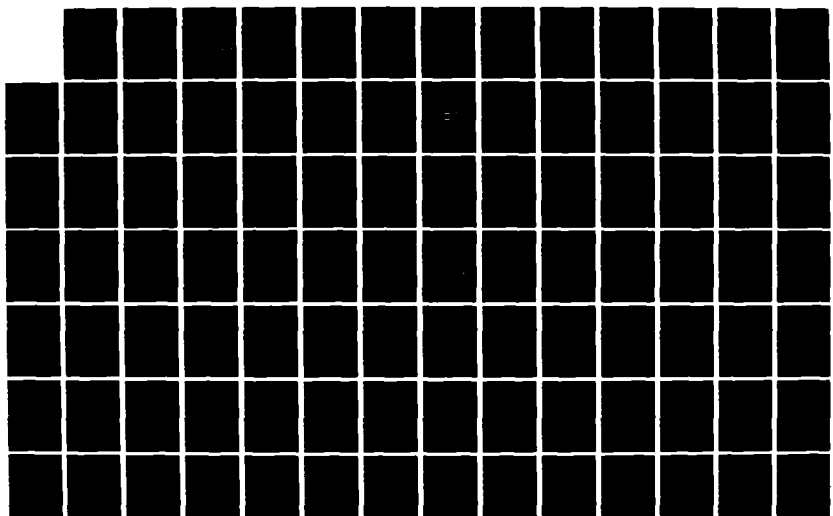

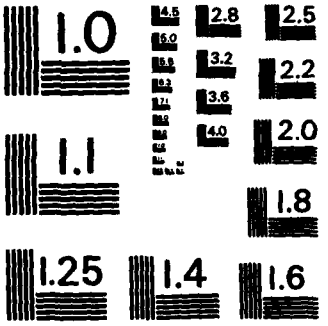

MICROCOPY RESOLUTION TEST CHART
NATIONAL BUREAU OF STANDARDS - 1963 - A

(12)

SECURITY CLASSIFICATION OF THIS PAGE (When Data Entered)

REPORT DOCUMENTATION PAGE		READ INSTRUCTIONS BEFORE COMPLETING FORM
1. REPORT NUMBER ONR-TR-19	2. GOVT ACCESSION NO. AD-A160329	3. RECIPIENT'S CATALOG NUMBER
4. TITLE (and Subtitle) Photodissociation Dynamics of Small Molecules		5. TYPE OF REPORT & PERIOD COVERED TECHNICAL REPORT 19 6. PERFORMING ORG. REPORT NUMBER
7. AUTHOR(s) William M. Jackson and Hideo Okabe		8. CONTRACT OR GRANT NUMBER(s) N00014-80-C-0305 O/C
9. PERFORMING ORGANIZATION NAME AND ADDRESS Laser Chemistry Division Department of Chemistry Howard University Washington, D.C.		10. PROGRAM ELEMENT, PROJECT, TASK AREA & WORK UNIT NUMBERS NR-051-733
11. CONTROLLING OFFICE NAME AND ADDRESS Office of Naval Research Department of the Navy Arlington, VA 22217		12. REPORT DATE October 4, 1985 13. NUMBER OF PAGES 94
14. MONITORING AGENCY NAME & ADDRESS(if different from Controlling Office)		15. SECURITY CLASS. (of this report) UNCLASSIFIED 15a. DECLASSIFICATION/DOWNGRADING SCHEDULE

16. DISTRIBUTION STATEMENT (of this Report)

Approved for public release; ~~reproduction is permitted for any purpose of the United States Government;~~ distribution is unlimited.

17. DISTRIBUTION STATEMENT (of the abstract entered in Block 20, if different from Report)

Distribution of this document is unlimited.

DTIC ELECTE OCT 16 1985 S D B

18. SUPPLEMENTARY NOTES

Prepared for publication in the Advances in Photochemistry, Vol. 13.

19. KEY WORDS (Continue on reverse side if necessary and identify by block number)

Photodissociation, lasers, laser induced fluorescence, quantum state analysis, photofragments, dissociation dynamics, water, hydrogen peroxide, formaldehyde, ozone, acetylene compounds, metal halides, alkyl halides, NH compounds, NO and NO_2 compounds, CO and CO_2 compounds, sulfur compounds.

20. ABSTRACT (Continue on reverse side if necessary and identify by block number)

The recent advancement of photodissociation dynamics of about 60 small molecules has been presented. The emphasis is placed on the primary photochemical process and the energy partitioning in photofragments. Compound discussed in this report include-

DD FORM 1 JAN 73 1473 EDITION OF 1 NOV 65 IS OBSOLETE
S/N 0102-014-6601

UNCLASSIFIED
SECURITY CLASSIFICATION OF THIS PAGE (When Data Entered)

OFFICE OF NAVAL RESEARCH

Contract N0O014-80-C-0305

Task No. NR 051-733

TECHNICAL REPORT NO. 19

PHOTODISSOCIATION DYNAMICS OF SMALL MOLECULES

by

William M. Jackson and Hideo Okabe

Prepared for Publication in Advances in Photochemistry, Vol. 13

Department of Chemistry
Laser Chemistry Division
Howard University
Washington, D. C. 20059

October 4, 1985

PG 1 Model paper for 15% reduction to 23×44 picas type page

Photodissociation Dynamics of Small Molecules

WILLIAM M. JACKSON AND HIDEO OKABE

Department of Chemistry
Laser Chemistry Division
Howard University
Washington, D.C. 20059

Contd

CONTENTS

Contd

Originator supplied keywords include:

See DD 1473

I. INTRODUCTION

The development of photochemical reaction dynamics has been extremely rapid over the last decade (1-7). The impetus behind this growth has been the availability of new technology that has given the photochemist highly sensitive tools that can be used to probe the unstable fragments of the photochemical process. Certainly, the laser is foremost among the new tools in the photochemical arsenal. With tunable lasers, photochemists can probe the quantum state distribution of photochemical fragments. Lasers can also be used to dissociate a molecule, often from a given rovibronic level of the excited state. Their high intensity is useful in producing enough fragments so that less sensitive analytical techniques may be used for detection and characterization of the photochemical process. The polarization characteristics of lasers allow the photochemist to gain new information about the lifetime of the excited state and the absorption transition moment in the dissociation process. The ultimate goal of all of these experiments is to obtain enough information so that the experimental data may be used to obtain accurate potential energy surfaces of the upper electronic state of the dissociating molecule.

With all of these new tools, it is no wonder that there has been an explosion of papers on photochemical dynamics, so much so that in this review we shall limit ourselves to those papers that have appeared over the last three years. Earlier reviews cover the work before this time, and the papers that are cited also give references to the earlier work. The papers that are covered are further limited to those that measure and discuss the detailed quantum state distribution of one or more of the photochemical fragments. Those papers that are limited to final product analysis are discussed only if the results bear directly upon the dynamics of the photochemical process. The review is organized so that molecules with similar chromophore groups are all discussed at the same time. This emphasizes the similarities and differences between these molecules. The discussion of the molecular systems begins after a brief discussion of some of the newer experimental techniques. In this review any earlier reviews that cover that molecule are cited along with the later papers on the subject.

There have been several experimental developments in the last few years that have resulted in more definitive experiments on photodissociation dynamics. First and foremost is the greater availability of intense laser sources, particular in the region below 300 nm (8,9). Excimer laser sources provide large numbers of photons at 157, 193, 222, 249, and 308

nm. Commercial Nd-YAG pumped-dye lasers and excimer lasers provide useful tunable photolytic sources between 217 and 300 nm. These same lasers can be shifted further in the UV region by stimulated Raman shifting in H_2 or D_2. Finally, there are various nonlinear mixing schemes that are reported to give tunable radiation in the VUV and EUV region. In some cases, intensities as high as 10^{12} photons/pulse have been reported (10). With these more intense light sources, more sophisticated experiments may be performed, since larger numbers of photolytic products are available after each laser shot. This large laser intensity can be both a blessing and a curse, since care has to be taken to be sure that simultaneous and sequential multiphoton processes do not occur.

Intense laser sources have been used to induce ionization or fluorescence of products in several kinds of photolytic experiments. Welge and his colleagues have used these sources to detect NO by multiphoton ionization (MPI) of the product. They have also used lasers that have been extended to the VUV region by various nonlinear mixing schemes as photoionization sources for mass spectrometric detection of reaction products. Recently, Brewer et al. (11,12) have reported on the use of lasers to induce the two photon transition in iodine and sulfur atoms, so that these atoms may be detected by fluorescence. Using this laser-induced fluorescence (LIF) technique, they have been able to determine branching ratios in the photolysis of various compounds.

Both Welge (13), and Wittig and his colleagues (14), have been able to use high resolution tunable lasers to measure the Doppler profile of the individual rotational lines of NO and CN fragments produced by photodissociation. They are thus able to determine all of the energetics (translational, rotational, and vibrational) associated with a particular fragment.

Coherent anti-Stokes Raman scattering (CARS) spectra of O_2 (15) and H_2 (16) have been recently obtained. This opens up a very important class of molecules to direct detection. It is now possible, with the right parent molecule, to study the dynamics of the molecular detachment process. It will be particularly interesting to see the dynamical results that will be obtained in the future on the VUV photodissociation of hydrocarbons, such as the vibrational and rotational excitation of the H_2 product.

Most of the detection schemes involve LIF as the means of detection of the unstable species. Recently, however, Kanamori et al. (17) and Wood et al. (18) have reported on the use of infrared tunable diode lasers to detect by absorption the SO and CO_2 photochemical fragments respectively. Undoubtedly, this will also be extended to various non-fluorescing molecules so that it is likely that more products

will be detected in the future.

Finally, one of the most exciting recent developments is the observation of fluorescence or Raman scattering from a molecule during the fragmentation process (19). This technique allows one to probe both the upper and ground potential surfaces, giving directly the information that is the ultimate basis for study of photodissociation dynamics.

II. HYDROGEN-OXYGEN COMPOUNDS

Most of the recent reviews on photodissociation dynamics have had an extensive section on the earlier work on water (2-4, 7,20) because it is an important component on the earth's atmosphere. In this section we shall concentrate on the more recent work on water and hydrogen peroxide, since $OH(X^2\Pi)$ is amenable to laser detection.

A. Water

Water absorbs only below about 185 nm (2,3). The first absorption spectrum is continuous (145-185 nm) corresponding to the transition $A^1B_1 \leftarrow X^1A_1$. Photodissociation in this region has been studied in detail by Welge and Stuhl (21) and recently by Andresen et al. (22-25). The main dissociation process (99%) at 157 nm (F_2 excimer laser) is

$$H_2O + h\nu \longrightarrow H + OH(X^2\Pi), \quad <242 \text{ nm} \qquad (1)$$

where the rotational distribution of $OH(X^2\Pi)$ is probed using LIF. About 88% of the excess energy is in translation, 10% is in vibration, and 2% is in rotation. When the molecule is cold (10 K) the $OH(^2\Pi)$ rotational distribution can be described as a Boltzmann distribution with a temperature of 475 K for the Q branch, but the P, R branches deviate from this distribution. The experimental arrangement used by Andresen et al. (25) to study the details of the photodissociation process at 157 nm is shown in Figure 1. The dissociation laser beam is directed along the X axis and the probe laser is propagated in the opposite direction to the excimer laser. The intensity of the LIF is measured along the Y axis. It was found that when H_2O is cold (10 K), the ratio of the Q to R branch increases with an increase in the OH rotational energy. Since the Q branch probes the π^- states (the upper levels of the λ doublets of $^2\Pi_{3/2}$ state), the results indicate a preferential population of the upper levels of the λ doublet. As shown in Figure 1, the unpaired p orbital of the π^- state is perpendicular to the rotational plane of OH, which coincides also with the molecular

PG 1 Model paper for 15% reduction
to 28×44 picas type page

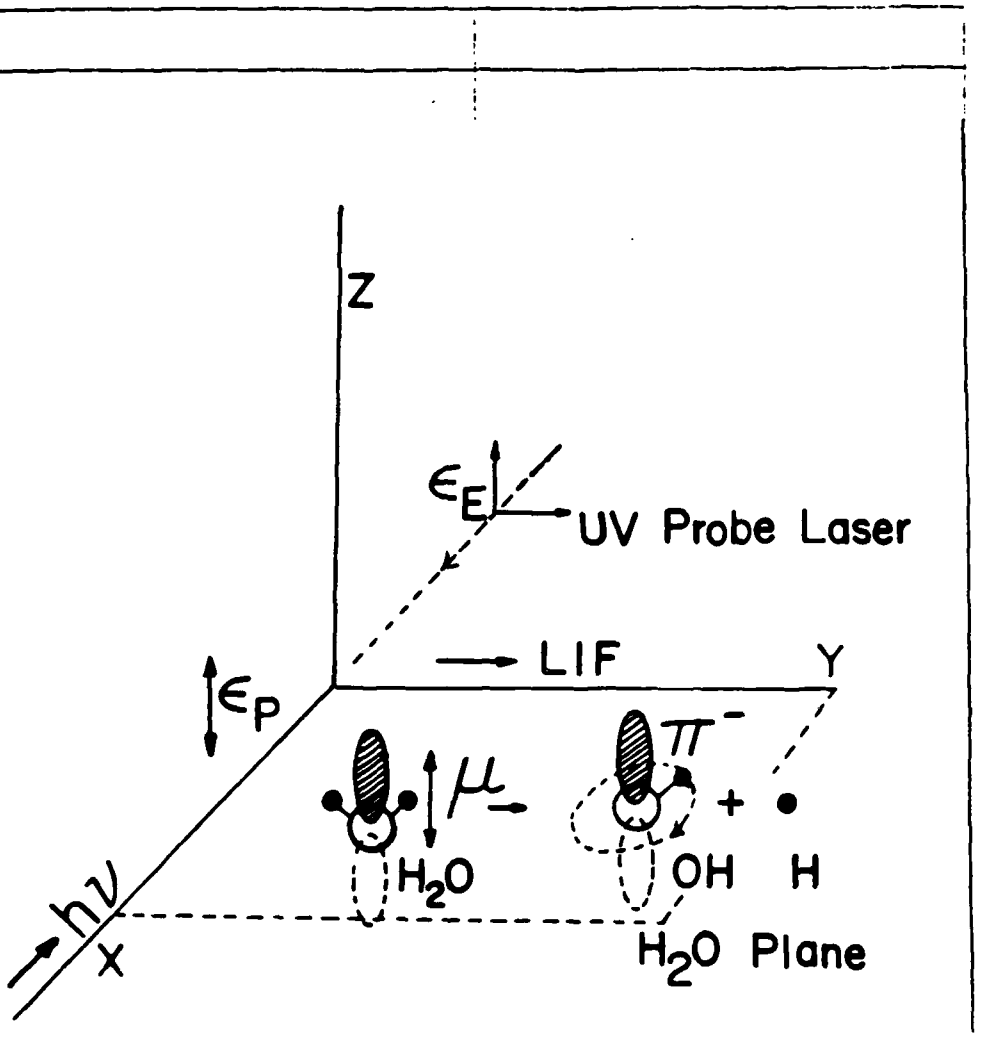

FIGURE 1. Polarization of laser induced fluorescence of $OH(X^2\Pi)$ photodissociated from H_2O in the 145-185 nm region. The absorption transition moment is perpendicular to the molecular plane corresponding to the transition A^1B_1-X^1A_1. The dissociated $OH(X^2\Pi)$ is also in the molecular plane, since the induced fluorescence intensity of OH is preferentially polarized along the Z axis (25) perpendicular to the molecular plane. The OH radical rotates on the H_2O plane (XY plane) after dissociation. The unpaired p-orbitals of excited H_2O and of dissociated OH are perpendicular to the molecular plane.

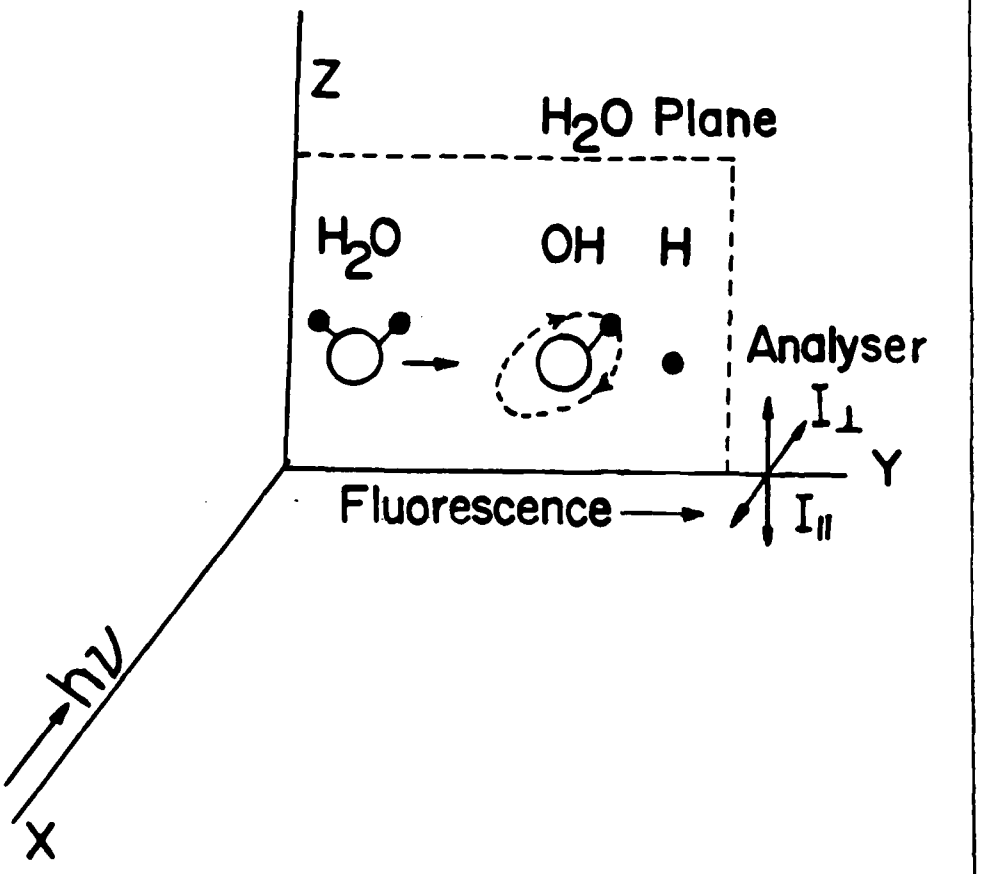

FIGURE 2. Production of $OH(A^2\Sigma)$ from the photolysis of H_2O in the 120-140 nm region. The beam of light is along the X axis and fluorescence is observed along the Y axis. The absorption dipole moment is in the molecular plane according to the transition B^1A_1-X^1A_1. The OH fluorescence is preferentially polarized perpendicular to the molecular plane corresponding to the emission dipole perpendicular to the OH internuclear axis (27).

plane. Hence, the preferential production of $OH(\pi^-)$ levels indicates the conservation of symmetry during photodissociation, that is,

$$H_2O + h\nu \longrightarrow H_2O(A^1B_1) \longrightarrow H + OH(\pi^-) \quad (2)$$

since $OH(\pi^-)$ has the same symmetry ($^1B_1$) as the excited water molecule.

The dissociation of OH within the molecular plane has also been suggested from the results of the fluorescence polarization. Referring to Figure 2, if the F_2 laser is polarized along the Z axis, the intensity of the OH fluorescence induced by the probe laser polarized along the Z axis to that polarized along the Y axis increased, at high J values and 10 K, to a limiting value of 3.3. The loss of polarization at low J is ascribed to the doublet mixing in OH. Even at higher temperatures, depolarization is relatively small, suggesting a fast dissociation. The preferential production of the upper levels of the doublets in photodissociation may explain the OH maser observed in the interstellar medium.

The second region of absorption (110-145 nm) in H_2O corresponds to the transition $B^1A_1 \leftarrow X^1A_1$ and is characterized by diffuse bands and sharp Rydberg bands which are superimposed on a continuum. In this region processes 3 and 4 have been found.

$$H_2O + h\nu \longrightarrow H + OH(A^2\Sigma^+), \quad <137 \text{ nm} \quad (3)$$

$$H_2O + h\nu \longrightarrow H_2 + O(^1D), \quad <117 \text{ nm} \quad (4)$$

Figure 2 shows a typical arrangement for measuring the fluorescence polarization of a photofragment produced by a polarized or unpolarized light source. The incident beam is directed along the X axis, and the fluorescence intensity of the photofragment is measured along the Y axis. The intensity of the fluorescence polarized perpendicular to the YZ plane is denoted $I_\perp$ and that polarized parallel to the Z axis is $I_\parallel$. The degree of polarization P is given by

$$P = (I_\parallel - I_\perp)/(I_\parallel + I_\perp) \quad (5)$$

Chamberlain and Simons (26) have shown by theory that when the absorption transition moment in H_2O is parallel to the molecular plane, the degree of polarization P is (-1/13), if the OH fluorescence transition moment is perpendicular to the internuclear axis, and P is (1/7) if it is parallel to the internuclear axis. Simons and Smith (27) and MacPherson and

Simons (28) have shown experimentally that P of OH fluorescence produced by process 3 near 130 nm is negative, suggesting that the absorption dipole moment is in the molecular plane and the OH fluorescence dipole moment is perpendicular to the internuclear axis. This agrees with the assignment of the H_2O transition $B^1A_1 \leftarrow X^1A_1$ and the observed OH fluorescence. The degree of polarization is largest if dissociation is direct, and it becomes less if the lifetime of the excited state is longer. The degree of polarization at 130 nm is largest at high Js, while it decreases at 121.6 nm where absorption to a Rydberg state occurs, resulting in a delay in the dissociation as the Rydberg state predissociates through a repulsive state. In contrast to the results obtained in process 1, large amounts of rotational energy are partitioned into the $OH(A^2\Sigma^+)$, that is, 61% of the excess energy resides in rotation and 10% in vibration (29). This indicates that a large change in bond angle (from 105 to 180°) occurs in the excitation providing the necessary torque for rotational excitation. Such a large partitioning of the excess energy into rotation is unusual in triatomic photodissociation (20). Process 3 occurs almost exactly at the calculated thermochemical threshold wavelength of 137 nm and with a maximum quantum yield of 11% at 130 nm (30). The OH fluorescence intensity produced from H_2O at 121.6 nm has been used to measure the water content in the straro-sphere (31).

The transition to the C^1B_1 state of H_2O was achieved by a two photon absorption of KrF laser light near 248 nm (32). The OH(A-X) fluorescence excitation spectrum in the 247.9-248.5 nm range follows the rotational structure of the $C^1B_1 \rightarrow X^1A_1$ transition. However, (i) the OH(A-X) fluorescence spectrum produced by the two photon dissociation of H_2O has a maximum population at $N' = 14$, while single photon absorption near 124 nm generates OH fluorescence spectrum with a maximum population at $N' = 20$; (ii) only absorption to $K_a = 1$ (and not $K_a = 0$ where K is the rotational angular momentum about the a axis) of the C^1B_1 state predissociates into $OH(A^2\Sigma)$ + H probably through the B^1A_1 state. Apparently, the two-photon absorption near 248 nm predominantly populates the C^1B_1 state, while the single photon process populates the B^1A_1 near 124 nm.

Reaction 4 is energetically possible below 177 nm but experimentally it is only significant (>10%) in the second absorption region (eq. 2), which indicates that there is a large (~2 eV) energy barrier. Theodorakopoulos et al. (33) calculated the minimum energy path for the symmetrical dissociation process 4. It is likely that the B^1A_2 state that is originally formed crosses the $^1A_2$ state at an excitation energy of 9.05 eV.

B. Hydrogen Peroxide

Hydrogen peroxide is an important minor constituent in the troposphere and stratosphere. Absorption starts at about 350 nm, and is continuous down to 170 nm (34,35). Between 137 nm and 170 nm two vibrational progressions were found (34). The primary process in the ultraviolet (>190 nm) is mainly (36)

$$H_2O_2 + h\nu \longrightarrow OH + OH \qquad (6)$$

Below 140 nm other processes also occur (36) to a minor extent

$$H_2O_2 + h\nu \longrightarrow H + HO_2 \qquad (7)$$

$$H_2O_2 + h\nu \longrightarrow H_2 + O + O \qquad (8)$$

The formation of $HO(A^2\Sigma^+)$ is thermochemically possible below 200 nm; experimentally, $HO(^2\Sigma)$ starts to appear below 172.2 nm (34).

$$H_2O_2 + h\nu \longrightarrow HO(X^2\Pi) + HO(A^2\Sigma) \qquad (9)$$

with a maximum quantum yield of 18% at 130 nm. Ondrey et al. (37) and jacobs et al. (38) studied the photolysis of H_2O_2 using lasers at 193 and 248 nm. More than 90% of available energy resides in translation and less than 10% in rotation. Almost no vibrational excitation was found. At 248 nm, the rotational distribution follows a Boltzmann distribution with a temperature of 1235 K, while at 193 nm at least two different rotational distributions were found, suggesting two different repulsive surfaces.

III. ALDEHYDES, KETONES, AND ACIDS

Most of the latest experimental techniques have been applied to the study of the photodissociation dynamics of these molecules. Part of the reason for the great interest in these molecules is a result of their long history in photochemistry and partly because there is a low lying absorption that is accessible to the available lasers. Formaldehyde is particularly important since it is the simplest molecules in the group and has been studied theoretically.

A. Formaldehyde

Spectroscopy (39) and photochemistry (40) of formaldehyde have been extensively studied. The rotational analysis of the absorption spectrum of H_2CO in the 250 to 360 nm region indicates that the transition is $A(^1A_2) \leftarrow X(^1A_1)$, which is forbidden by the electric dipole selection rules but is vibronically allowed with excitation of ν_4' vibration of b_1 symmetry. Low resolution absorption spectrum of H_2CO is shown in Figure 3. The notation $2^n_0\ 4^1_0$, for example, denotes a vibronic transition from zero vibrational level of the ground state to the upper A_2 state with n quanta of ν_2' vibration and 1 quanta in the ν_4'. Moore (40) has given an excellent review of the formaldehyde photochemistry up to 1983 that includes over 100 references. The photochemistry of H_2CO consists of three main primary events:

(i) dissociation to H + HCO

$$H_2CO + h\nu \longrightarrow H + HCO, \quad <331.5 \text{ nm} \tag{10}$$

As shown in Figure 3, this process occurs below 331.5 nm. The quantum yield increases to a maximum of 0.8 near 300 nm and then decreases to 0.3 near 260 nm (41).

(ii) dissociation to H_2 + CO

$$H_2CO + h\nu \longrightarrow H_2 + CO, \quad \Delta H = -0.47 \text{ kcal/mol} \tag{11}$$

The quantum yield of this process is near unity in the 331-355 nm region, as shown in Figure 3. Process 11 is not the direct decay from A^1A_2 (S_1) to H_2 + CO but is considered to be a sequential process involving high vibrational levels (S^*_0) of the ground state S_0.

$$S_1 \longrightarrow S^*_0 \longrightarrow H_2 + CO \tag{12}$$

This sequential process rather than the direct, $S_1 \rightarrow H_2 + CO$ decay was invoked to explain the rapidly increasing decay rate with an increase of total energy.

(iii) fluorescence lifetime

The fluorescence ($S_1 \rightarrow S_0$) lifetime of H_2CO changes from several microseconds to several nanoseconds as the vibrational energy increases from zero to several thousand wave numbers in the S_1 state (see Figure 3, the 0-0 transition is located at 28188 cm^{-1} = 3.49 eV). However, the rotational state lifetime

PG 1 Model paper for 15% reduction
to 28×44 picas type page

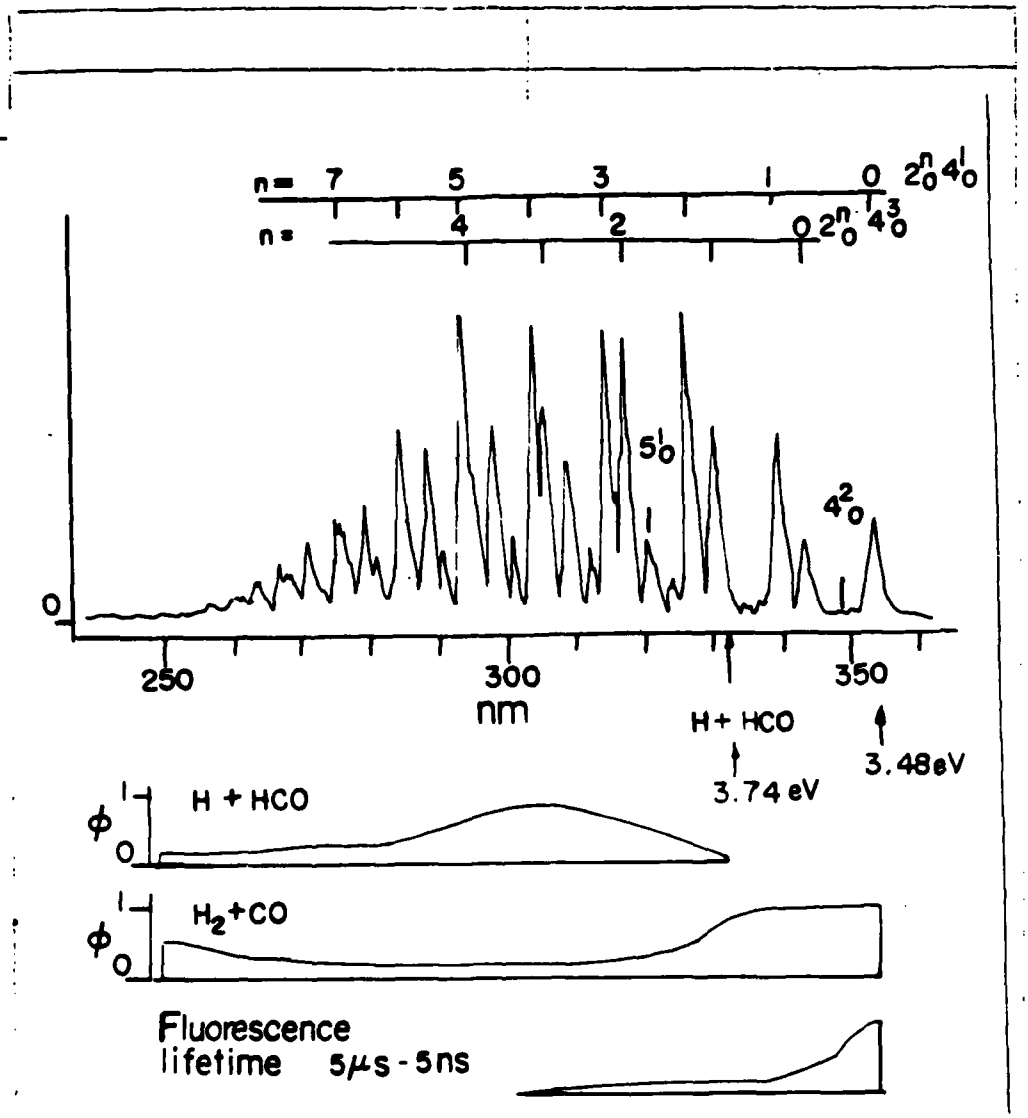

FIGURE 3. Low resolution absorption spectrum of H_2CO in the 250-360 nm region (39). The electronic transition (A^1A_2-X^1A_1) is forbidden by electric dipole selection rules but is allowed by vibronic transition; 4^1_0 means a transition from zero vibrational levels of the ground state to v'_4=1 of the upper state. The process $H_2CO \rightarrow H_2 + CO$ occurs throughout the absorption region. The quantum yield is unity between 330 and 360 nm. Below 330 nm another process, $H_2CO \rightarrow H + HCO$, sets in. The fluorescence lifetime decreases from several μs to several ns as absorption changes from 355 nm to 300 nm. Within each vibronic band, the lifetime changes drastically with change in J' and K'_a. Reproduced from reference (39) with permission from Annual Reviews, Inc.

within each vibronic band ($2^n_0 4^3_0$ series) changes drastically with J' and k'_a component and apparently no systematic variations have been found.

Ho et al. (42) studied the photolysis of H_2CO under collisionless conditions using the TOF molecular beam method and laser light at 383.9 nm. At this wavelength the radical dissociation (H + HCO) is predominant (see Figure 3). The time of flight analysis of the product HCO indicates that the HCO radicals have only a very small fraction (<10%) of the available energy in translation, implying that HCO radicals are highly internally excited. On the other hand, a large fraction of the translation energy goes into the products H_2 and CO. Ho et al. (42) also studied the photolysis at 339 and 357 nm (corresponding to absorption by the $2^1 4^1$ and 4^1 bands; see Figure 3) where the primary process is mainly H_2 + CO production. At 339 nm, 65% of the available energy, 55 kcal/mol, is translational energy in the products. The H_2 can be vibrationally excited up to v" = 3. The vibrational population of H_2 has recently been determined using (CARS) by Pealat et al. (16). They found that v = 1, 2, and 3 are comparatively populated. At 355 nm excitation (43-45) the product CO, detected by vacuum UV laser excited fluorescence, was rotationally excited from J" = 26 to 63 but vibrationally cold. Cheng et al. (46) monitored the product CO vibrational state by infrared emission. They found that more than 95% of CO formed is in v" = 0 at 355 nm excitation. At 317 nm the population ratio of 77:20:4 was found for v" = 0, 1, and 2 by infrared laser absorption. They conclude that the initially produced CO is in high rotational states, which are subsequently deactivated to lower J's by collisions.

Bamford et al. (45) have recently studied the photolysis of H_2CO near the S_1 origin. The complete rotational distribution has been obtained for CO, which was detected by vacuum ultraviolet laser induced fluorescence. The distribution has a peak at J" = 42 and highly nonthermal, suggesting that energy randomization does not occur during dissociation. The population in CO J" < 20 is absent. The vibrational population of v" = 1 is 14 ± 5% as large as that of CO (v" = 0). The CO(v" = 1) has nearly the same rotational distribution as CO(v" = 0).

B. Ketene

The photolysis of CH_2CO has been extensively studied (2,4). The primary processes in the ultraviolet are:

$$CH_2CO + h\nu \longrightarrow {}^3CH_2 + CO, \quad <373.4 \text{ nm} \tag{13}$$

$$CH_2CO + h\nu \longrightarrow {}^1CH_2 + CO, \quad <336.0 \text{ nm} \tag{14}$$

where $^3CH_2$ and $^1CH_2$ are X^3B_1 and a^1A_1 respectively. Hayden et al. (47) studied the photolysis of CH_2CO at 351 and 308 nm. From TOF measurements of the CO and CH_2 photofragments, the translational energy distribution of the fragments is derived. The center-of-mass energy distribution of the fragments produced using a laser at 351 nm, has a peak at 2.3 kcal/mol and a high energy limit of 3.8 kcal/mol. The difference of 81.4 kcal/mol (for 351 nm light) and 3.8 kcal/mol is the bond energy $D_o(H_2C\text{-}CO)$ = 77.6 kcal/mol. The high limit of the translational energy at 308 nm is 6.7 kcal/mol. The enthalpy change for the production of $^1CH_2$ + CO is then 92.8 - 6.7 = 86.1 kcal/mol. Hence the energy difference $^1CH_2$ - $^3CH_2$ = 8.5 kcal/mol is obtained. The energy distribution curve of the fragments at 308 nm has only one peak suggesting only $^1CH_2$ is produced.

Sonobe and Rosenfeld (48,49) have measured the 4.7 μm infrared emission of CO. The extent of the CO vibrational excitation can be estimated using a cold gas filter containing CO and a 4.7 μm filter. If CO is vibrationally excited there is a smaller amount of attenuation of 4.7 μm fluorescence by the cold gas filter. When ketene is photolyzed at 193 nm, they estimate from their data that the rotational and vibrational temperatures are about 6700 and 3700 K, respectively. A high rotational temperature suggests that the C-C-O angle is bent in the excited state. The CO vibrational excitation becomes less for longer excitation wavelengths.

The photolysis of CH_2CO at 193 nm has also been studied by Fujimoto et al. (50). A CO laser was used to probe the vibrational excitation of the CO produced. The product CO contains an average vibrational energy of 6.4 kcal/mol. The vibrational population distribution corresponds to about 4000 K in good agreement with Sonobe and Rosenfeld (49,50).

C. 3-Cyclopentenone

The photolysis of 3-cyclopentenone at 193, 249, and 308 nm has been studied by Sonobe et al. (51,52). The vibrational population of CO produced in the reaction

$$\text{3-cyclopentenone} + h\nu \longrightarrow \text{butadiene} + \text{CO} \qquad (15)$$

was probed by time-resolved CO laser absorption. The CO excitation is less than that calculated by statistical theory assuming that all available energy, (i.e., $[h\nu - \Delta H]$, is used for internal excitation of the products. They suggest that a biradical intermediate is formed, which requires an activation energy. Once the

intermediate is formed it dissociates, converting most of the excess energy into translational recoil energy between the products. Hence the net internal excitation of the fragments becomes much less than the maximum available energy.

D. Acrylic Acid and Methacrylic Acid

The photolysis of acrylic acid and methacrylic acid has been performed by Rosenfeld and Weiner (53) at 193 and 249 nm.

$$CHCH_2COOH \longrightarrow C_2H_4 + CO_2 \quad (16)$$

$$CH_3CCH_2COOH \longrightarrow CH_3CHCH_2 + CO_2 \quad (17)$$

The infrared emission of the CO_2 that is formed, and its attenuation by a cold gas filter containing CO_2 and a 4.3 μm filter were observed. If all available energy ($h\nu$ + exothermicity of the reaction) is used to excite the products assuming strong coupling between the products, far more excited CO_2 would be produced. Thus, only part of the available energy may be used for internal excitation of the products, and the remaining energy is spent on forming carbenes (e.g., CH_3HC:).

E. Pyruvic Acid

Rosenfeld and Weiner (54) photolyzed pyruvic acid at 193, 249, 308, and 351 nm and measured the infrared emission of the product CO_2.

$$CH_3COCOOH + h\nu \longrightarrow CH_3CHO + CO_2 \quad (18)$$

They postulate the formation of the carbene intermediate, (CH_3COH), to explain the discrepancy between the observed CO_2 excitation and much larger excitation that is calculated on the basis of a statistical theory that uses strong coupling in the exit channel as the photofragments dissociate.

F. Glyoxal

Recently (55) it has been shown that the S_1 state of glyoxal photodissociates in the absence of collisions. It was only natural that a study on the photodissociation dynamics should quickly follow, since many interesting questions were raised in the original study. Through product analysis they could identify two primary processes, namely,

$$C_2H_2O_2 + h\nu \longrightarrow \begin{cases} H_2CO + CO & (19) \\ H_2 + 2CO & (20) \end{cases}$$

It was suggested that vibrationally hot H_2CO^* formed in reaction 19 decomposed to form a H_2 molecule and CO which was plausible since this kind of dissociation is known to occur in formaldehyde. They also suggested that there must be another primary process, since their product yields could not be reconciled with just these two primary process. Hepburn et al. (56) did a TOF experiment in which they excited the 8^1_0 band of glyoxal at 439.8 nm. They were able to show from TOF measurements of mass 28 that there was indeed a third primary process, that is, corresponding to the third low energy peak.

$$H_2C_2O_2 + h\nu \longrightarrow HCOH + CO \quad (21)$$

This third primary process produced the hydroxymethyl radical which was needed to explain the third low energy peak in the translational energy distribution curve. From the areas associated with each of the peaks in the translational distribution curves they were able to determine that the relative quantum yields for each of these primary process were 9,4,1, and respectively, for reactions 19, 20, and 21.

Preliminary measurements on the LIF spectra of the CO produced in the photolysis of glyoxal in the 8^1 transition have also been reported (57). The results show that CO is formed within in the 0.87 μs lifetime of glyoxal and that the complexity of the observed spectra indicates that the CO is formed vibrationally excited. It will be interesting to see what the final vibrational distribution of the CO will be in light of the previous demonstration that there are three primary processes that lead to CO.

IV. GROUP SIX TRIATOMIC OXIDES

Sulfur dioxide (2,4) and oxone are important atmospheric constituents. Particularly ozone acts as a radiation shield of sunlight below about 300 nm. A great deal of work has been done to understand the photodissociation dynamics of these molecules. While a great deal of progress has been made, it will be clear from the following discussion that much remains to be done for complete understanding.

A. Sulfur Dioxide

The photodissociation of SO_2 occurs below 219.4 nm, corresponding to $D_o(OS-O) = 5.65$ eV (2). Freedman et al. (58) and Kawasaki et al. (59) have studied a time-of-flight distribution of SO formed by the photolysis of SO_2 at 193 nm. Because the geometry of the excited state (C^1B_2) is markedly different from that of the ground state, it is expected that a large fraction of the excess available energy goes into rotational and vibrational energy of the SO fragments and hence the fragment recoil energy distribution must have a peak at a value much lower than the available energy. The peak is indeed at about 7 kcal/mol (59), or 11 kcal/mol (60), corresponding to $v'' = 3$ or 4 of SO, while the excess available energy is 19 kcal/mol. The instrumental resolution was not sufficient to resolve vibrational structure.

Kawasaki et al. (60) have measured the angular distribution of SO using a polarizer. No angular dependence was found for four angles of the polarization direction of the laser light with respect to the detector axis, indicating that the excited molecule does not dissociate immediately. Freedman et al. (59) believe that the strong vibrational excitation of the SO fragment is primarily due to the drastic change in SO bond length on excitation. Further work is desirable to probe SO vibration and rotation by laser induced fluorescence.

The intense laser beam at 248 nm is capable of dissociating SO_2 by sequential two-photon absorption (60-62). Further excitation of the SO and S fragments was observed to occur by one and two photon processes, respectively (see Figure 4):

$$SO_2 + h\nu \longrightarrow SO_2(B^1B_1) + h\nu \longrightarrow SO_2 \quad \text{(G Rydberg state)} \tag{22}$$

$$SO_2(G) \longrightarrow SO(X^3\Sigma^-) + O \tag{23}$$

$$SO(X^3\Sigma^-) + h\nu \longrightarrow SO(B^3\Sigma^-) \tag{24}$$

$$SO_2(G) \longrightarrow S(3P^4\ ^3P) + O_2 \tag{25}$$

$$S(3P^4\ ^3P) + 2h\nu \longrightarrow S(8P\ ^3P) \longrightarrow S(4S\ ^3S_1^0) \tag{26}$$

$$S(4S\ ^3S_1^0) \longrightarrow S(3P^4\ ^3P) + \text{182-nm emission}) \tag{27}$$

The ultraviolet fluorescence of SO(B, $v' = 2$) → SO(X, v'') and

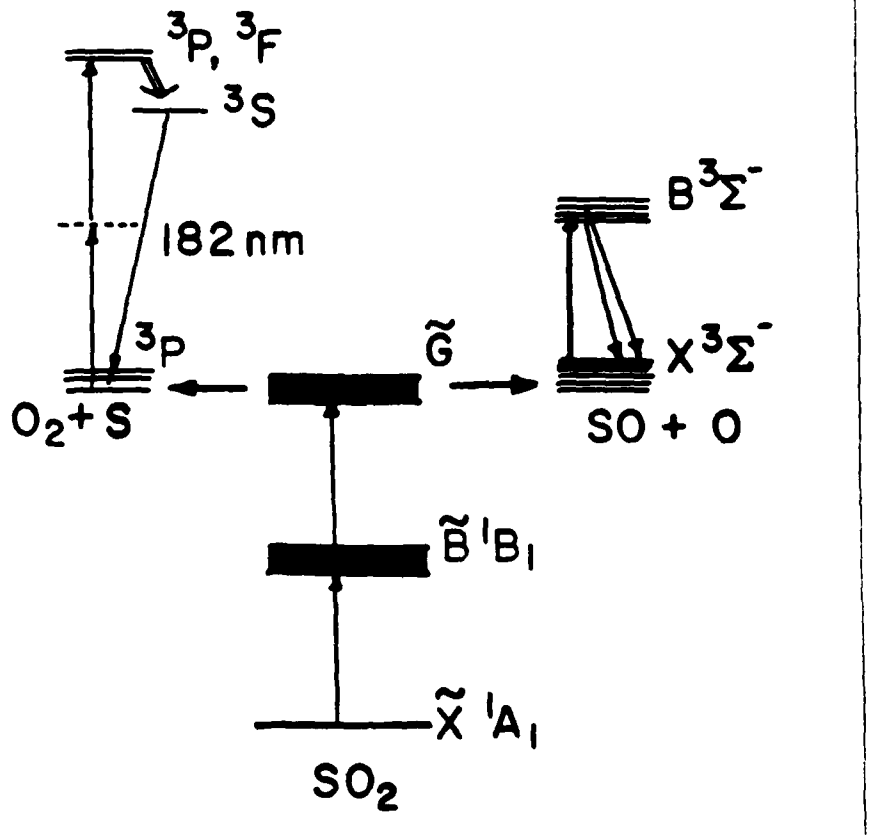

FIGURE 4. Schematic diagram of the 248 nm laser photolysis of SO_2; ground state $S(^3P)$ and $SO(X^3\Sigma^-)$ are produced by sequential two photon absorption by SO_2. These species are further promoted to the electronically excited $S^*(^3P)$ and $SO(B^3\Sigma^-)$; the $S^*(^3P)$ atoms relax (radiatively) to ^3S then return to ^3P by the emission of 182 nm light. From reference (215) with permission of the American Institute of Physics and the authors.

the atomic emission $S(4s\ ^3S^0) \rightarrow S(3P^4\ ^3P)$ at 182 nm were thus observed. The 182 nm atomic fluorescence is delayed 50 ns after the photolysis laser suggesting that the initially formed $S(3p^4\ ^3P)$ is relaxed to the lowest ^3S level from which 182-nm emission is produced. Venkitachalam and Bersohn (63) have shown that laser light in the 285-311 nm region produced 145, 147.6 nm SO emission as well as 166.7 nm S atom emission by the following processes:

$$SO_2 + h\nu \longrightarrow SO_2(B^1B_1) \tag{28a}$$

$$SO_2(B^1B_1) + h\nu \longrightarrow SO_2 \quad \text{(G. Rydberg)} \tag{28b}$$

$$SO_2\ (G) \longrightarrow SO(X^3\Sigma) + O \tag{29}$$

$$SO(X^3\Sigma) + 2h\nu \longrightarrow SO(E^3\Pi) \longrightarrow SO(X^3\Sigma) + (145\text{-}146.7\ \text{nm emission}) \tag{30}$$

$$SO_2\ (G) \longrightarrow S(3P\ ^1D) + O_2$$

$$S(3P\ ^1D) + 2h\nu \longrightarrow S(^4P\ ^1F_3) \longrightarrow S(4s'\ ^1D) \longrightarrow S(3P\ ^1D) + (166.7\ \text{nm}) \tag{31}$$

Above 218 nm, below the dissociation limit, fluorescence from the SO_2 (C^1B_2) state has been observed.

When the molecule is cooled by supersonic expansion, and excited with a very narrow linewidth laser in the 218-235 nm region, quantum beats are observed by Ivanco et al. (64,65) in the fluorescence decay curves. They proposed that vibronic interaction between the X state and C state produces coupled levels that give rise to quantum beats in the fluorescence decay. Watanabe et al. (66,67) also found quantum beats in the fluorescense decay of A^1A_2 state formed by absorption of laser light at 304.3 nm under an applied weak magnetic field. In addition they found that all of the rovibronic levels in the 300-320 nm region exhibit a biexponential decay with a short lifetime of 3-5 μs and a long life of 15-30 μs when SO_2 is excited by a laser with a 0.02 cm^{-1} bandwidth. This suggest that the initially prepared $^1A_2$ state couples with a small number of other levels. On the other hand, Holtermann et al. (68) found but one decay of 13.4 μs with a 0.2 cm^{-1} bandwidth laser. Watanabe et al. (67) have explained the differences that are observed in these decay curves as being due to the differences in the bandwidths of the lasers that were used.

The self-quenching rate constant of 21 x 10^{-10} cm^3/molecule s that was measured in these studies is unusually large (69). Quenching by various gases and collision induced rotational transitions have also been measured (68,69). The quenching cross sections by He and Ar in a supersonic jet increase at very low temperature (70), indicating the formation of collision complexes.

Kimel et al. (71) have used the combination of ultraviolet and infrared lasers to excite SO_2 near 300 nm. Sharp peaks superimposed on a quasi-continuum were observed in the fluorescence spectrum excited by the UV laser. When the CO_2 laser was fired after the UV laser, the sharp peaks decreased and a broad band emission appeared towards the shorter wavelength region of the exciting wavelength. The fluorescence lifetime decreased when the CO_2 laser was combined with the UV laser. The results are interpreted as being due to more efficient coupling of the excited vibronic states with the highly excited vibrational levels of the ground electronic state.

B. Ozone

The photodissociation of ozone (2,4,20) in the ultraviolet region is important in atmospheric chemistry, since its main product, $O(^1D)$, reacts further with H_2O and N_2O to produce OH and NO (2). Recent studies (72-76) have shown that in the Hartley continuum (250-300 nm), 90% of the process is:

$$O_3 + h\nu \longrightarrow O(^1D) + O_2(a^1\Delta), \qquad <310 \text{ nm} \qquad (32)$$

and 10% is (72,74,77)

$$O_3 + h\nu \longrightarrow O(^3P) + O_2(X^3\Sigma^-_g), \qquad <1180 \text{ nm} \qquad (33)$$

The quantum yield of $O(^3P)$ has been determined by resonance absorption at 130 nm (76), resonance fluorescence (73,75), and time-of-flight (TOF) mass spectrometer (72,74). The quantum yield of $O(^1D)$ decreases from 0.9 to 0.1 in the 300 to 320 nm region (73). The production of $O(^1S)$ is 0.1% or less in the entire region from 170 to 240 nm (78). Above 310 nm both O_3 absorption and the $O(^1D)$ quantum yield increase with vibrational excitation of O_3 (79). For example at 314 nm, which is about 500 cm^{-1} below the thermochemical threshold for process (32), the absorption cross section increases more than 8 times and the quantum yield increases 6 times.

Imre et al. (80) have recently succeeded in measuring very weak Raman scattering (or fluorescence) of strong laser light at 266 nm. Ozone dissociates almost immediately ($<10^{-15}$ s) upon absorption of light but a very small fraction ($<10^{-6}$) of light is re-emitted before the molecule falls apart. The observed resonance enhanced Raman scattering spectrum provides information on the potential surfaces of the ground and electronically excited states. As shown in Figure 5, the spectra consist of emissions associates with the ν_1 (symmetric stretch) and ν_3 (antisymmetric stretch) frequencies but does not contain the ν_2 (bending) vibration of the ground state. The highest ν_1 vibrational level that is observed (i.e., $v''_1 = 7$) is only about 5000 cm^{-1} below the dissociation limit. The absence of the ν_2 vibration shows that the upper state has the same bond angle as the ground state. From the relative intensities of various fundamentals, overtones, and combinations, the configuration of the upper state may be derived. The upper state potential thus derived has a maximum with respect to the ν_3 normal coordinate at the ground state equilibrium geometry and tends to dissociate into $O_2 + O$, with the O_2 being formed vibrationally excited.

A CARS experiment has recently been done to determine the amount of vibrational and rotational excitation that occurs in the $O_2(a^1\Delta)$ molecule when O_3 is photodissociated (81,82). Valentini used two lasers, one at a fixed frequency (266 nm) and the other that is tunable at lower frequencies. The 266 nm laser light is used to dissociate O_3, and the CARS spectrum of $O_2(a^1\Delta)$, the photolysis product, is generated using both the fixed frequency and tunable lasers. The spectral resolution (0.8 cm^{-1}) is sufficient to resolve the rotational structure. Vibrational levels up to $v'' = 3$ are seen. The even J states are more populated than the odd J states by some as yet unknown symmetry restrictions. Using a fixed frequency laser at 532 nm (83) to photolyze O_3 and to obtain the products $O(^3P) + O_2(X^3\Sigma^-_g)$, a non-Boltzmann vibrational population up to $v'' = 4$ (peaked at $v'' = 0$) is observed from the CARS spectrum. The rotational population is also non-Boltzmann peaked at J=33, 35 33, 31 and 25 for $v'' = 0,1,2,3$, and 4, respectively. Most of the available energy, 65-67%, appears in translation; 15-18% is in rotation and 17-18% is in vibration. A population inversion between $v'' = 2$ and 3 is also observed.

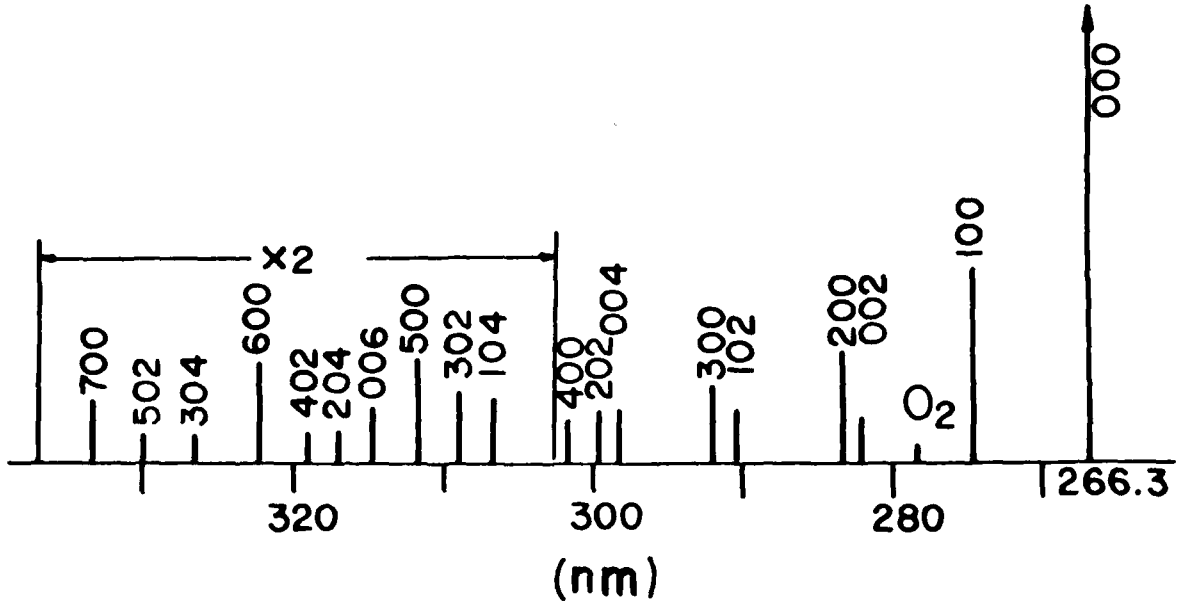

FIGURE 5. Schematic diagram of low resolution (0.8 nm) Raman scattering spectrum of O_3 excited at 266 nm. The spectrum consists of overtones and combination bands in ν_1 (symmetric stretch) and ν_3 (antisymmetric stretch up to v" = 7 and v_3 = 6. No bands with ν_2 (bending) are evident, suggesting that the bond angle remains the same during the transition. Reproduced from reference (80) with permission from the American Chemical Society.

V. NITROGEN-OXYGEN COMPOUNDS

Some molecules in this group (HONO, NO_2, N_2O, $HONO_2$) have been extensively studied because the photofragments OH and NO can be probed by tunable lasers. These molecules are important minor constituents in the earth atmosphere and their photochemistry plays a major role in air pollution. Atmospheric pollutants NO_x (NO, NO_2, NO_3) are formed from combustion of fuel and subsequent chemical reactions in the atmosphere. Photolysis of alkyl oxides produces NO and NO_2 that can be probed by LIF; the internal energy distribution provides an important clue to the mechanism of photodissociation.

A. Nitrous Acid

Nitrous acid in the gas phase is in equilibrium with NO, NO_2, and H_2O together with N_2O_3, N_2O_4, and a trace of HNO_3. The transform is lower in energy by about 0.5 kcal/mol than the cis form. Nitrous acid is present in the troposphere during the night time and is photodissociated rapidly after sunrise (84). The photofragment OH may subsequently attack organics, starting a chain photooxidation.

The first weak absorption band in the 300-400 nm range is diffuse, consisting of the ν_2 (-N=O) vibrational progression; the second much stronger band in the 190-270 nm region is continuous.

The primary processes are (2):

$$HONO + h\nu \longrightarrow HO + NO, \quad <593 \text{ nm} \tag{34}$$

$$HONO + h\nu \longrightarrow H + NO_2, \quad <369 \text{ nm} \tag{35}$$

with process 35 occurring to an extent of 10% or less. The photolysis of HONO in the first absorption band has recently been studied by Vasudev et al. (85,86) at 341.8, 354.7, and 368.9 nm. The transition is A^1A''-X^1A, that is, the transition moment is perpendicular to the molecular plane. The photofragment $OH(X^2\Pi)$ was probed by a polarized tunable laser in combination with Doppler spectroscopy. Because HONO always contains NO and NO_2, the internal energy of the other photofragment NO cannot be probed by a tunable laser. The results provide information on the angular distribution and translational, rotational, and vibrational energy of OH. The experimental arrangement is shown in Figure 6. The photolysis and probe laser are counterpropagated along the X axis and the electric vector of

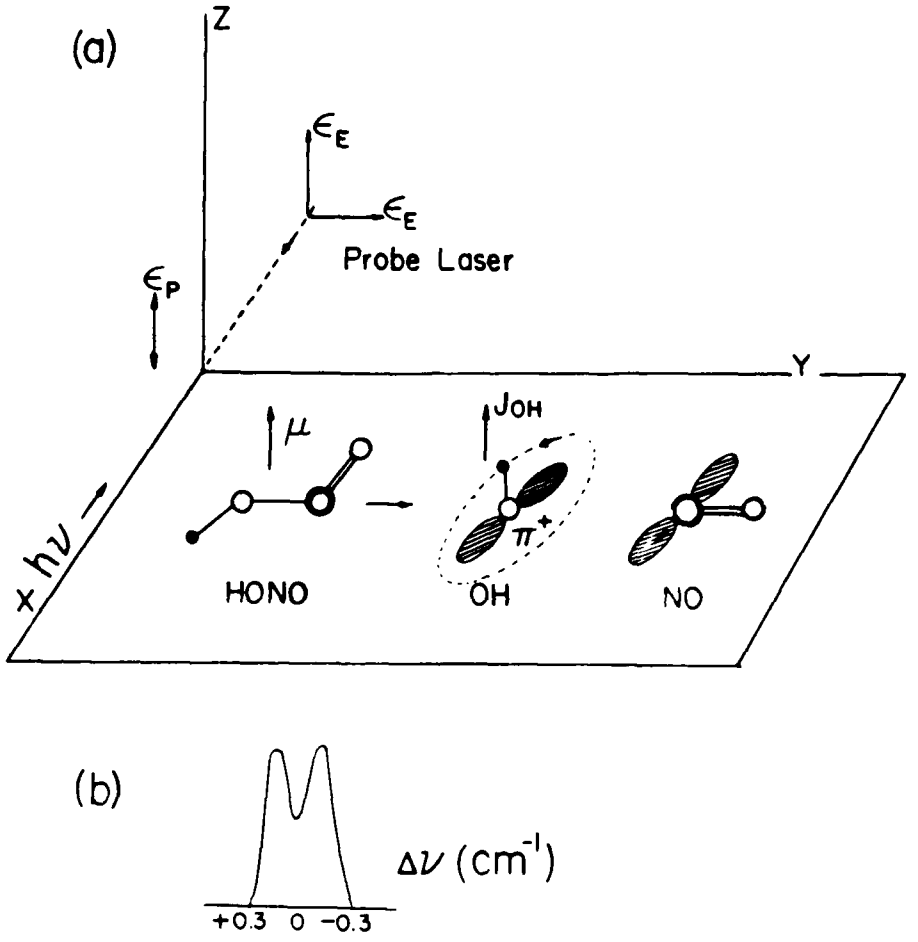

FIGURE 6. The photodissociation of HONO in the 300-400 nm region. (a) The photolysis and probe laser beam are coaxial and propagated in the opposite direction along the X axis; the electric vector, ε_p, of the photolysis light and that of the probe light, ε_E, are along the Z axis. The induced fluorescence intensity is measured along the Z axis. The transition moment of HONO in the 300-400 nm region is perpendicular to the molecular plane; the dissociated OH fragment rotates on the molecular plane and the unpaired π orbital is on the plane of rotation (π^+). (b) The Doppler line of OH dissociated from HONO profile probed with a tunable laser light near 285 nm; line width is approximately 0.1 cm^{-1} and ε_p is parallel to ε_E (86).

the photolysis laser and that of the probe laser are polarized along the Z axis. The induced fluorescence is viewed along the Z axis. It was found (86) that: (i) The $OH(^2\Pi_{1/2})$ state is more populated than the $^2\Pi_{3/2}$ state; (ii) The rotational temperature is near room temperature; (iii) The OH rotational angular momentum at the high J limit is parallel to the photolysis vector (i.e., after dissociation OH rotates in the molecular plane as shown in Figure 6a). This conclusion is deduced from the intensity ratios for P, R, and Q branches when ε_p is parallel to ε_E and when ε_p is perpendicular to ε_E (for details see references 85 and 86). (iv) The $v'' = 1$ levels are not excited. (v) When the electric vector of the photolysis light is parallel to the Z axis, the Doppler profile has two peaks indicating that more fragments with high velocity components than with low velocity components are moving forward and backward along the OH probe axis (see Figure 6b). The observed line shape can be reproduced if the Doppler width is 0.61 cm^{-1} and the direction of fragment recoil is perpendicular to the parent transition moment. If the direction of fragment recoil is parallel to the parent transition moment (i.e., the Z axis, the Doppler profile would have a peak at the center frequency).

The Doppler width of 0.61 cm^{-1} arises from the OH fragment velocity of 2.58 km/s, equivalent to a translational energy of 4720 cm^{-1}. This is 46% of the total energy available to the fragments. As shown in Figure 6a, OH radical dissociates from HONO in the molecular plane. This coplanar dissociation is possible if the half-filled π orbital of OH lies in the molecular plane. This orbital corresponds to π^+ (symmetric with respect to the molecular plane) and the lower rotational levels of the $OH(^2\Pi_{3/2})$ state. When π^+ levels are more populated, the intensities of the P, R branches become stronger than those of the Q branches. Similar preference of the $OH(^2\Pi)$ π^+ levels is found in the product $OH^2\Pi_{3/2}$ state produced from the reaction given below (87)

$$H + NO_2 \longrightarrow OH + NO \qquad (36)$$

This suggests that there is a HONO coplanar transition state formed during this reaction. The initial parent vibrational excitation in -N=O(ν_2) has no effect on the energy content of the OH product, suggesting that dissociation is so rapid that the ν_2'(-N=O stretch) vibration does not interact effectively with the fragmentation coordinate ν_4'(O-N stretch), that is, the ν_2' vibration is localized.

B. Nitrogen Dioxide

The spectroscopy and photochemistry of NO_2 have been extensively studied because the molecule is an important precursor for the formation of photochemical smog and it absorbs light throughout the ultraviolet and visible regions (2). Because of the strong perturbation between the excited and ground state, the spectrum is extremely complex. Two overlapping transitions in the visible region are the Douglas Huber system A'^2B_1 or $(^2\Pi_u) \leftarrow X(^2A_1)$ and the π-π^* system $A^2B_2 \leftarrow X^2A_1$ transition (88, 89). The dissociation to produce the ground state O atoms occur below 397.8 nm (90) (=3.12 eV)

$$NO_2 + h\nu \longrightarrow NO(X^2\Pi) + O(^3P) \qquad (37)$$

The production of $O(^1D)$ occurs below 243.9 nm (=5.08 eV)

$$NO_2 + h\nu \longrightarrow NO(X^2\Pi) + O(^1D) \qquad (38)$$

The photodissociation of NO_2 at 337 nm (N_2 laser) has been studied by Zacharias et al. (91) with a tunable probe laser near 235 nm to detect NO by LIF using its $A^2\Sigma^+ \leftarrow X^2\Pi$ transition. Almost 70% of the excess energy appears as rotational and vibrational energy of NO and 30% goes into kinetic energy of fragments. Of the 70% of the excess energy that appears as internal energy, 50% is in NO vibration and 20% is in NO rotation. The vibrational population is inverted with fractional populations of 0.2, 0.3, and 0.5 for $v'' = 0,1$, and 2, respectively. The rotational distribution also deviated from a Boltzmann distribution with two different slopes corresponding to 65 and 1600°K. These results suggest that the excited state involved has an equilibrium bond angle and bond length substantially different from those of the ground state. The two likely states involved, the A^2B_2 and A'^2B_1, have bond angles of 111 and 180°, respectively, substantially different from 134° of the ground state. The equilibrium bond length in the ground state is 1.193 Å while those in the A^2B_2 and A'^2B_1 state are 1.31 and 1.23 Å, respectively. Recently, Slanger et al. (92) have studied photodissociation at 248.5 nm near the origin of the $B^2B_2 \leftarrow X^2A_1$ transition at 249.2 nm (88). The 248.5 nm photolysis of NO_2 produces NO with an inverted vibrational population peaking at $v'' = 7$ where the NO vibrational excitation was probed by a tunable dye laser. The results are similar to those by Zacharias et al. (91), two rotational temperatures, 130 and 750 K, were obtained. The B^2B_2 state at 249.2 nm has an equilibrium

bond angle of 120.8° and bond length of 1.31 Å, substantially different from the corresponding ground state values. Hence rotational and vibrational excitation results when photodissociation occurs. Bigio et al. (93) have examined the photolysis of NO_2 in the 220-227 nm region and compared the results with the isoenergetic two-photon process near 450 nm excitation (94). They found a drastic difference between the one- and two-photon dissociation processes; the former produced an inverted vibrational population with a maximum at $v'' = 2$, while the latter formed NO mainly in $v'' = 0$ and 1. The NO was probed by the two-photon resonance-enhanced ionization process. In this wavelength region (220-227 nm), process 38 is almost exclusively operative since only vibrational levels in the NO up to $v'' = 2$ were observed. The threshold for process 38 was also observed in this study. The dramatic difference in the vibrational energy distribution is attributed to the presence of real intermediate states which are reached by the absorption of the first photon in the two-photon process. Because of the strong perturbation of these intermediate states with the ground state, the intramolecular relaxation or energy redistribution occurs before the absorption of the second photon.

The absorption and fluorescence cross sections of NO_2 have been measured by Lee and Chiang (95) in the 106-162 nm region.

C. Nitrous Oxide

Absorption of N_2O starts below about 210 nm (2). The absorption spectrum in the 172-197 nm region has recently been studied by Selwyn and Johnston (96). The spectrum consists of a weak continuum superimposed on diffuse bands of v_2' bending mode which increased in intensity with temperature. The transitions observed are probably $^1\Sigma^- \leftarrow X^1\Sigma^+$ and $^1\Delta \leftarrow X^1\Sigma^+$. Photodissociation in the 185-210 nm region is a spin-allowed process

$$N_2O + h\nu \longrightarrow N_2 + O(^1D), \qquad <341 \text{ nm} \qquad (39)$$

Subsequent reactions of $O(^1D)$ are

$$O(^1D) + N_2O \longrightarrow 2NO, \qquad k_{40} \qquad (40)$$

$$O(^1D) + N_2O \longrightarrow N_2 + O_2, \qquad k_{41} \qquad (41)$$

Reactions 40 and 41 are almost equally important. Reaction 40 is a major source of NO in the stratosphere. The branching ratio, $k_{40}/(k_{40}+k_{41})$, has recently been reported in several

papers (97,100), both at 23 and -96°C. The ratio is 0.62 and is independent of the partial He pressure (97,98). The NO product formed in reaction 40 was probed by one-photon enhanced ionization spectroscopy of the NO γ bands $A^2\Sigma^+ \leftarrow X^2\Pi$ by Goldstein et al. (101). The vibration of NO is broadly excited up to $v'' = 11$ and no single level appears to dominate.

The photolysis of N_2O with focussed 193 nm laser light produced NO in the highly excited D and E states (102). The excited NO is apparently formed by three sequential steps involving processes 39 and 40 and photoexcitation of NO produced by (40).

D. Methyl Nitrite

The photolysis of CH_3ONO in the ultraviolet leads to (103, 104)

$$CH_3ONO + h\nu \longrightarrow CH_3O + NO, \quad <689 \text{ nm} \qquad (42)$$

with $D_o(CH_3O\text{-}NO) = 41.5$ kcal/mol (105). In the vacuum ultraviolet, two processes are found (106,107)

$$CH_3ONO + h\nu \longrightarrow CH_3O + NO(A^2\Sigma), \quad <170 \text{ nm} \qquad (43)$$

$$CH_3ONO + h\nu \longrightarrow CH_3O(A^2A_1) + NO, \quad <217 \text{ nm} \qquad (44)$$

The internal and translational energy distributions of product NO at 355 nm photolysis of CH_3ONO have been studied by Lahmani et al. (107). The internal distribution of NO was probed by a two-photon LIF method. The translational energy was deduced from the Doppler profile of the linewidth of individual rotational transitions. The vibrational population has ratios 0.25:0.5:0.2:0.05, for $v'' = 0,1,2,3$ and deviates from a Boltzmann distribution. The rotational distribution deviates also from the Boltzmann and has a peak at about $J'' = 35.5$. The total translational energy of the photofragments observed is 5100 cm^{-1}, which is 36% of the available energy (14320 cm^{-1}). The vibrational energy of NO observed is 1900 cm^{-1} and the rotational energy is 1775 cm^{-1}. The distributions deviate strongly from those calculated on the basis of a direct impulsive model. That is, the observed translational and rotational energies are much less than the calculated energies, while the observed vibrational energy is more than the calculated energy. To explain the discrepancy, the geometry of the excited state must also be considered. Radhakrishnan and Estler (108) photolyzed CH_3ONO at

382 nm and detected the product NO by multiphoton ionization. The NO rotational excitation is very large and direct dissociation was suggested. Ebata et al. (109) have found the A→X fluorescence of CH_3O (process 44) at the 193 nm photolysis. The CH_3O A state is highly rotational and vibrationally excited. Below an excitation wavelength of 161 nm, the production of $NO(A^2\Sigma)$ was observed (107,108).

E. t-Butyl Nitrite

The photolysis of $(CH_3)_3CONO$ has been studied by Schwartz-Lavi et al. (110) at 266, 355, 454, 474, and 494 nm. The rotational and vibrational distribution of the product NO was probed by two-photon LIF. At shorter wavelengths the vibrational population of NO shifts from $v'' = 0$ to higher levels. At 355 and 266 nm $v'' = 0$ was not immediately observed since it is produced from $v'' > 0$ by quenching. At 266 nm NO is highly rotationally excited (J'' up to 40).

F. Dimethylnitrosamine

The photolysis of $(CH_3)_2NNO$ at 363.5 nm has been performed by Dubs and Huber (111). The product NO was detected by two-photon LIF and the translational energy was derived from the Doppler profile of the individual rotational transitions. A large fraction (70%) of the available energy is converted into translational energy of NO. The rotational distribution has a peak at $J'' = 22.5$ and strongly deviates from the statistical distribution. The vibrational population is 0.65:0.29:0.06 for $v'' = 0,1$, and 2. These results suggest the direct dissociation on a repulsive S_1 surface with a large change in -NNO bond angle in excitation. Geiger et al. (112) found the infrared emission $v'' = 1 \rightarrow v'' = 0$ in 350 nm photolysis. The quantum yield of dissociation was unity.

G. Trifluoronitrosomethane

Spectroscopy and photochemistry of CF_3NO in the visible region have been extensively studied by Roellig and Houston (113,114), Bower et al. (115), Jones et al. (116), and Spears and Hoffland (117). Trifluoronitrosomethane has a weak structured absorption spectrum in the visible near 700 nm. Absorption of light in this region induced fluorescence as well as dissociation, which is similar to the H_2CO photochemistry in the ultraviolet described earlier.

$D_o(F_3C\text{-}NO) = 42$ kcal/mol

The primary process in the visible region is

$$CF_3NO + h\nu \longrightarrow CF_3 + NO, \qquad <722 \text{ nm} \qquad (45)$$

Bower et al. (115) have studied the photolysis of CF_3NO in the visible region in a supersonic jet expansion. The internal energy distribution of NO was probed by one- or two-photon LIF. Various vibronic levels of CF_3NO were excited and the appearance time of NO was measured. It was found that: (1) the appearance time of NO decreased nearly monotonically with increasing energy above the S_1 origin (716 nm) and is equal to the fluorescence lifetime of the excited CF_3NO; (2) the NO rotational distribution is nearly statistical up to 600 cm^{-1} above the S_1 origin with a maximum at $J'' = 7.5$. As the photon energy increased, the vibrational population of $NO(v'' = 1)$ increased much more than that expected on statistical theory. Apparently, the excess energy in the NO stretch is not totally redistributed before the occurrence of dissociation. The most likely dissociation mechanism suggested by Bower et al. (115) is the internal conversion from S_1 to S_o^* (vibrationally excited S_o) followed by rapid dissociation. The ν_{12} (torsional mode) is the promoting mode for internal conversion. Another primary step,

$$CF_3NO + h\nu \longrightarrow CF_3 + NO(A^2\Sigma^+), \qquad <172 \text{ nm} \qquad (46)$$

was found by Lahmani and Lardeux (107) by 140 nm excitation.

H. Nitromethane

The photolysis of CH_3NO_2 by 193 nm laser light was studied by product emission spectroscopy and molecular beam photofragment translational energy spectroscopy by Butler et al. (119). Blais (120) also studied the photolysis by the TOF method. The primary process is

$$CH_3NO_2 + h\nu \longrightarrow CH_3 + NO_2, \qquad <476 \text{ nm} \qquad (47)$$

and $D_o(H_3C\text{-}NO_2) = 60.1$ kcal/mol. The total translational energy distribution obtained from the CH_3 fragment has only one peak at about 16 kcal/mol. The major process is

$$CH_3NO_2 + h\nu \longrightarrow CH_3 + NO_2(^2B_2) \qquad (48)$$

where NO_2 is formed in the electronically excited state $^2B_2$ which fluoresces in the 400 to 900 nm region with a lifetime of 35 μs. The available energy for process (48) is about 60 kcal/mol since the electronic energy of $NO_2(^2B_2)$ is 27.9 kcal/mol. Hence about 45 kcal/mol or 73% of the available energy is left for excitation of rotation and vibration of the CH_3 and NO_2 fragments. Another minor process corresponding to the second (smaller translational energy) peak from CH_3 is

$$CH_3NO_2 + h\nu \longrightarrow CH_3 + NO_2^{\dagger} \quad (49)$$

$$NO_2^{\dagger} \longrightarrow NO + O \quad (50)$$

where $NO_2^{\dagger}$ signifies vibrationally and rotationally excited NO_2. $NO_2^{\dagger}$ contains more than 72 kcal/mol internal energy and it immediately dissociates into NO and O.

I. Nitric Acid

The photolysis of $HONO_2$ in the near ultraviolet leads to the formation of OH and NO_2 (2).

$$OHNO_2 + h\nu \longrightarrow OH + NO_2, \quad <599 \text{ nm} \quad (51)$$

The internal state distribution of the product $OH(X^2\Pi)$ was probed by Jacobs et al. (38) using laser induced fluorescence. The rotational distribution has a peak at K" = 6 and approaches zero at about K" = 18. The only 3% of the available energy goes into rotation. The distribution deviates from that of the Boltzmann at lower K's. The vibrational population of v" = 1 is less than 0.05. The $^2\Pi_{1/2}$ and $^2\Pi_{3/2}$ were equally populated. The lower energy components (π^+) of the λ doublet states are more populated at higher rotational energies, that is, $\pi^+/\pi^- = 2.6 \pm 0.5$. This population ratio of the λ doublet states is inverted from those of the $OH(X^2\Pi)$ states (more π^- than π^+) produced by H_2O photolysis (see process 2). Suto and Lee (121) and Okabe (122) have observed $OH(A^2\Sigma^+)$ emission produced by the photolysis of $HONO_2$ in the vacuum ultraviolet. The rotational and vibrational distribution of the OH emission (A-X) have been measured (123). The rotational distribution has a maximum at K' = 9 by 123.6 nm photolysis.

$$HONO_2 + h\nu \longrightarrow OH(A^2\Sigma^+) + NO_2, \quad <204 \text{ nm} \quad (52)$$

The observed threshold for process (52) is at 154 nm (2). The production of the electronically excited NO_2 (NO_2^*)

$$HONO_2 + h\nu \longrightarrow OH + NO_2^*(^2B_2 \text{ or } ^2B_1) \qquad (53)$$

has been detected (121,123) below an excitation wavelength of 220 nm.

VI. NITROGEN-HYDROGEN COMPOUNDS

Even though ammonia, hydrazine, and hydrazoic acid have nitrogen-hydrogen bonds, their photochemistry is very different. In hydrazoic acid the photochemistry is dominated by the weak HN-N bond while in ammonia and hydrazine the fragmentation of the N-H bond appears to be the most important process.

A. Ammonia

Ammonia has well-structured absorption bands that extend from 220 nm to deep within the VUV region below 110 nm (124). The width of the bands suggests that each of the excited states is strongly predissociated. Most of the recent work has been aimed at determining the branching ratio for the various possible primary processes. These primary processes are listed in Table 1 with their threshold wavelengths (124).

In the first absorption band of ammonia, where the A^1A_2'' excited state is produced, it is generally agreed that the principal fragments are NH_2 and H. Most of the NH_2 radicals are formed in the ground electronic state, but 2-3% (124) of them are produced in the excited electronic state via reaction (2) in Table 1. The same authors measured the fluorescence yields from the B and C state of NH_3, and found that these yields ranged from 3 to 7%. Their results further indicate that both of these states are predissociated by the same repulsive state. This is in agreement with the conclusions from a wavelength-resolved multiphoton ionization study (125). In that study, the authors matched the observed 3+1 multiphoton ionization spectrum with a computed one, and ascribed any observable differences to predissociation. In this manner, they were able to show that the C'^1A_1' and B^1E'' were predissociated by nonadiabatic coupling to high vibrational levels of the A^1A_2'' state. They also suggested that the D, D', and E states also predissociate via the same mechanism. This predissociation is thought to involve the inversion mode of the excited state, so that it is to be expected

TABLE 1. Ammonia Product Threshold Wavelengths[a]

	Process	Threshold wavelength (nm)
1	$NH_3 + h\nu \longrightarrow NH_2(X^2B_1) + H(^2S)$	283.1
2	$NH_3 + h\nu \longrightarrow NH_2(A^2A_1) + H(^2S)$	219.4
3	$NH_3 + h\nu \longrightarrow NH(X^3\Sigma^-) + H_2$	297.3
4	$NH_3 + h\nu \longrightarrow NH(A^3\Pi_i) + H_2$	157.8
5	$NH_3 + h\nu \longrightarrow NH(X^3\Sigma^-) + 2H(^2S)$	143.3
6	$NH_3 + h\nu \longrightarrow NH(a^1\Delta) + H_2$	226.2
7	$NH_3 + h\nu \longrightarrow NH(a^1\Delta) + 2H(^2S)$	124.5
8	$NH_3 + h\nu \longrightarrow NH(b^1\Sigma) + H_2$	182.6
9	$NH_3 + h\nu \longrightarrow NH(b^1\Sigma) + 2H(^2S)$	109.9
10	$NH_3 + h\nu \longrightarrow NH(c^1\Pi) + H_2$	129.0

[a]From reference (124).

that the NH_2 radical should be produced rotationally excited. There is some evidence that this is the case, because LIF studies do not detect the NH_2 radical until after the radical has undergone several collisions.

Suto and Lee have also shown that the thresholds for reactions 8 and 10 in Table occur at 182.3 and 127.9 nm, respectively. The quantum yields that they measure in this region suggest that even though these excited fragments are produced, they are minor photolysis channels. Slanger and Black (126) have shown that the channels that produce NH + $2H(^2S)$ represent 90% of the quantum yield at 121.6 nm. Since the fluorescence quantum yield is only a minor fraction of this yield, it is likely that the NH radicals are produced in the lowest singlet and ground triplet state via reactions 5 and 7. Because the threshold for reaction 7 is so close to 121.6 nm, it is to be expected that this should be less important than reaction 5 in Table 1. Little

is known about the quantum state distribution of this fragment, but if the predissociation mechanism involves the inversion vibrational mode of NH_3, then it should be rotationally excited.

B. Hydrazine

There have been two recent reports on the photolysis of this compound at 193 nm (127,128). Hawkins and Houston studied the photolysis by probing for the NH_2 radical using the LIF technique. They were able to show that the primary photolysis product was N_2H_3 and H atoms rather than two NH_2 radicals. Their time-dependence studies showed that there was an inducation period for the formation of the NH_2 and that this inducation period depended upon the initial concentration of N_2H_4. Adding inert gases such as He and N_2, instead of accelerating the appearance of the NH_2 radical, slowed down the appearance of this radical indicating that NH_2 is not formed in vibrationally excited state. The NH_2 radical is produced by the reaction of H atoms with N_2H_3 to product NH_2. Haak and Stuhl suggested that it was difficult to see how a N_2H_3 with 12,100 cm^{-1} of energy formed in the primary process could survive in a photolysis system as long as 10 s at a pressure of 0.1 torr. It would seem that this is possible if the energetic N_2H_3 radical is rapidly quenched by N_2H_4 rather than reacting with it. Under these circumstances the radical would exhibit a long lifetime because its only mode of decay would be by diffusion or radical disproportionation, which is slow at low radical concentrations.

C. Hydrazoic Acid

A pulsed beam study of NH_3 photolysis at 248 nm was recently reported (129). They used the LIF technique to probe for the $NH(^1\Delta, v'' = 0$ and 1) states as well as the $NH(^3\Sigma)$ state. They found that the $NH(^1\Delta, v' = 1)/NH(^1\Delta, v' = 0) \leq 5.1\%$, while the $NH(^3\Sigma^-)/NH(^1\Delta)$ was $\leq 1.0\%$. Thus, most of the radicals are produced in the $NH(^1\Delta, v' = 0)$ state. The rotational distribution of this fragment is non-Boltzmann and peaks at $J'' = 1$, while in a static gas cell at 300 K, the rotational distribution is completely different and peaks at $J'' = 5$ and can be described with a Boltzmann distribution of 1150 K. It is estimated that NH_3 has a rotational temperature of 3 K in the pulsed molecular beam. The NH distribution at 300 K is very similar to that obtained for this same molecule at 266 nm (130). From this, they conclude that the upper electronic state is steeply repulsive, so that dissociation takes place on a very short time scale. The

observed rotational distribution of the NH radical fragment observed in the pulsed molecular beam must be due to the original angular momentum present in the parent molecule. Most of the available energy must appear as translational energy in the two fragments.

VII. CYANIDE COMPOUNDS

A great deal of work has been done on the photodissociation dynamics of the cyanide compounds. This is undoubtedly due to the well known spectroscopy and the strong oscillator of the $B^2\Sigma \rightarrow X^2\Sigma$ transition in CN. The spectra are confined in a narrow region of wavelength and occurs in a readily accessible wavelength region. Furthermore, most of the molecules that contain this chromophore have absorption bands in the near ultraviolet region which can be excited with strong lasers.

A. Hydrogen Cyanide

Very little has been reported on the photodissociation dyamics of HCN leading to the production of the CN X and A state fragments, despite the fact that this is the simplest triatomic cyanide compound. This is probably because the absorption above 150 nm is very weak and structured so that a laser in the VUV region is needed. Nevertheless, some results from a recent study on the photodissociation dynamics of HCN at 193 and 157 nm have been presented at the Sixteenth Informal Conference on Photochemistry (131).

HCN has a weak absorption band in the 160 to 200 nm region which is partially forbidden in the linear configuration since the upper state is a $^1\Delta$ or $^1\Sigma^-$. This band has been analyzed by Herzberg and Innes (132) who have determined that the excited state is bent with a bond angle of 125°. When Eng et al. (131) photolyzed HCN at 193 nm and probed the X state radicals, they found the radicals to be both vibrationally and rotationally excited. The X state radicals are observed with vibrational excitation up to $v'' = 4$, which corresponds to an energy of about 8300 cm^{-1}, while rotational temperatures for this fragment were found to vary from 800 K for $v'' = 0$ to about 400 K for $v'' = 4$. No attempt was made to look directly for the A state fragments.

When the photolysis was done at 157 nm, a much larger signal could be obtained, so that the experimental conditions could be adjusted over a wider range. They again noted that a large amount of vibrational and rotational energy was present in

the $CN(X^2\Sigma^+)$ fragment. The results of collisional quenching studies suggest that the $CN(A^2\Pi)$ is also produced. This is the expected result, since it is known that the upper state that is excited correlates with this fragment (5). It will be very interesting to see the final outcome of this study.

B. Cyanogen Iodide

This was the first molecule studied that used both a laser to excite it to a dissociating state and another tunable laser to determine the quantum state distribution of the photochemical fragment (133). The photodissociation dynamics of ICN has been studied more than that of any other molecule, because its first absorption band is in a readily accessible region, the quantum states of both fragments can be measured, and a large amount of theoretical work has been done on this molecule since it contains only three atoms.

Previous workers had used the molecular beam TOF technique (134) and the VUV flash photolysis LIF technique (135). Ling and Wilson (136) had suggested that either the $A(^2\Pi)$ state of CN is produced in the original photolysis process or that I atoms were produced in the $^2P_{1/2}$ and $^2P_{3/2}$ states. It had been previously shown (135), by collisional quenching studies, that the A state of CN was not produced. This earlier work has been reviewed by Baronvaski (137) but recently both he and others have done further work on this molecule using excimer laser sources in both static gases and pulsed molecular beams.

Wittig and his co-workers (138) have studied the photolysis at 266, 320, and 355 nm in a static gas cell as well as in a pulsed molecular beam. At each of these wavelengths they report only on the $CN(X^2\Sigma^+, v'' = 0)$ radical product.

The rotational distribution that Nadler et al. (138) measured at 266 nm clearly has three components, with low, mid, and high rotational quantum numbers N", which agrees with the recent results of Baronavski (139). The pulsed beam studies at this wavelength indicate that the low N" quantum numbers are enhanced relative to the high N", suggesting that these low N" come from ICN molecules that are rotationally and/or vibrationally cold. It is further suggested that these low N" are produced along with $I(^2P_{1/2})$ and $I(^2P_{3/2})$ atoms. This interpretation differs from the one given by Baronavski. More recent work by Wittig's group (140), in which the Doppler profile of individual rotational lines is measured, suggest that the $I(^2P_{1/2})$ atom is associated with CN radicals with rotational quantum numbers between $N'' = 0$ and $N'' = 40$. The $I(^2P_{3/2})$ is

associated with CN radicals in the N" = 20 state up to the observed rotational limit.

Photolysis of ICN at 320, and 355 nm yields a smooth but non-Boltzmann rotational distribution. The latter observations must come from hot bands, since no CN could be observed in the pulsed beam studies at these wavelengths.

Krieger and his co-workers (141) photolyzed ICN at 266 nm and obtained essentially the same experimental results as Baronavski. They used various theories to try to explain their results and finally decided that the simple Frank-Condon (142) model could not be used to reproduce their observations. They suggested that an interfragment interaction during dissociation must be invoked to account for the high rotational temperature peak. The deviation of the lower temperature peak from theory was explained by invoking dynamic axis switching during the collinear dissociation, which is different than the interfragment interaction proposed by Baronavski. Photodissociation in the hot bands of ICN using multigas excimer lasers at 351, 337, and 308 nm has also been recently reported (143). There is not enough energy to produce the electronically excited CN radicals or I atoms at any of these wavelengths.

The quantum state distribution of the CN fragment was measured with a tunable dye laser. A "quasi-Boltzmann" behavior for the rotational distribution of the fragments is observed at all three wavelengths, in agreement with the earlier work. The deviation from a Boltzmann distribution is larger as the photon energy increases. In general, the average rotational energy increases with increasing photon energy but the fraction of the available energy that appears in rotation stays almost constant.

At 308 nm a bimodal rotational distribution is observed for the radicals that are produced in the v" = 0, 1, and 2 levels.

When the quasi-diatomic Franck-Condon model was compared with the experimental results it was found that it could predict the observed vibrational distribution as well as the observation that the translational energy is much greater than the rotational energy. The theory could not, however, predict the observed proportionality between the average rotational energy and the available energy. A simple classical description of the impulsive dissociation of a rotating molecule does predict this observed linear proportionality.

In a recent report the same authors have extended their original work to other wavelengths (144). ICN was photolyzed in the A continuum using an excimer laser at 222 nm (KrCl), 249 nm (KrF), and 308 nm (XeCl). The fractional amount of energy that appears in rotation for the v" = 0 is 0.16, 0.15 and 0.18,

respectively. This fraction increases with increasing vibrational energy. Excited vibrational levels are observed at each of these wavelengths. The maximum excited vibrational level that is observed increases from v" = 3 at 308 nm to v" = 6 at 222 nm. The observed vibrational populations decrease monotonically with increasing vibrational energy. Note, however, that the amount of vibrational excitation is much less than that predicted by the theory of Pattengill (145). Franck-Condon arguments predict that the vibrational energy should decrease sharply at 308 nm but not necessarily at the shorter wavelengths. It does predict that the amount of vibrational energy at the shorter wavelengths should be comparable to that observed at longer wavelengths.

Since the fraction of available energy that appears in rotation remains nearly constant with increasing energy, the vibrational excitation that observed comes at the expense of the translational recoil energy. The highest observed internal energy is always less than the amount of available energy, so that some minimum amount of energy must appear in translation.

The observed rotational distributions are in agreement with the ideas of Baronavski on the ICN photolysis but disagree with the theoretical calculations. These rotational distributions are not, however, simply Boltzmann distributions.

The results of all of these studies are summarized in Table 2. They show that, in the work with excimer lasers, a higher fraction of the radicals are detected in the higher vibrational levels. This higher observed fraction in the upper vibrational levels probably does not occur because of any discrepancy between the different studies but is the result of the difficulty of detecting small amounts of vibrationally excited radicals in the presences of large amounts of v" = 0 radicals that have a substantial amount of rotational excitation. Fisher et al. had to make a special effort to determine the vibrationally excited radicals in the presence of rotationally excited CN(v" = 0).

Photodissociation dynamics studies in a nozzle-cooled beam have been reported along with an elegant analysis of the data (146). Only CN radicals in the v" = 0 level are reported because of the difficulty of detecting small amounts of excited radicals in the upper vibrational level. The results that were obtained by fitting the observed rotational distributions with Boltzmann rotational distribution functions are summarized in Table 3.

At each of the wavelengths, the observed rotational distributions were determined by successively stripping the higher rotational distribution out of the total distribution. It is clear from the results in this table that complex rotational distributions are observed at all wavelengths.

TABLE 2. Energy Partitioning in the Photolysis of ICN

λ(nm)	E_{avail} (cm^{-1})	v''	$f_{v''}$	Average energy (cm^{-1})	
				E_{rot}	E_{tr}
220[a]	19350	0	0.76	3020	16330
	17290	1	0.14	4213	13077
	15260	2	0.02	nr[b]	
	13260	3	0.02	nr	
		4+5	0.03	nr	
		6	<0.01	nr	
249[a]	14460	0	0.92	2197	12263
	12410	1	0.05	2949	9461
	10380	2	0.02	3376	7004
	8375	3	0.004	nr	
		4+5	0.002		
266[c]	11896	0	0.99	1500	10396
299.4[c]	7703	0	0.91	1160	6543
	5643	1	0.06	1367	4276
	3616	2	0.02	1293	2323
308[d]	6770	0	0.88	1252	5518
	4710	1	0.10	1400	3310
	2650	2	0.02	900	1750
337[d]	3977	0	>0.97	610	3367
351	2793	0	>0.94	420	2373

[a]From reference (144).

[b]Not reported.

[c]From reference (139).

[d]From reference (143).

In the analysis of the data the authors applied a model that consisted of a Franck-Condon transition to three different surfaces. Once the molecule was on one of these surfaces it was allowed to undergo a classical trajectory to a final product. The upper potential surface was chosen to be of the type given below,

TABLE 3. Fitting Parameter Obtained by Fitting the Observed Rotational Distributions with a Boltzmann Function[a]

λ_p (nm)	$\langle E_{avail} \rangle$ (cm^{-1})	T_i (K)	f_i x 100	$\langle E_{rot} \rangle$ (cm^{-1})	$\langle E_{trans} \rangle$ (cm^{-1})	b x 100 (Å)
235	8700	113 ± 6	2.3 ± 6	78 ± 4	8622 ± 4	6.1 ± .2
	16303	20.0 ± 3 x 10^3	98 ± 18	6600 ± 200	9600 ± 200	53 ± 1
248	6470	59 ± 3	11 ± 3	40 ± 2	6430 ± 2	5.1 ± .1
	6470	550 ± 20	24 ± 5	380 ± 17	6090 ± 17	16 ± .4
	14073	4600 ± 170	65 ± 10	3040 ± 90	11030 ± 90	33.7 ± .6
266	3741	57 ± 4	21 ± 9	39 ± 3	3702 ± 3	6.6 ± .3
	3741	380 ± 18	31 ± 9	263 ± 12	3478 ± 12	17.6 ± .5
	11344	5600 ± 300	48 ± 11	3300 ± 100	8100 ± 100	41 ± .1
280	1861	74 ± 4	38 ± 14	51 ± 3	1811 ± 3	10.7 ± .3
	9464	4000 ± 200	62 ± 13	2470 ± 80	7000 ± 80	38.1 ± .1
290	630	140 ± 15	16 ± 7	96 ± 10	530 ± 10	27 ± 2
	8233	2700 ± 180	84 ± 25	1800 ± 100	6500 ± 100	34 ± 1

[a]Adapted from reference (146). λ_p = photolysis wavelength; $\langle E_{avail} \rangle = h\nu - D_0 - E_e$, where D_0 is the dissociation energy and E_e is the electronic energy of the iodine atom; b = impact parameter.

$$V(R,Z) = D_0 + EI + A \exp(-\alpha^* R)[1-kZ_o^2 + k(Z-Z_o)^2] \quad (54)$$

Each of the three potential surfaces was then adjusted by changing A, α, k, and Z_o until a reasonable fit was produced between the observed rotational distributions and the calculated distributions. Each surface results in a unique set of values that gives the best fit in all of the observed data. The comparison between theory and experiment is given in Table 4.

TABLE 4. <Theoretical E_{rot}> and <Experimental E_{rot}> for the Photolysis of ICN[a]

λ_p (nm)	Channel	Surfaces	<E_{rot}>(cm^{-1}) Theoretical	Experimental
235	I	3	6273	6639
	I*	2	84	78
248	I	3	5434	3039
	I*	2	83	276
266	I	1 and 3[b]	3371	3274
	I*	2	73	172[c]
280	I	1	2022	2466
	I*	2	67	51
290	I	1	1757	1788
	I*	2	[d]	96

[a]Adapted from reference (146).

[b]The results are weighted by the relative absorption to each surface.

[c]This is the average of two distributions. See Table 2.

[d]Little absorption at this wavelength for this surface.

It is clear that the theory does not completely match the experiment. The authors noted this and suggested that the observed discrepancies might be due to diabatic interactions between the departing fragments. It was further suggested that the molecules might be excited to only one excited state, and that the complexity that is observed at the different wavelengths might all be due to diabatic interactions between the departing

fragments. Despite the good agreement they get with experiment using the derived potentials, these potentials must be inadequate since they cannot predict any of the observed vibrational excitation in the fragments. Clearly, as the authors indicate, this can not be the complete story.

Waite et al., (147) have also tried to use the observed rotational distribution to derive a potential energy surface for the excited states of ICN. They have been able to obtain not only the average rotational energy at 266 nm but have also been able to reproduce the shape of the rotational distribution. It will be interesting to see if the same curves can do as well at other wavelengths.

Recently Shokoohi et al. (14) obtained high resolution LIF spectra from the photolysis of ICN at 266 nm. Using these spectra, they were able to show that the population of the F_1 and F_2 spin components associated with each rotational level varied with both rotational and vibrational quantum number. For CN radicals with $v'' = 0$ and $N'' < 43$ the population of F_1 level < F_2 level, for $N'' = 43$ the population of F_1 level $\sim$ F_2 level, and for $N'' > 43$ the population of F_1 level > F_2 level. In the $v'' = 1$ level more of the CN radicals are produced in the upper N'' levels than in the lower levels and for these upper levels the population of F_1 level > F_2 level. In the $v'' = 2$ level, no radicals are observed below $N'' = 17$, and the population of F_1 level > F_2 level. These results can be qualitatively understood in the following manner. The iodine atom can be produced in the $^2P_{1/2}$ and the $^2P_{3/2}$ spin-orbit states. Spin-orbit interaction between the recoiling iodine atom and the CN fragment can result in alignment of the spin of the CN radical relative to the molecular frame of the dissociating fragment. This in turn, as a result of electron correlation, will lead to orientation of the unpaired spin relative to the CN nuclear motions. It is known (136,148, 149) that there are both parallel and perpendicular components to the transition moment at 266 nm and that both spin components of the I atoms are produced in the dissociation process. Thus, it is likely that certain rotational levels and spin components of the CN radicals are associated with one or the other spin components of the I atoms. Further quantitative statements require more detailed theoretical work.

Quite a bit of the work done earlier on the ICN photolysis at shorter wavelengths has been thoroughly reviewed (3). Recently Long and Reilly (150) have investigated the photodissociation dynamics of ICN at 157.8 nm using a F_2 laser to dissociate the molecule. The quantum state distribution of the CN radicals produced in the B state was measured by dispersing the direct fluorescence from this state using a 3/4 nm monochromator in the second order. Their results indicate that the B state is

formed vibrationally and rotationally hot. Further collisional quenching studies and fluorescent spectra of the B state at longer delay times indicate that the A state of the CN radical is also produced in the primary process. The results from the quantum state distribution measurements of the B state are shown in Table 5. No quantum state distribution of the A state of CN was determined.

TABLE 5. Quantum State Distributions of $CN(B^2\Sigma^+)$ Formed in the Photolysis of ICN at 157.8 nm

E_{avail} (cm^{-1})	v''	$F_{v''}$	T_{rot} (K)	$\langle E_{vib}\rangle E_a$	$\langle E_{rot}\rangle / E_a$
12,480	0	0.64 + 0.05	14,000 + 4000	.076	.60
	1	0.27 + 0.04	6,000 + 2000		
	2	0.05 + 0.02	3,000 + 1000		
	3	0.03 + 0.02	1,800 + 800		

[a]Adapted from reference (150).

Most of the available energy appears as rotation in the B state fragment, indicating that the upper state is bent. The vibrational excitation that is observed in this study is considerably higher than the distribution observed by Ashfold and Simons (151) at 156 nm, even though there is more energy available at this wavelength. This in turn implies that within the vibrational band of the Rydberg level there can be large changes in the vibrational disposal in the products. Could it be a reflection of the interfragment interaction as the CN fragment departs from the I atom during dissociation? At the shorter wavelength the initial recoil velocity is larger, so that there is less time for this interaction.

They also point out that the rotational distributions that are observed are smooth, with no indication that there is an abrupt change at any of the thresholds that would be appropriate for $I(^2P_{1/2})$ formation. The collisional quenching studies suggest that the $A(^2\Pi)$ must be produced vibrationally excited up to v'' = 10. It would be interesting to probe how the dynamics of this state varies as the available energy is varied.

C. Cyanogen Bromide

In recent years, several workers have studied the photodissociation dynamics of this molecule in its various absorption bands. Two principal techniques are used, namely emission spectroscopy at wavelengths below the threshold for the production of $CN(B^2\Sigma^+)$ and the LIF technique for $X^2\Sigma^+$ and $A^2\Pi$ state CN radicals at wavelengths above this threshold. The former work has been adequately reviewed (3).

Several groups (138,144,152-154) have reported on LIF studies of CN following the photolysis of BrCN in the A continuum at 193 nm and longer wavelengths. These studies have been done in a pulsed molecular beam as well as in a static gas cell. A summary of the results of these studies is given in Table 6.

The static gas cell work of Halpern and Jackson (153) showed that the upper electronic state of BrCN is bent, in accord with the predictions made from their spectroscopic observations of Rabalais et al. (155). An example of the observed rotational distribution is given in Figure 7. Included in this figure is the rotational distribution obtained at 10^{-4} torr and one that was obtained after a few collisions. This latter distribution is identical to one that had been obtained earlier by Heaven et al. (152) and shows that their distribution was not a nascent distribution, since it could not be obtained in a static gas cell after several collisions. One can conclude from the work at 193 nm that the $CN(X^2\Sigma^+)$ is produced rotationally hot mainly in the $v'' = 0$ and less than 6% of the radicals are formed vibrationally excited.

There is a recent indication that a few CN radicals may be produced in the $(A^2\Pi)$ state (156). An LIF spectra obtained in a static gas cell in the photolysis of BrCN at 193 nm by these authors is given in Figure 8. The spectra were obtained after several collisions with BrCN and show that both $v'' = 0$ and $v'' = 1$ levels are present in the system. This spectrum is comparable to an earlier LIF spectrum of the LeBlanc system of CN (157). The authors estimate that the $A^2\Pi$ state radicals represent only 1% of the radicals produced as a result of laser photolysis. LIF spectra of these radicals obtained at lower pressure indicate that the A state is produced rotationally hot. This is what one would expect if this fragment arises from the same electronic state that produces the X state fragment.

Nadler et al. (138) photolyzed BrCN at 266 and 320 nm. They only observed an LIF spectra at 266 nm. The experiments were done in a static gas cell as well as in a pulsed molecular beam. In the static gas cell experiments, the CN radicals are formed in the $v'' = 0$, 1, and 2 levels. The highest rotational level observed for the $v'' = 0$ and $v'' = 1$ levels of the X state

TABLE 6. Summary of LIF Studies on the Photolysis of BrCN

λ (nm)	E_{avail} (cm^{-1})	v"	$f_{v"}$	$E_{avg\ rot}$ (cm^{-1})	$E_{avg\ tr}$ (cm^{-1})
193[a]	21810	0	0.78	5767	16043
	19750	1	0.15	5329	14421
	17720	2	0.03	nr[b]	nr
	15720	3	0.01	nr	nr
		4+5	0.03	nr	nr
		6	<0.01	nr	nr
193[c]	21810	0	>0.94	6785	14025
222[a]	15040	0	0.77	3806	11234
	12980	1	0.16	4883	8097
	10950	2	0.03	nr	nr
	8950	3	0.02	nr	nr
		4+5	0.03	nr	nr
249[a]	10160	0	0.72	3344	6816
	8098	1	0.24	3514	4584
	6068	2	0.03	2691	3377
	4066	3	0.005	nr	nr
	2091	4	<0.02	nr	nr

[a]Reference (144). The total pressure was 0.1 torr and the time delay was 1.0 μs.

[b]Not reported.

[c]Reference (153). The total pressure was 10^{-5} torr and the time delay was 0.2 μs.

were N" = 57 and 51, respectively. Since at these rotational levels it is energetically impossible to produce $Br(^2P_{1/2})$ atoms when the radicals are formed in these rotational levels, they conclude that the major channel is given by

$$BrCN + h\nu \longrightarrow CN(X) + Br(^2P_{3/2}) \qquad (55)$$

In the pulsed beam studies most of the radicals that are observed are in the v" = 0 level with very low N" quantum numbers. These low v" quantum numbers are also observed in a static gas cell for the v" = 0 level, but not for the v" = 1 and 2 levels. They conclude that the dissociation that is observed

PG 1 Model paper for 50% reduction
to 28x44 picas type page

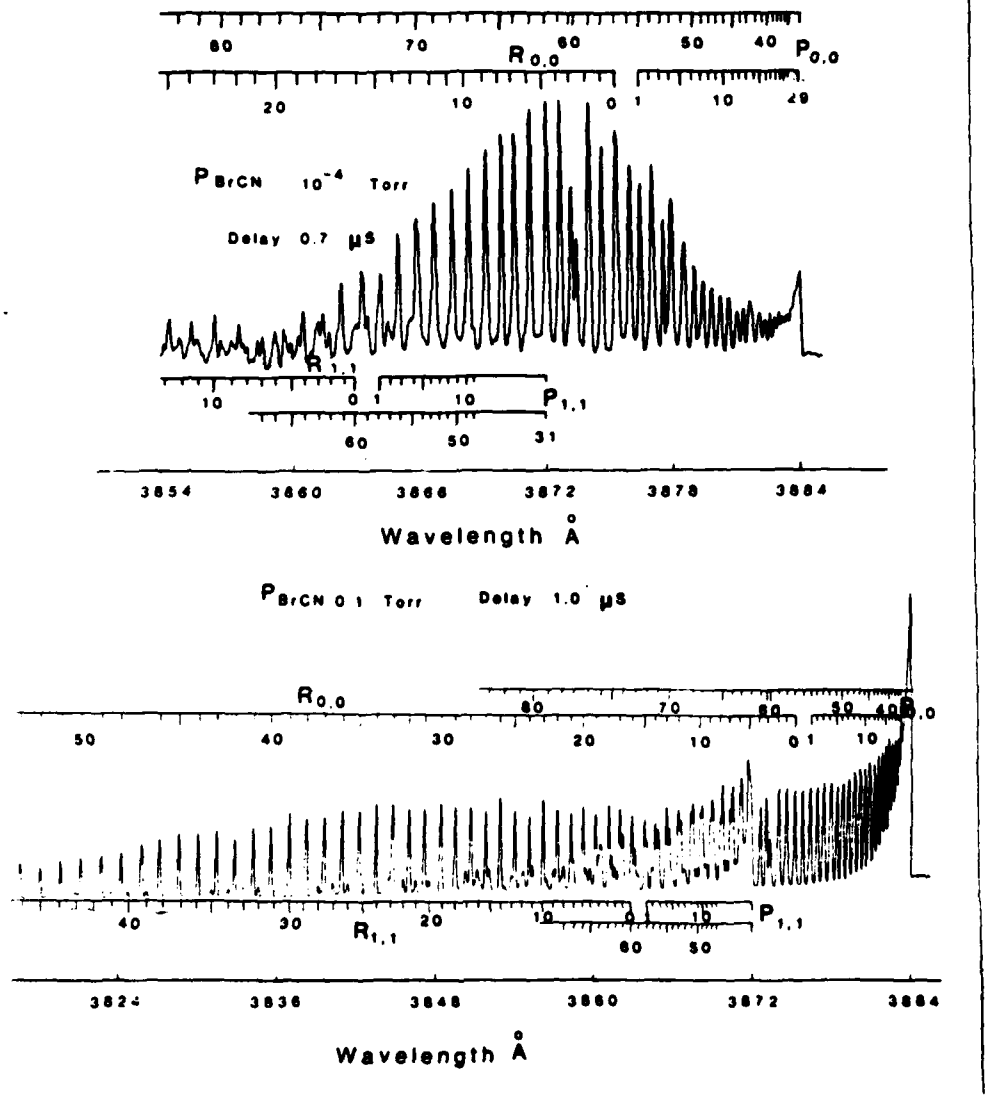

FIGURE 7. Laser induced fluorescence (LIF) spectrum of the CN($X^2\Sigma^+$) fragment produce in the ArF laser photolysis of BrCN. Note that the recoil fragment energy is such that the recoil velocities of nascent CN produced with Br($^2P_{3/2}$) or Br($^2P_{1/2}$) fragments are 3.3 x 10^5 and 2.0 x 10^5 cm/s, respectively. The collision frequency will be up to a factor of six higher than it is at room temperature.

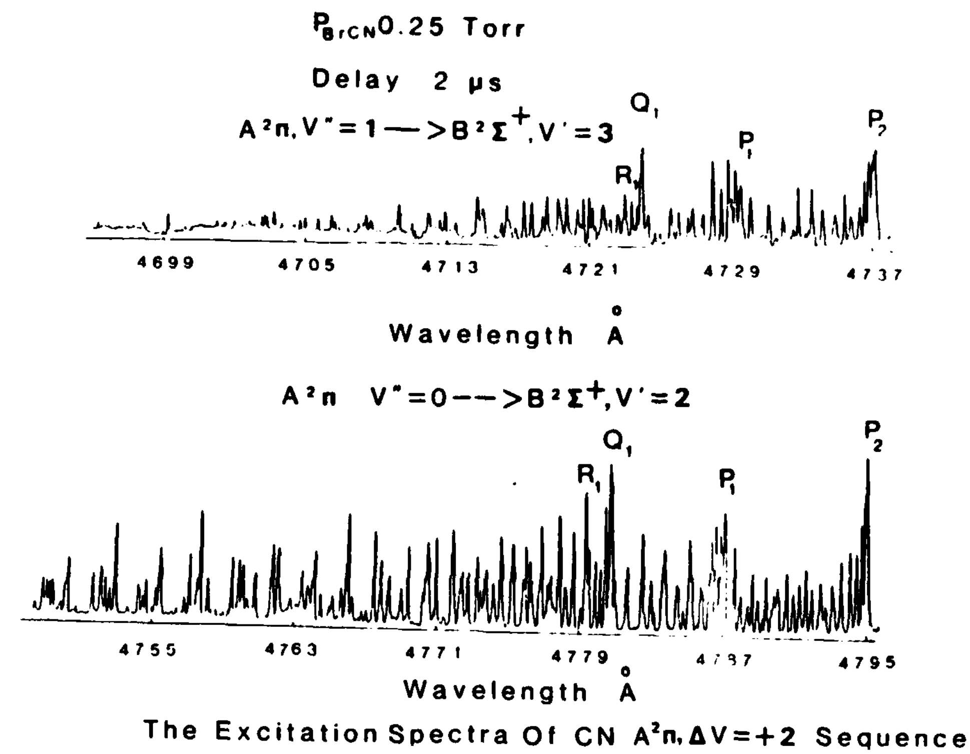

FIGURE 8. An LIF spectrum of the $CN(A^2\Pi)$ fragment produced in the photolysis of BrCN at 193 nm. The upper and lower spectra correspond to the radical in the v" = 1 and v" = 0 levels, respectively.

at 266 nm is from the (000) vibrational level of BrCN and that it occurs via a linear excited state. Dissociation from the (010) vibrational level of BrCN occurs at this wavelength through a bent excited state and results in the formation of rotationally hot radicals.

Recently Fisher et al. (144) reported on the photolysis of BrCN in a static gas cell at 193, 222, and 249 nm. At each of these wavelengths they observed vibrationally excited CN radicals. The fraction of the available energy that appears in rotation decreases from 0.33 to 0.25 to 0.26 at 249, 222, and 193 nm, respectively. Fragments with the highest observed internal energy are always significantly below the amount that is available, which suggests that there is a minimum amount of energy that must go into translation. Note that a significant population is observed in higher vibrational levels at 193 nm. This is in direct contradication to the results of Lu et al. (154) and suggests that collisions may be responsible for these

vibrational levels.

D. Cyanogen Chloride

Other than the earlier work reviewed by Ashfold et al. (3), only three studies on the photodissociation dynamics have been reported for this molecule (153,154,158). The first study reported the quantum state distribution of the CN radical obtained in an effusive molecular beam and in a static gas cell, while the second study reported the observations in a pulsed molecular beam. The dynamics remains the same despite the fact that the initial internal state distribution of the ClCN molecule changes. This of course shows that hot bands are not important in the photodissociation of this molecule at this wavelength.

A summary of the findings of these studies for the internal state distribution of the CN radical is given in Table 7. It is clear from this table that the CN radical is produced with quite a bit of rotational energy. This was interpreted as being due to the excitation of the ClCN molecule from a linear configuration in the ground state to a bent configuration in the excited state. Thus both ClCN and BrCN have bent excited states in the A continuum. The excited states of ICN are apparently more complex probably as a result of spin-orbit interaction splitting the degeneracies in the excited state.

TABLE 7. Quantum State Distribution of the $CN(X^2\Sigma^+)$ Produced in the Photolysis of ClCN[a]

λ (nm)	E_{avail} (cm^{-1})	v''	$f_{v''}$	$E_{avg\ rot}$ (cm^{-1})	$E_{avg\ tr}$ (cm^{-1})
193	16800	0	0.69	7300	9500
	14740	1	0.22	6744	7996
	12680	2	0.09	5489	7191
	10620	3	trace	nr[b]	nr

[a]Reference (153).

[b]Not reported.

In the pulsed molecular beam studies, the results were used to calculate an impact parameter for the photodissociation process. From these impact parameters it was concluded that the recoiling CN fragment did not take the lowest energy path when it was departing from the halogen atom. Rather, because of strong impulsive motion, the trajectory that the CN radical

follows has a higher impact parameter.

Recently Li et al. (156) have observed that a small amount of CN radicals are formed in the $A^2\Pi$ state in the 193 nm photolysis of ClCN. An example of the LIF spectra that they obtained is shown in Figure 9. At the pressure and delay time of this spectrum the radical would have undergone some collisions so that little can be said about the nascent rotational distribution.

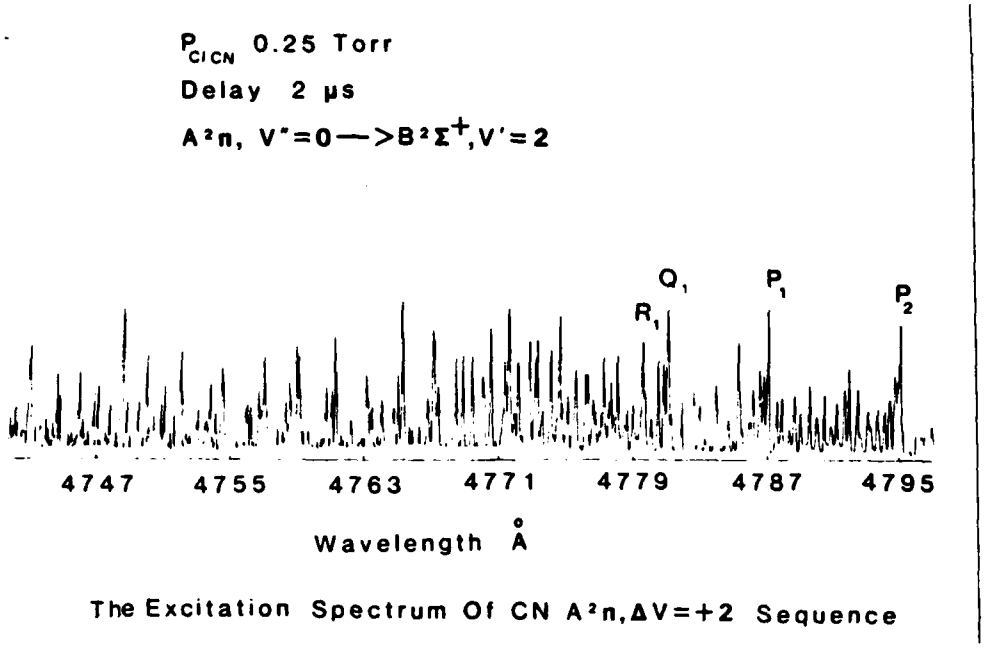

FIGURE 9. An LIF spectrum of the CN($A^2\Pi$, v" = 0) radical produced in the 193 nm laser photolysis of ClCN.

Guest et al. have studied the polarization of the fluorescence that results from the B($^2\Sigma^+$) when ClCN is photolyzed at 157.6 nm with a F_2 laser (158). They find that the absorption dipole is parallel to the ClCN internuclear axis and that the photodissociation process is direct.

E. Cyanogen

Cyanogen was the first molecule where the LIF method was used to determine the quantum state distribution of a photochemical fragment (159,160). In that work a VUV broadband flash

lamp was used to detect the nascent quantum state distribution of the ground state $CN(X^2\Sigma^+)$ fragment that was produced when the $(C^1\Pi_u)$ of C_2N_2 was excited. The structure that is observed in the absorption band of C_2N_2 suggests that the molecule fragments by a predissociation mechanism rather than by a direct dissociation. Collisional quenching studies suggested that CN radicals were also formed in the $A^2\Pi$ state, which agrees with the $C^1\Pi_u$ assignment of the absorption band because such a state would adiabatically correlate with the states of the CN fragments that are observed.

Recent work (161) with a tunable VUV flash lamp has shown that the $CN(A^2\Pi)$ can be detected directly using the LIF technique. Thus one is able, in principle, to determine the vibrational and rotational population of each of the fragments $(CN(X^2\Sigma), (A^2\Pi))$. The tunable UV flash lamp allows one to measure these quantum state distributions as a function of the vibrational frequency of the upper electronic state. The results from these studies thus far are summarized in Table 8.

TABLE 8. Energy Distribution of the $CN(X^2\Sigma^+)$ Fragment Produced in the Photodissociation of C_2N_2

Photolysis Wavelength λ (nm)	E_{avail} (cm^{-1})	v''	$F_{v''}$	T_{rot} (K)	$\langle E_{vib}\rangle/E_{av}$
164 ± 4	5208	0	0.60 ± 0.07	1020 ± 45	0.18
		1	0.28 ± 0.04	825 ± 85	
		2	0.09 ± 0.04	nd[a]	
157 ± 1.4	7926	0	0.54 ± 0.06	1710 ± 65	0.15
		1	0.35 ± 0.05	1170 ± 80	
		2	0.12 ± 0.04	nd	
154 ± 1.4	9167	0	0.42 ± 0.07	1685 ± 40	0.18
		1	0.36 ± 0.07	1110 ± 85	
		2	0.22 ± 0.13	nd	

[a]Not determined.

The results indicate that the fraction of the radicals formed in higher vibrational levels increases as the available energy increases but ratio of the average vibrational energy to the available energy remains constant. The rotational excitation also remains fairly constant and the rotational distribution can be described by a Boltzmann distribution. The latter obser-

vation is consistent with the idea that the excited state predissociates and has ample time to sample phase space.

The CN A state fragment has been detected, but the detailed quantum state distributions are still being obtained so that the full dissociation dynamics scheme has not been completed.

The ratio of the A/X state concentration can also vary with the vibrational excitation in the excited state since, energetically, predissociation may occur through the vibrational continua of the various electronic states of C_2N_2. It might be expected that this predissociation would be a strong function of the excess available energy. This ratio has been determined by measuring the change in the CN X state concentration as a function of time (162). The A/X ratio is then the ratio of final CN concentration divided by the initial CN concentration minus one.

Taherian and Slanger (162) have reported on the direct detection of the A state fragment produced when the C_2N_2 molecule is dissociated with a F_2 laser at 157.3 nm. Their results indicate that the A state fragment is produced at this wavelength with vibrational energy up to what they thought was the thermodynamic limit (i.e., $v' = 5$). Eres et al. (163) have shown however that the D_0 of C_2N_2 is 133 kcal mol rather than 128 kcal/mol; thus the true thermodynamic limit is $v' = 4$ rather than $v' = 5$. This, coupled with the fact that there is some evidence that there are multiphoton effects in their experiments, throws some doubt upon this interpretation. Their results are in direct contradication with the results obtained with the VUV flashlamp and, if both are correct, then it may indicate that the predissociation dynamics are sensitive to the exact point within an absorption band where the molecule is excited. A laser source, of course, excites only at one point in the band, while the flashlamp integrates over many points. In the first case, the molecule is formed on only one point on the upper potential surface, while in the latter case the molecules are formed on a manifold of points on this surface.

Predissociation through the ground state continuum has also been observed in the ArF laser photolysis of C_2N_2 at 193 nm (164). This work was done in an effusive molecular beam source, so that the C_2N_2 molecules had initial vibrational and rotational distributions appropriate for a gas at 300 K. It was found that CN radicals were only formed in the ($X^2\Sigma^+$) state. The CN radicals were observed in both the $v'' = 0$ and the $v'' = 1$ levels of this state, with rotational distributions for both levels that can be described by a Boltzmann distribution with a temperature of 900 K. It was first thought that these results could be explained with a simple model, where the original rotational angular momentum of the parent is equally divided into angular

momentum of the fragments. This would predict that when the molecule is cooled in a pulsed molecular beam, the fragments would have a well-defined and predictable rotational temperature, and that the vibrational populations should remain unchanged. When the experiments were carried out (154), it was found that the rotational temperature did not decrease as much as the model would have predicted and the vibrational populations did not remain unchanged. These results were interpreted as showing that a significant amount of the angular momentum came from the angular momentum present in the bending modes of C_2N_2. The change in the vibrational population was shown to be due to the relative branching between the excitation of C_2N_2 in the (00000) and (00010) levels. Each of these levels are excited to different points on the upper potential curve, which leads to a different branching between the vibrational levels of the fragments.

In an elegant series of experiments, Eres et al. (164) have used the LIF method to measure both the angular and velocity distributions of CN fragments of the individual rotational and vibrational states that are produced in the photodissociation of C_2N_2 at 193 nm. From the results they have been able to redetermine the bond dissociation energy, so that it is now known to be 133 ± 1 kcal/mol rather than 128 ± 1 kcal/mol. Because they count and determine both the signal and the laser intensity on each laser pulse, they are able to obtain data with a better signal-to-noise ratio than Lu et al. (154). Their rotational distributions extend to higher rotational energies and can be fitted with a simple phase space theory model. Each of the velocity distributions can also be fitted with this phase space model. They also report that 75% of the available energy appears as translational energy in the product, while 18.6% and 6.4% of the energy appears as rotational and vibrational energy, respectively, of the products.

F. Nitrosyl Cyanide

In a recent series of papers C. Wittig and his group have reported on the photolysis of NCNO in its first absorption band (540 - 900 nm). These experiments have been done both in a static gas cell (165) and in a pulsed molecular beam (166). This molecule is ideal for photodissociation dynamics studies, since it has allowed excited states in the visible region of the spectrum which is more easily accessible with tunable lasers. Both products can in principle be detected using the LIF method, though at the present time only the product distribution of the CN radical has been measured, since NO is often present as an impurity. The spectroscopy is also well studied

(167), so that both the initial state from which the NCNO is excited, and the state to which it is excited, are well characterized. These advantages are somewhat counterbalanced by the fact that both the ground and the excited states are nonlinear, which increases the possibility that vibronic interactions may be important. The weak N-C bond may also mean that the results may not be easily generalized to molecules with stronger bonds. Finally, the NO molecule can only be probed by a one-photon process with laser light in the 150 to 230 nm region, which is a difficult region to work in. Two-photon methods may be employed for detection, but the relative quantum state distributions are difficult to obtain from such methods.

Despite the fact that the NO fragment distribution has not yet been measured, they have made considerable progress in the understanding of the photodissociation dynamics of this molecule. In the first paper, they were able to show that there is a competition between one-photon and two-photon photodissociation. The latter process is not competitive with the former above the thermodynamic threshold. Furthermore, as long as the available energy was kept below the thermochemical threshold for the production of vibrationally excited CN radicals, it was possible to fit the observed rotational distributions with phase space theory. The upper electronic state that is involved in the two-photon dissociation was shown to originate below 22,000 cm^{-1} and is thought to be repulsive. It could be the same state that has its absorption maximum at 270 nm.

The same authors were able to measure the high-resolution absorption spectrum of NCNO by detecting the two-photon photodissociation product rotationally hot CN radicals as a function of wavelength. This method allowed them to assign the constants for the ground and excited states.

In a more recent paper, they have been able to observe the two-photon and one-photon dissociations of NCNO near the threshold, using a pulsed nozzle source to cool the rotational degrees of freedom in the beam. From these studies, they have found that near threshold the CN fragment has energies as low as 0.4 cm^{-1}, and have concluded from this that the one-photon process is the result of vibrational predissociation through the ground state. Ordinary phase space theory explains the rotational distributions as long as the wavelength is below the threshold for the production of CN(v" = 1). Above this threshold, and the threshold for production of the v" = 2 level, they were only able to predict the observed distributions using a statistical ensemble theory (168). At the threshold wavelength for dissociation they find, through Doppler measurements of the line profile, that the translational energy of CN is low. Also near threshold, the appearance time of the CN radical varies

from 31 ns to less than the 10 ns time resolution of their apparatus. RRKM calculations show that this fast increase in the dissociation rate is inconsistent with the small increase in the excess available energy. To explain this, they invoke a tunneling mechanism through a very small barrier, 1-2 cm^{-1}, to explain dissociation near the threshold.

VII. SULFUR CONTAINING COMPOUNDS

Sulfur is the group six element in the second row of the periodic tabke and it might be expected that the photodissociation dynamics of its compounds should be similar to the analogous oxygen compounds. While some similarities exist, a great deal of the dynamics is influenced by the fact that the sulfur atom is heavy and spin-orbit coupling breaks down. This leads to large perturbations between the singlet and triplet states, resulting in new photodissociation dynamics. The sulfur containing compounds absorb in the near UV region where intense laser light can be used to photodissociate and probe photoproducts.

A. Hydrogen Sulfide

The photochemical dynamics of H_2S has been studied in its first absorption band between 180 and 260 nm (2) using LIF measurements to determine the quantum state distribution of the SH fragment (169-171), as well as TOF measurements of the velocity distribution of H atom fragment (172). In the former case, the vibrational and rotational distribution of the SH fragment was only measured in the $v'' = 0$ level because fewer radicals with $v'' > 0$ are produced and the LIF technique does not efficiently detect these excited radicals.

The TOF measurements of the H atom produced in the photodissociation of H_2S indicate that a substantial number of HS radicals are produced vibrationally excited at each of the wavelengths studied. Their results are summarized in Table 9.

The results show that SH radicals are observed in higher vibrational levels as the available energy increases, but that the average amount of vibrational energy $\langle E_{vib} \rangle$ relative to the available energy does not increase in the same manner. Rather, a peak is observed in the relative amount of vibrational energy appearing in the fragment.

The observed vibrational excitation is explained using a predissociation mechanism. It is postulated that the $^1B_1$ state is excited by direct absorption, and is crossed at two different S-H internuclear distances r_{SH} and r'_{SH} by a $^1A_2$ repulsive state.

TABLE 9. Energy Distributions of the HS Fragment Produced in the Photolysis of H_2S[a]

Photolysis Wavelength λ (nm)	E_{avail} (cm^{-1})	v"	$F_{v"}$	$<E_{vib}>/E_{avail}$
193	19957	0	89.5	0.04
		1	1.5	
		2	2.2	
		3	2.2	
		4	2.7	
		5	1.9	
222	13598	0	82	0.078
		1	1	
		2	10	
		3	7	
248	8466	0	94.5	0.017
		1	5.5	

[a]Data adapted from reference (172).

One of the crossings at r_{SH}, which is close to the ground state internuclear distance of the SH radical, produces the SH radical in the v" = 0 level. The vibrationally excited radicals are produced by predissociation to the same $^1A_2$ state, which intersects the $^1B_1$ curve at the larger r'_{SH} distance. Fragmentation resulting from this crossing produces a SH fragment with an extended S-H bond distance, resulting in the observed vibrational excitation. The r'_{SH} internuclear distance changes with excitation energy. Though they do not say so, this mechanism suggests that the ratio of the [SH(v" > 0]/[SH(v" = 0)] is proportional to the predissociation rate at these two extremes of the potential energy surface. The change in the relative amount of vibrational excitation with wavelengths is thus due to changes in the probability at the two extremes of the potential energy surface.

Recent calculations by Kulander (173), using model potentials that mimic those suggested by van Veen et al., confirm that the proposed model could be used to explain the observations. Without accurate upper potential surfaces one cannot, however, exactly reproduce the observed vibrational distributions.

The angular distributions of the SH fragments in the center of mass (CM) system was also determined using the polarization technique. The results of these measurements suggest that the anisotropy parameter β for radicals formed in the $v'' = 0$ level varies as the photolysis wavelength is changed. This variation is given in Table 10, which has been adapted from the original work.

TABLE 10. Anisotropy Parameter β for the $v'' = 0$ of H_2S as a Function of Photolysis Wavelength[a]

Laser photolysis wavelength (nm)	Anisotropy parameter
248	-0.48 ± 0.01
222	-0.42 ± 0.01
193	-0.33 ± 0.33

[a]Data adapted from reference (172).

The anisotropy curve could only be obtained for the $v'' = 0$ level because the signal/noise ratio was too low for the upper vibrational levels. They were still able to show, however, that the angular distributions of the upper vibrational levels were peaked at the same angle as that for the $v'' = 0$ level.

The increases that are observed in the anisotropy parameter with increasing wavelength are thought to be due to the non-negligible lifetime of the $^1B_1$ state, which proves that predissociation must be occurring in the photolysis. There is no indication in the absorption spectra that this is the case, which illustrates how photodissociation dynamics can reveal new details about the upper electronic states of the molecule.

The angular distributions that were observed were also used to determine the symmetry of the upper electronic state that is predissociating. The results confirm that the upper state symmetry of the bound state is $^1B_1$.

The TOF results suggest that the geometry of the excited state is very similar to the geometry of the ground state, in agreement with the observation of Hawkins and Houston, who found very little rotational excitation in the SH fragment. The LIF technique was used to map out the rotational, and nominally the vibrational distribution, of the SH fragment. Very little vibrational excitation was observed, presumably because the detection sensitivity is much less for $v'' > 0$.

The LIF studies of Hawkins and Houston were done in a static gas cell and with a pulsed molecular beam. Even though there is almost 20,000 cm^{-1} of available energy, very little rotational excitation is observed. The rotational temperatures that were observed under both experimental conditions are summarized in Table 11.

TABLE 11. Rotational Temperatures T_r of the Spin-Orbit Components of the HS Fragment Produced in the Photolysis of H_2S at 193 nm[a]

Experimental conditions	T_r (K)		Spin-orbit ratio
	$HS(^2\Pi_{3/2})$	$HS(^2\Pi_{1/2})$	$(^2\Pi_{3/2}/^2\Pi_{1/2})$
Static cell (300 K)	375 ± 15	220 ± 15	3.75 ± 0.2
Pulsed beam (few K)	188 ± 10	75 ± 10	1.97 ± 0.15

[a]Data adapted from reference (171).

In their first paper on the photolysis of H_2S at 193 nm, Hawkins and Houston suggested that the observed rotational distribution in the HS fragment was the result of the partitioning of the original angular momentum of the parent into angular momentum of the SH fragment. This would suggest that as the parent cooled, the angular momentum of the fragment should be reduced. The Table 11 shows that this does in fact occur. The other conclusion of their original work is not, however, in agreement with the conclusions drawn from the time-of-flight work. Hawkins and Houston suggested that the photodissociation process in H_2S was direct because a simple quasi-diatomic kinematic model could be used to fit their data. The experimental evidence from the time-of-flight data disagrees with this conclusion. Since the dissociation process is not direct, it explains why the oscillations predicted by the distorted wave approximation are not observed. The delay that occurs between excitation and dissociation can average these oscillations. Even though the dissociation process is not direct, predissociation is fast enough that the essential elements of the rotational distribution are explained by a quasi-diatomic model.

Very little work has appeared on the photodissociation of H_2S from higher electronic states. Most of the work that has appeared has already been reviewed by Ashfold, Macperson, and

Simons (3). It suggests that at wavelengths below 200 nm two channels exist that may lead to atomic sulfur, namely;

$$H_2S \longrightarrow H_2 + S(^3P),\ S(^1D),\ S(^1S) \qquad \lambda < 406\ nm,\ 245\ nm,\ 186\ nm \qquad (56)$$

$$H_2S \longrightarrow 2H(^2S) + S(^3P),\ S(^1D),\ S(^1S) \qquad \lambda < 165\ nm,\ 143\ nm,\ 121\ nm \qquad (57)$$

These assertions have not been confirmed, and the true thresholds for the above processes are unknown.

At wavelengths below 162 nm the following reaction may occur.

$$H_2S \longrightarrow H + SH(A^2\Sigma^+) \qquad (58)$$

Reaction 58 has been observed, and the rotational distribution measured is thermal, in marked contrast to similar measurements in H_2O. Theoretical calculations suggest that this is because there is an exit valley that lies close to the bent geometry of the H_2S molecule. Thus, the excited state can dissociate without producing a large amount of angular momentum in the SH fragment.

B. Carbon Disulfide

The recent work on the photodissociation dynamics of this molecule has centered around the ArF laser wavelength at 193 nm. The frequency of this laser line corresponds to the excitation of the strong $^1\Sigma_u^+(^1A')$ absorption band (3,174). This band correlates with the production of $CS(X^1\Sigma^+) + S(^1D)$ and most of the dynamics work has revolved around determination of the $S(^1D)/S(^3P)$ ratio.

Butler et al. (175) measured the LIF spectra of the ground state of the CS radical, and found that it was produced vibrationally excited. Their vibrational distribution curve peaks at $v'' = 3$ and extends to $v'' = 6$ (see Figure 10). Their high resolution studies indicated that the rotational population could be described with a "temperature" of about 700 K. Addison et al. (176) directly measured the $S(^1D)$ concentration change in time using resonance fluorescence detection. From the time dependence they extrapolated the concentration back to zero time and determined the nascent atom concentration for the ^1D. The yield of the $S(^3P)/S(^1D)$ ratio was obtained by measuring the

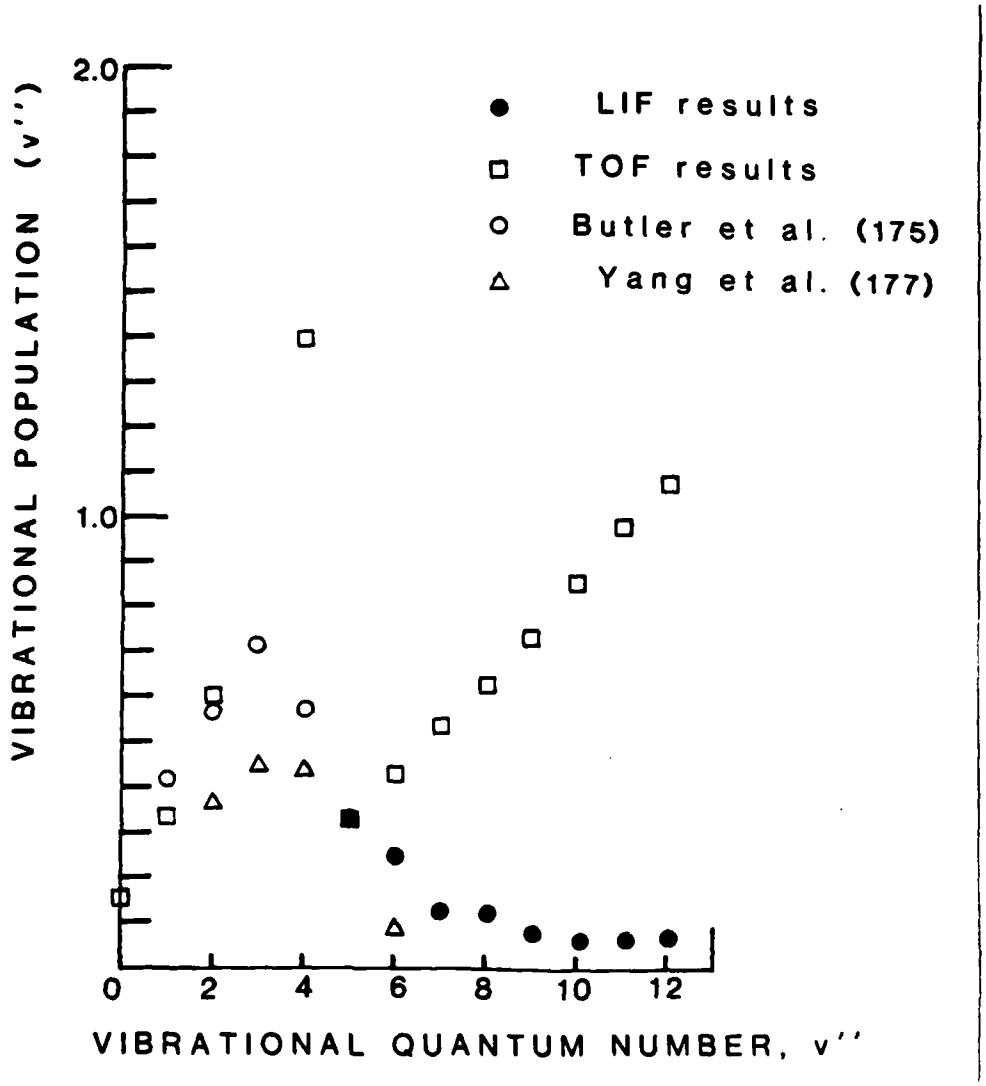

FIGURE 10. The vibrational distribution of the CS radical derived from TOF measurements and from LIF measurements. All of the measurements have been normalized to v" = 4. The TOF measurements of Lu et al. (178) were obtained by using a logarithmic extrapolation for the $S(^3P)$ in the translational energy regime where both $S(^3P)$ and $S(^1D)$ can be formed. The vibrational distributions were then derived from the observed curves.

increase in the $S(^3P)$ concentration when singlet D atoms are quenched by N_2. They estimated that the $(S^3P)/S(^1D)$ ratio was between 5.7 and 3. A large ratio like this implies that the upper state must predissociate through a lower triplet state, by violation of spin conservation rules. The state that is excited directly only correlates directly to a $S(^1D)$ atom. This is not inconsistent with the pronounced structure that is observed in this absorption band.

Yang et al. studied (177) the photolysis of CS_2 at 193 nm in an effusive molecular beam. The quantum state distribution was determined from both time-of-flight measurements of the S fragment at right angles to the molecular beam, and by LIF on the CS fragment. Angular distributions were measured by polarizing the ArF laser with a stacked plate polarizer. No difference was observed in the intensity of the signal with the polarization direction. This suggests that photodecomposition occurs via predissociation, since the predissociation lifetime must be long; otherwise there would be an observed change in the signal with polarization direction.

They also measured a LIF spectrum of the CS radical, which showed that the vibrational distribution peaks at v" ' 3 and decreases at higher vibrational levels. These measurements only extended up to v" = 6 because of the low Franck-Condon factors for transitions from higher vibrational levels of CS(X) in the band sequence they measured.

A break was observed in the translational energy probability curve for CS radicals at the thermochemical threshold for the production of $S(^1D)$. It was then assumed that only ^1D atoms were produced below this threshold, while only ^3P atoms were produced above this threshold. With this assumption they were able to derive a lower limit of 0.25 for the $S(^3P)/S(^1D)$ ratio. They were also able to calculate a vibrational distribution from the TOF curve that agrees with the LIF measurements. The overall conclusions of this paper are in direct disagreement with the work of Addison et al.

Recently Lu et al. (178) have reported time of flight measurements based upon TOF measurements of CS traveling coaxially with the molecular beam. This detection geometry is not biased toward high energy fragments, and they do indeed see a larger proportion of the fragments at lower recoil velocities. From their results and using the adiabatic theory of Kresin and Lester (179), they derive a $S(^3P)/S(^1D)$ ratio of 2, which is in reasonable agreement with Addison et al. (176). The vibrational distribution (see Figure 10) that they derive from their time-of-flight curve using the theory suggests that CS radicals should be produced in higher vibrational levels. LIF measurements exciting the $\Delta v = -2$ and -3 sequences, and cross fluorescence

detection, show that this is the case, since CS radicals are observed up to the thermochemical limit of v" = 12.

Dornhofer, Hack, and Langel (180), in a detailed study of the fluorescence that is induced by an ArF laser, have been able to show that an intense ArF laser can distort the observed vibrational distribution by photodissociating CS radicals with v" > 5. The ArF laser absorption by CS will also produce electronically excited CS which, when it emits, will redistribute the vibrational populations. Probing the CS quantum state population under these conditions could distort the CS ground state populations. The LIF measurements will underestimate the amount of CS radicals that are produced, while the direct detection methods will overestimate the amount of $S(^3P)$ atoms because of the secondary photolysis of CS. The vibrational distribution of Lu et al. (178) will be less prone to this secondary photolysis because very low laser powers (< 1 mJ) were used. Dornhofer, et al. concluded from their results that the $S(^3P)/S(^1D)$ ratio was 3, which is in reasonable agreement with the LIF measurements of Lu et al.

In summary, the recent work on CS_2 at 193 nm suggests that photodissociation at this wavelength produces three times as many S atoms in the ^3P state as in the ^1D state. The CS radical is produced with a bimodal vibrational distribution, peaking at low vibrational levels at v" = 3 but extending to higher vibrational levels up to v" = 13. Polarization measurements suggest that the upper state predissociates with a fairly long lifetime. The predissociation must simultaneously be occurring through both the vibrational continuum of the upper state which leads to $S(^1D)$ and the vibrational continuum of a triplet state which leads to $S(^3P)$.

C. Carbonyl Sulfide

There is a coincidence between the F_2 laser line and the strong $^1\Sigma$ to $^1\Sigma$ absorption that occurs between 160 and 154 nm. Recent work in Bersohn's laboratory (181) has exploited this coincidence to measure the time of flight of the S atom fragment produced in the laser photolysis of this compound.

A supersonic beam was used to cool the OCS molecule to very low rotational levels. Because the transition is a Σ to Σ transition, there is no change in the electronic angular momentum and cooling in a supersonic nozzle ensures that there is little change in the rotational angular momentum. Thus it is not necessary to consider how changes in angular momentum in the parent molecule affect the observed product energy distributions.

The observed TOF spectra are fitted with models, rather than inverting the laboratory distribution into a center-of-mass dis-

tribution. From this fitting procedure they obtain a vibrational distribution that is basically described by

$$P(n) = NO^{0}(n) \exp[8.5\ E(n)/E_{avail}] \tag{59}$$

In this equation N is the normalization constant, E(n) the energy of the nth vibrational level, and $P^{o}(n)$ the prior distribution over final states n, which is proportional to $[E_{avail} - E(n)]^{1/2}$. This equation yields a reasonable fit between the simulated curve and the experimentally obtained TOF curve. A better fit is obtained if the same equation is used with a prior distribution that is defined by

$$P^{o}(n) = (1 - f_n)^{1/2} \tag{60}$$

where f_n is equal to $E(n)/E_{avail}$.

The simulation of the TOF curves suggests that the CO fragment is produced with an inverted vibrational population which peaks at the v'' = 5 level. The average fraction of the available energy, $\langle E_v \rangle / E_{avail}$ that appears in vibration is 0.734 or 12,041 cm^{-1}, so that the average that appears in translation is 4,363 cm^{-1}.

The results that are obtained from the TOF curves are compared to three models, namely a Franck-Condon model, a spectator model, and a quasi-oscillator model. It is concluded that the quasi-oscillator model has the right kind of qualitative potential to explain the results. This quasi-oscillator potential has a series of quasi-minima, about which the R_{CO} oscillates while R_{CS} gradually increases.

D. Thiophosgene

Photodissociation dynamics of this molecule were studied using the TOF technique to determine the velocity distribution of the fragments when the molecule is photolyzed with a KrF laser at 248 nm (182). Absorption at this wavelength leads to the excitation of the second singlet state, the B^1A_1 state, from the X^1A_1 ground state. From the TOF spectra of the CS fragment they were able to show that both of the following reactions occur:

$$CSCl_2 + h\nu \longrightarrow CSCl + Cl \tag{61}$$

$$CSCl_2 + h\nu \longrightarrow CS + Cl_2 \tag{62}$$

They estimate that the quantum yield of reaction 61 if 0.8 while that of reaction 62 is C.2. The fraction of available energy

that is channeled into translational energy for reaction 61 is 0.29. The remaining energy results in internal excitation of the CSCl fragment. It is suggested that an impulsive spectator model can adequately describe the results. No polarization studies are reported.

IX. HALOGEN CONTAINING COMPOUNDS

A great deal of work has been done on the photodissociation dynamics of the halogen containing compounds. This is partially due to the production of halogen atoms and radicals that can be studied by TOF and partially due to the fact there are intense absorption bands in the ultraviolet and near ultraviolet region. These reasons, coupled with the fact that the spectroscopy of some precursor molecules is fairly well understood, have resulted in many workers looking at these compounds. Finally, some of these compounds have been studied as possible candidates for various types of lasers.

A. Hydrogen Iodide

The absorption by hydrogen iodide starts at about 310 nm and is continuous down to 180 nm; $D_0(H\text{-}I) = 3.054$ eV (2). Because of its relatively small dissociation energy, H atoms produced by photolysis are expected to have large translational energy and are amenable to Doppler spectroscopy. Schmiedl et al. (183) have measured the line shape of H atom absorption using tunable vacuum ultraviolet light near 121.6 nm. From the observed Doppler line profile it is possible to derive the recoil energy, the angular distribution of fragments, and the branching ratio of $I(^2P_{1/2})$ and $(^2P_{3/2})$. Figure 11a shows a schematic diagram of the Doppler spectroscopy of H atoms produced from the photolysis of HI at 266 nm (184). The photolysis laser beam at 266 nm is along the X axis with its electric vector E_D either parallel (Figure 11b) or perpendicular (Figure 11c) to the direction of the laser probe beam K_p along the Z axis. The LIF emission from the Lyman α line is viewed along the Y axis. The probe beam frequency ν is given by

$$\nu = \nu_o \ (1 + w/c) \tag{63}$$

where $w = v \cdot k_p$ is the projection of H atom velocities v to the probe beam direction K_p (k_p is the unit vector along K_p). When the electric vector E_D is along the probe beam direction, Figure 11b, the parallel transition A (the transition dipole or E_D being parallel to the internuclear axis) produces a line profile with

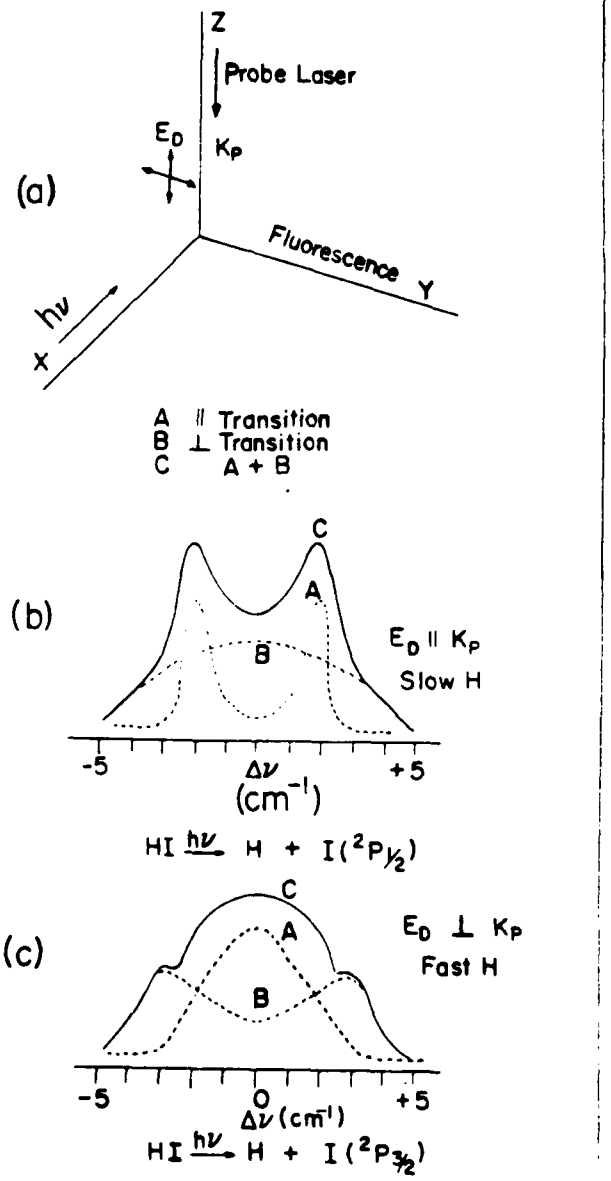

FIGURE 11. LIF Measurements of the Doppler width of the Lyman α line. The H atoms are produced in the photolysis of HI.

two maxima, one corresponding to the probe beam direction and the other in the opposite direction. On the other hand, the perpendicular transition B does not show any Doppler shift. If E_D is 90° to the probe beam direction, the parallel transition A does not show any Doppler shift, while the perpendicular transition B shows two maxima since the recoil direction is now the probe beam direction or opposite to it. The Doppler shift in (c) is larger than in (b) since (b) corresponds to process 64

$$HI(^1\Sigma_o) + h\nu \longrightarrow HI(^3\Pi_o^+) \longrightarrow H + I(^2P_{1/2}) \qquad \Delta\Omega = 0 \qquad (64)$$

that is, the $I(^2P_{1/2})$ is 0.94 eV above the $I(^2P_{3/2})$ and hence the H atom has less kinetic energy. On the other hand, the distribution in (c) corresponds to process (ii)

$$HI(^1\Sigma_o) + h\nu \longrightarrow HI(^3\Pi_1) \longrightarrow H + I(^2P_{3/2}) \qquad \Delta\Omega = \pm 1 \qquad (65)$$

and hence H atoms must have $h\nu - D_o(H\text{-}I) = 1.61$ eV kinetic energy. This energy corresponds almost exactly to v = 17,500 m s of recoil velocity. Thus, the Doppler line profile provides information on the H atom recoil energy, the angular distribution (whether H atom is produced in parallel or perpendicular transition) and the branching ratio for $I(^2P_{1/2})$ and $I(^2P_{3/2})$.

Photofragment TOF measurements of the H atom produced in the photolysis of HI at 248, 222, and 193 nm have also been recently reported (184). Two peaks were observed in the TOF spectra, and each of these peaks had a different polarization dependence. The slow peak was associated with the dissociation channel that produces an H atom and an $I(^2P_{1/2})$ fragment, while the fast peak was identified with the channel that produces the $I(^2P_{3/2})$ fragment. From the polarization measurements they could obtain the anisotropy parameter β, and this along with the TOF spectra could be used to derive the branching ratio between the two channels as a function of wavelength. Combining this information with the measured extinction coefficients, they were able to derive the partial extinction coefficients to the upper states that correlate with each of the channels. A modified δ approximation was then combined with all of this information to calculate the upper repulsive potential curves that lead to dissociation into these products. Four upper states are involved in the dissociation in this region. The symmetries of these four states are $^3\Pi_1$, $^1\Pi$, $^3\Pi_o$, and $^3\Sigma_1$. The first two states produce $I(^2P_{3/2})$ atoms, while the latter two states produce $I(^2P_{1/2})$ fragments in agreement with the predictions of Mullikan (185). These calculations suggest however that the $^3\Sigma_1$ state is much lower than Mullikan predicted.

B. Methyl Iodide

There has been a flurry of recent activity in the study of the photodissociation dynamics of this molecule (186,187,188). Hermann and Leone used the infrared luminescence technique with a circular variable filter to determine the IR emission as a function of frequency when this molecule was photolyzed with lasers at 248 and 266 nm. From their results, they were able to show that the umbrella bending ν_2 mode of the CH_3 radical was the only mode of CH_3 that was excited in the photofragmentation of CH_3I. This is in accord with the idea that the photodissociation of this molecule is unusually simple, and involves primarily the scission of the C-I bond with the simultaneous relaxation of the pyramidal structure of the CH_3 part of the molecule into its final planar form. The data are used to obtain a vibrational distribution of the CH_3 radical that peaks at v" = 2 and extends all the way out to the v" = 10 level.

Theory suggests (189,190) that the $n \rightarrow \sigma^*$ transition is between the $N(^1A_1)$ ground state and $^3Q_0(^3D)$ excited state of the molecule. The latter state is repulsive and correlates with a CH_3 radical and an iodine atom in the $^2P_{1/2}$ state. This repulsive state is also crossed by another repulsive state, the ^1Q state, that correlates with a $I(^2P_{3/2})$ ground state of the atom. TOF measurements at 266 nm had already shown that both fragments are produced. Van Veen et al. (184) and Barry and Gorry (188) show that this is also the case at 248 nm. Van Veen et al. also measured the anisotropy parameter, showing that it is appropriate for the $^3Q_0 \leftarrow\!\!- \ ^1A_1$ transition, so that ground state iodine atoms must be produced as a result of a curve crossing between the $^3Q_0$ state and the ^1Q state. From the width of the TOF curves both authors were able to derive two different vibrational distributions of the CH_3 radical. One of these is associated with the production of $I(^2P_{1/2})$ peaks at v" = 2 and extends out to v" = 6. The other is associated with the production of $I(^2P_{3/2})$ atoms and peaks at v" = 2, extending out to v" = 8 The distribution that is associated with the $I(^2P_{1/2})$ channel disagrees markedly with the theoretical predictions of Shapiro and Bersohn (191), which lead Van Veen et al. to suggest that the potential surface that they used needed modifying.

C. Iodobromomethane

This polyatomic molecule has two halogen chromophores attached to it, so that in principle it is possible to excite one of them and determine which of the halogen bonds is broken. Lee and Bersohn (192) did just this experiment. The molecule has two absorption bands, one with a maximum at 213 nm and the other with

a maximum at 258 nm. The first of these bands is thought to be due to the excitation of the C-Br chromophore while the second is thought to be due to the C-I chromophore. However, since each of the bands are stronger and shifted to the red when compared to the corresponding monohalide, it is thought there is a moderate degree of coupling between them.

Lee and Bersohn photodissociated this molecule in the long wavelength band centered at 268 nm. They used a broadband high-pressure Hg-Xe arc lamp that had a filter solution that cut off both the shorter UV radiation and the longer IR radiation. They then measured the photofragment mass spectrum that is produced when the molecule is irradiated, along with the angular distribution of the I atom fragment. From the photofragment mass spectral pattern they were able to determine that photodissociation in this wavelength band produced Br atoms with a quantum yield of 0.14 and I atoms with a quantum yield of 0.86. The anisotropy parameter was found to be 1.42 ± 0.14, which is lower than the value of 1.81 ± 0.33. Because the anisotropy parameter is significantly lower than the value of 2 expected for a parallel transition, they have suggested that there is a small admixture of another state with a different symmetry than the predominant ^3E symmetry of the first absorption band. This would explain the small observed yield of Br atoms so that a level crossing does not have to be invoked. They also concluded that even though the anisotropy parameter was reduced, it is still high enough that the dissociation is probably direct.

D. Difluorodibromomethane

The photodissociation dynamics of this molecule, which is similar to CH_3I and CH_2IBr, have recently been investigated by Krajnovich et al. at 248 nm (193) using the molecular beam TOF technique. Previously (194) it had been suggested that this molecule dissociates to yield Br_2 and CF_2. The TOF results prove that the only primary process at 248 nm is

$$CF_2Br_2 + h\nu \longrightarrow CF_2Br + Br \qquad (66)$$

The average CM recoil energy is 21.4 kcal/mol with a FWHM energy spread of 8.0 kcal/mol. From the angular distribution they were able to determine that the anisotropy parameter was equal to 1.21. This parameter suggest that the transition dipole moment is polarized parallel to a line through the two Br atoms. While they could not determine whether the Br atom is produced in the $^2P_{1/2}$ or the $^2P_{3/2}$ state, they were able to determine that the CF_2Br radical does not spontaneously decay. Normally, this might suggest that the $^2P_{1/2}$ state is produced, but because of the

uncertainties in the dissociation energies and the possibility that the CF_2Br might be formed rotationally hot, one could not draw this conclusion.

E. Halogenated Ethanes

These molecules have absorption bands that are characteristic of the Br and/or I chromophores. Just as in the case of CH_2IBr, one can in principle excite the long wavelength band which should be associated with the I atom and look for preferential dissociation of the C-I bond. Similarly, one could excite the short wavelength band and look for preferential dissociation of the C-Br bond. Earlier, Pence et al. (195) had suggested that excitation in the respective wavelength regions did lead to independent dissociation of the molecule. Krajnovich et al. (193), using the TOF method and each of the monohalides as a control, were able to show that this was not the case.

C_2F_5Br absorbs at 193 nm but not at 248 nm. At the shorter wavelength photodissociation occurs via

$$C_2F_5Br + h\nu \longrightarrow C_2F_5 + Br(^2P_{3/2}) \quad \text{or} \quad Br(^2P_{1/2}) \qquad (67)$$

The CM recoil energy of the fragments was 30 kcal/mol with a FWHM of 11 kcal/mol. No angular distribution was determined because of the low signal-to-noise ratio.

C_2F_5I absorbs at 248 nm but not at 193 nm. TOF measurements of the photodissociation products at the former wavelength indicate that the I atom is produced only in the $^2P_{1/2}$ state, which is in agreement with the results of the quantum yield measurements (196). The average recoil energy of the fragments is 20.9 kcal/mol with FWHM of 6.8 kcal/mol, which represents 51% of the available energy. The anisotropy parameter β is 1.87, which indicates that the transition moment is parallel and that the dissociation occurs on a short time scale with respect to rotation.

In agreement with previous studies (197), the photodissociation of $1,2\text{-}C_2F_4BrI$ at 266 and 248 nm produces mostly $I(^2P_{1/2})$. The average CM recoil translational energy is 17.8 and 19.5 kcal/mol, with FWHM of 9.5 and 11.1 kcal/mol, respectively. At 266 nm, 53% of the available energy appears as translation recoil energy, while only 48% appears in this degree of freedom at 248 nm. A parameter of 1.8 is found at both wavelengths, indicating a parallel transition of the type $^3Q_0 \leftarrow N$ followed by direct dissociation. It is important to note that even though there is enough energy for fragmentation of the C-Br bond, it does not occur, indicating that the available energy is not randomized in the molecule.

TOF measurements of the photodissociation fragments of this molecule at 193 nm indicate that both Br and I atoms are produced in the primary process. These measurements cannot determine if the atoms are produced in one or both spin-orbit states. The average CM translational recoil energy for the chennel that produces I atoms is 27 kcal/mol with a FWHM of 13 kcal/mol, whereas it is 25.5 kcal/mol with a FWHM of 9.0 kcal/mol for the Br atom. The β for both channels is 1.85, indicating that a parallel transition is occurring. It was also determined that the ratio of C-I to C-Br bond fission was 1.7, so that even though the Br chromophore is excited, almost twice as much fragmentation occurs in the C-I bond. The authors have interpreted these results as indicating that a curve crossing occurs, during the dissociation process, from the state that is excited through the Br chromophore to a repulsive state that leads to C-I bond breakage. This is supported by the fact that no Br is observed at 248 and 266 nm, both of which are probably below the energy of the curve crossing.

The anisotropy parameter indicates that this is a parallel transition ($^3Q_0 \leftarrow N$) and the absorption coefficient suggests that it is much stronger than the corresponding CH_3Br transition. While the authors suggest that this is a mystery, it could be that the absorption strength is a result of the heavy I atom breaking down the spin selection rule.

Wight and Leone have remeasured the $I(^2P_{1/2})$ yield at 193 nm, and found that the yield is 0.50 ± 0.14, while it is 0.14 ± 0.04 for the $Br(^2P_{1/2})$ channel. Krajonovich et al. (193) have shown that the total yield of Br is 0.33, so that the yield for $Br(^2P_{3/2})$ must be 0.33 - 0.14 = 0.19. The corresponding yield that Wight and Leone measured for the $I(^2P_{1/2})$ state is in agreement, within their experimental error, with the TOF results, suggesting that most of the I atoms are produced electronically excited. The TOF studies (198) of the photodissociation of 1,2-chloroiodoethane at 248 and 266 indicate that the only two important primary process are

$$CH_2ClCH_2I + h\nu \longrightarrow \begin{cases} CH_2ClCH_2 + I(^2P_{1/2}) & (68) \\ CH_2ClCH_2 + I(^2P_{3/2}) & (69) \end{cases}$$

The measured branching ratios of $I(^2P_{1/2})/I(^2P_{3/2})$ were 1.5 and 3.0 at 248 and 266 nm, respectively. The ratio of the average amount of translational energy $\langle E^*_T \rangle$ to available energy E_{av} that appears in the excited I atom channel is 0.58 at 248 nm and 0.57 at 266 nm. The corresponding ratio for the ground state atom is 0.46 at both wavelengths. The measured anisotropy parameter β was 1.8 for both channels, which indicates that the

absorption excites a transition that is parallel to the C-I bond. This means that the excitation is a $^3Q_0 \leftarrow N$ transition, which only correlates to an iodine fragment in the $^2P_{1/2}$ state. The ground state iodine atoms must be produced by a curve crossing to a state at lower energies with which it correlates. Similar results have been found for the other alkyl halides, which is in accord with Mullikan's idea about $n \rightarrow \sigma^*$ in halogen containing compounds.

F. Halogenated Propanes

The relative quantum yield for the production of $I(^2P_{1/2})$ atoms from $\underline{i}$-C_3F_7I and $\underline{n}$-C_3F_7I has been measured as a function of wavelength between 265 and 336 nm (199). For both molecules the quantum yield is found to be 1 within experimental error up to 298 nm. From that wavelength to 336 nm, the quantum yield decreases for each of these molecules, but the yield decreases faster for the $\underline{n}$-C_3F_7I. These results could be explained by either a curve crossing, or by the excitation of a weak absorption to the $^3Q_1$ as well as the $^3Q_0$ state. In light of the results obtained in other alkyl halides the former explanation seems more likely.

G. Atomic versus Molecular Elimination in Halogenated Hydrocarbons

In a recent paper (200), TOF measurements of the photodissociation products of C_2HBr, C_3H_3Br, C_3H_3Cl, C_2H_5Cl, and $\underline{i}$-C_3H_7Cl at 193 nm were determined. It has been suggested (2) that the alkyl halides can dissociate via direct C-X bond breakage as well as by molecular elimination of HX. This suggestion may be tested by determining whether the HX compound is formed in the dissociation in a molecular beam. In addition to determining whether this is the case for saturated and unsaturated hydrocarbons, one can ascertain for the unsaturated compounds how the presence of the chromophore associated with the π bonds affects the overall dissociation process.

The translational energy probability $P(E_T)$, obtained from TOF measurements of the Br atom from HC_2CH_2Br at 193 nm shows two peaks at 30 and 120 kJ/mol. The fast Br atoms are thought to come from excitation of the σ^* orbital on the Br atom via the process

$$HC_2CH_2Br + h\nu \longrightarrow HC_2CH_2Br(S,\sigma^*) \longrightarrow C_3H_3 + X \qquad (70)$$

HBr is also observed in the photodissociation of this compound, and it is thought to arise along with slow Br atoms from an

intersystem crossing which can be represented by

$$HC_2CH_2Br + h\nu \longrightarrow HC_2CH_2Br(S,\pi^*) \longrightarrow (T) \longrightarrow \begin{matrix} C_3H_3 + B & (71) \\ C_3H_2 + HBr & (72) \end{matrix}$$

The peaks of the $P(E_T)$ for the Br atom from reaction 71 and for the HBr formed in reaction 72 occur at 30 and <20 kJ/mol, respectively.

Methyl, ethyl, and i-propyl chloride give fast Cl atoms as a result of the reactions

$$CH_3Cl + h\nu \longrightarrow CH_3 + Cl \quad (73)$$

$$C_2H_5Cl + h\nu \longrightarrow C_2H_5 + Cl \quad (74)$$

$$i\text{-}C_3H_7Cl + h\nu \longrightarrow C_3H_7 + Cl \quad (75)$$

The peaks of the $P(E_T)$ curves occur at an E_T of 240, 150, and 140 kJ/mol for reactions 73, 74, and 75, respectively. In addition to reaction 74, the ethyl chloride molecule also yields and C_2H_4 and HCI molecule via reaction 76.

$$C_2H_5Cl + h\nu \longrightarrow C_2H_5Cl(S,\pi^*) \longrightarrow (T) \longrightarrow C_2H_4 + HX \quad (76)$$

The peak of the $P(E_T)$ for this reaction occurs at <20 kJ/mol, similar to the other reactions of this type.

Propargylchloride (HC_2CH_2Cl) undergoes two primary process that can be depicted by

$$HC_2CH_2Cl + h\nu \longrightarrow \begin{matrix} HC_2CH_2 + Cl & (77) \\ C_3H_2 + HCl & (78) \end{matrix}$$

Reaction is thought to be a result of a σ^* transition associated with the Cl atom chromophore, while reaction 78 is the result of excitation of the π^* chromophore associated with the π bond. The peak of the $P(E_T)$ curve occurs at 140 and <20 kJ/mol for reactions 77 and 78, respectively. Angular distributions of the Cl atom signal in reaction 77 indicate that the distribution is anisotropic, and that the dissociation is direct with a lifetime of the order of a few picoseconds. Reaction 78 is thought to occur via a singlet-triplet intersystem crossing, followed by the dissociation of the resultant triplet state.

The fraction, f_T, of the available translational energy that appears in the fragments from the channel that produces molecular products (HX) is low, suggesting that a lot of the excess energy remains in the internal modes of the fragments. The f_T that appears in the atomic fragments (X) is large, and suggests that an impulsive model for dissociation is the correct theoretical interpretation of the results. In fact, the spectator model appears to predict the f_T that are observed.

H. Interhalogens

ICl and IBr have been recently studied by De Vries and colleagues, using the TOF technique and a tunable flash-lamp pumped-dye laser (201). Although there have been previous dynamics studies on these molecules, none of them have really addressed the problem of the potential surface in the curve-crossing region. In the region of the absorption spectrum where these experiments were performed (480 to 530 nm), it is possible to excite the molecule to both the $^3\Pi_0^+$ state and the $^3\Pi_1$ state. The latter state adiabatically correlates to two ground state fragments, while the former one correlates to a ground state iodine atom and an excited bromine atom. The $^3\Pi_0^+$ state dissociates either into $I(^2P_{3/2}) + Br(^2P_{1/2})$ or into the ground state I and Br atoms by curve crossing to the repulsive 0^+ state which leads to the ground state I and Br atoms.

The TOF spectrum of the Cl or Br atom is measured as a function of wavelength, with the polarization of the laser selected so that only $^3\Pi_0^+$ is excited. The peaks that are observed in the spectrum can be identified with atoms in either the $^2P_{3/2}$ or $^2P_{1/2}$ state, so that the experimental data can be used to determine the probability, P, for the diabatic crossing. The Landau-Zener formula for this probability is given by

$$P = \exp(-4\pi^2 H_{12}^2 / v_{rad}\Delta Fh) \tag{79}$$

in which μ is the reduced mass, E_x the potential energy at the crossing, E_{int} the internal energy of the molecule, $h\nu$ the photon energy, and E^*_{rot} the rotational energy at the crossing. $E_{int} - E^*_{rot}$ is small compared to the other terms, allowing them to replace $h\nu - E_{int} + E^*_{rot}$ with a Boltzmann averaged E. Combining the two equations, they then obtained

$$(\ln P)^{-2} = a(E - E_x) \tag{81}$$

$$a = (h/4\pi^2)^2(2/\mu)(H^2_{12}/\Delta F)^{-2}. \tag{82}$$

A plot of $(\ln P)^{-2}$ versus E should give a straight line, whose slope is related to $(H^2_{12}/\Delta F)$ and whose intercept is equal to E_x. Figure 12 shows the results that they obtained for each of these molecules along with a comparison obtained from theory. The results could also be used to obtain the repulsive part of the potential near the equilibrium distance. This is shown in Figure 13. All of these results illustrate how TOF measurements can supply detailed information about the upper potential surface of a molecule.

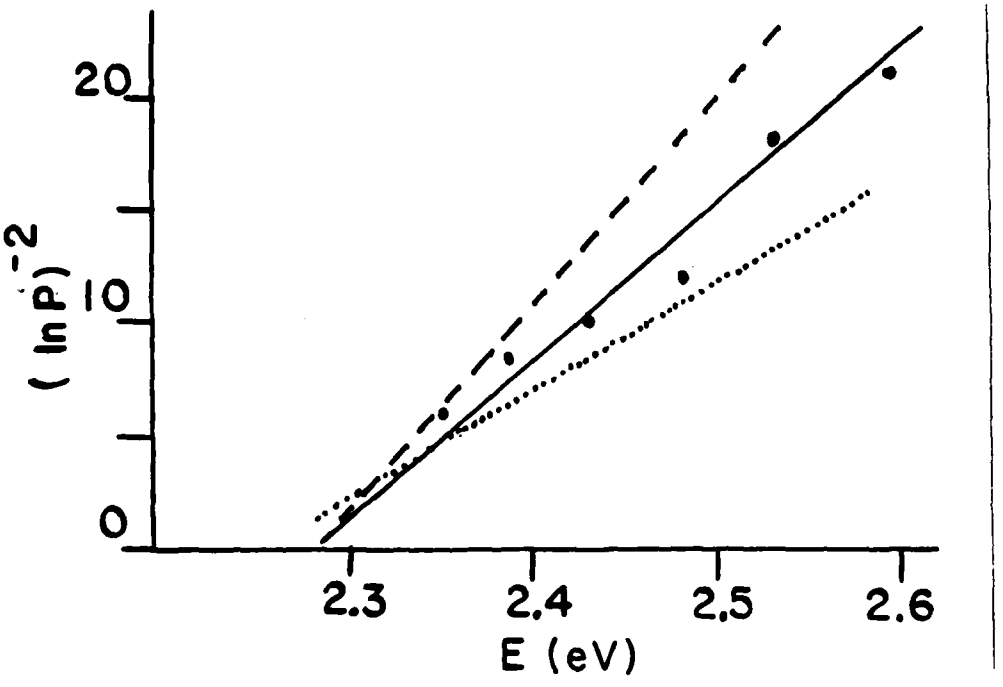

FIGURE 12. A plot of the $(n\ P)^{-2}$ versus E for the curve crossing in ICl. P is the probability for passing the crossing diabatically and E is the excitation energy. The dots are the experimental points and the solid line is the least-squares fit to these points. The dashed and dotted lines were taken from references (215) and (216), respectively. The figure was taken from reference (201) with permission of Elsevier Science Publishers.

I. Alkali Halides

Using a surface ionization detector and a tunable dye laser, Van Veen and his colleagues (202) studied the photolysis of KI between 265 and 335 nm using the TOF technique. They were able to show from the TOF spectra that only ground state $K(^2S_{1/2})$ were produced. From 335 to 305 nm only ground state $I(^2P_{3/2})$ atoms

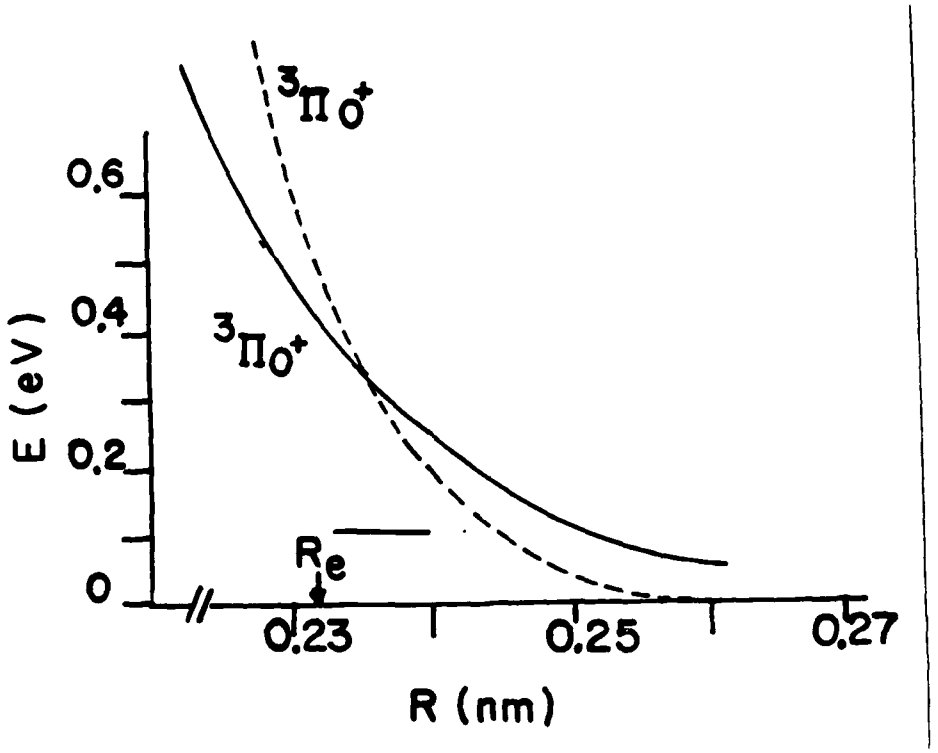

FIGURE 13. The dashed curve is part of a repulsive potential curve for ICl constructed from experimental data (201). The solid line is taken from Child and Bernstein (216). Re denotes the ground state equilibrium distance and the horizontal line is the Franck-Condon region probed in the experiment. The figure was reproduced from reference (201) with permission of Elsevier Science Publishers.

are produced, while from 265 to 295 nm only $I(^2P_{1/2})$ atoms are produced. Between 305 and 295 nm, both ground and excited state I atoms are produced. No polarization measurements are reported in this work.

In a later paper, Van Veen et al. (203) extended the original work to the other alkali halides (KBr, NaI, NaBr) and measured the anisotropy parameter for photodissociation at a variety of wavelengths. These data were used to separate the continuous absorption into the contribution from the two upper states corresponding to a parallel and a perpendicular transition. With their data they were also able to derive the upper potential curves in the Franck-Condon region. The relative absorptions to the two different repulsive curves in this region suggest that the ground state has a mixed but mainly ionic character. Their data indicate that there is no crossing inside

the Franck-Condon region, and, because of the previously determined symmetry in the fluorescent region, this crossing must occur at large internuclear distances.

J. Thallium, Indium, and Tin Halides

In a comprehensive work, Van Veen et al. (204) have studied the photofragment spectra of TlCl, TlBr, TlI, and InI obtained by TOF measurements at a number of different wavelengths. As the spectra in Figure 14 show, all of these molecules exhibit the same type of absorption bands, but they are shifted to different wavelength regions. Thus, by exciting the molecules in the various spectral regions that exhibit similar spectral characteristics, they were able to determine branching ratios for the production of $Tl(^2P_{1/2})$, $Tl(^2P_{3/2})$, $Tl(^2S_{1/2})$, $X(^2P_{1/2})$, and $X(^2P_{3/2})$ at the various wavelengths. The anisotropy that is observed in the angular distributions was used to determine the character of the upper state, and the time scale of dissociation. The TOF data were used to redetermine the bond dissociation energies of the TlX with an uncertainty of 0.02 eV. Finally, the spectra were used to derive schematic potential energy diagrams of the upper potential curves for these TlX molecules. Some data are also reported on the photolysis of InI at 193 nm. The principal results are summarized in Table 12. There is certainly enough experimental data in these studies to warrant a comprehensive theoretical calculation of the upper potential surface, especially in light of the importance of these molecules in the understanding of photodissociation lasers of the MI type. TOF and polarizations measurements of the photodissociation dynamics of $SnCl_2$ at 193 nm have been measured (205). The results indicate that the SnCl fragment is produced in the $X^2\Pi$ state along with a $Cl(^2P)$ atom. The SnCl radical has about 0.5 eV of vibrational energy. Using the spectator model, they estimate that less than 0.1 eV of rotational energy appears in the SnCl fragment. Some of the available energy is used to produce the various spin multiplet components of the $SnCl(^2\Pi_{1/2}$ or $^2\Pi_{3/2})$ and $Cl(^2P_{3/2}$ or $^2P_{1/2})$ fragments.

The polarization measurements showed that the Cl atoms and SnCl fragments had the same anisotropy factor $\beta = 0.21 \pm 0.01$, which, if the dissociation is fast compared with molecular rotation, suggests that there is a angle of $46.5 \pm 0.4°$ between the transition dipole moment and the dissociation direction. The transition dipole moment lies in the plane of the molecule rather than perpendicular to this plane. A model was developed in which charge transfer occurs in the excited $(SnCl_2)^*$ molecule, resulting from photoexcitation between the nonbonding p orbital on the Cl atom and the p_x orbital on the Sn atom. This model

TABLE 12. A Summary of the Results from the TOF Studies on InI and TlX Molecules[a]

Electronic state	MX	λ (nm)	(M + X)[b]	f_c	β	θ(deg)	Fraction of the transition character ⊥	∥
B	TlBr	332.5	Tl,Br	1	-0.40	22	1	
	TlCl	308	Tl,Cl	1	-0.32	15	1	
C	TlI	308	Tl,I*:Tl*,I	1	-0.32	35	1	
	TlI	300	Tl,I*:Tl*,I	1	-0.15	24	0.81	0.19
	TlBr	269	Tl,Br*	0.77	-0.38	18	1	
			Tl*,Br	0.16	-0.28	45		
	TlBr	266	Tl,Br	0.19				
			Tl,Br*	0.65	-0.26	14	0.91	0.09
			Tl*,Br	0.16				
	TlCl	248	Tl,Cl:Tl,Cl*	0.29	0		0.67	0.33
			Tl*,Cl	0.71	-0.29	15	1	
D	TlBr	248	Tl,Br*	0.33	0.60	11	0.19	0.81
			Tl*,Br	0.69	0.57	14	0.19	0.81
	TlI	248	Tl,I*:Tl*,I	1	-0.19	15	0.81	0.19
	TlCl	193	Tl*,Cl:Tl*,Cl*	1	0.36	5	0.40	0.60
E	TlI	193	Tl*,I*	0.47	0.75	12	0.14	0.86
			Tl**+I	0.53	0.68	31		1
	InI	193	In*,I*	0.75	0.68	10	0.18	0.82
			In**,I	0.25	0.28	39		1

[a] Adapted from reference (204). $I(\theta) = \sigma_0[1 + 2\beta P_2(\theta)]$ where σ_o is the maximum cross section, β is the anisotropy factor, θ is the shift angle, and $P_2(\theta)$ is the Legendre polynomial.

[b] X^* represents $X(^2P_{1/2})$, M^* represents $M(^2P_{3/2})$, and M^{**} represents $M(^2S_{1/2})$.

Fig 1 Model cable for 15-a reduction
to 38-44 picas type cage

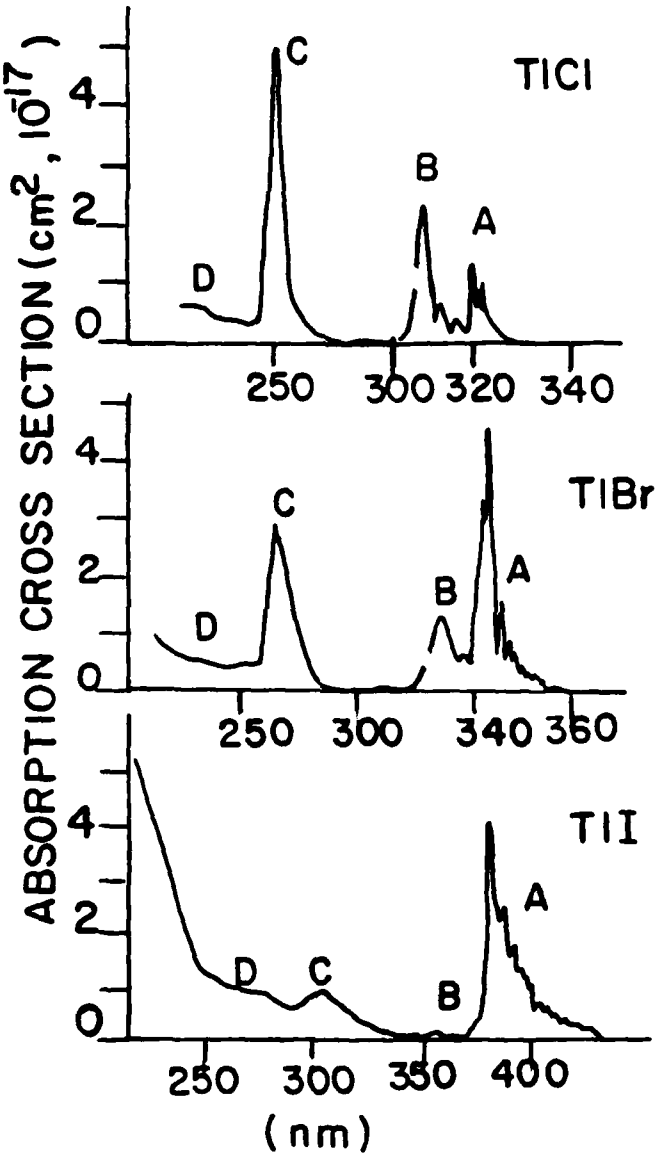

FIGURE 14. The UV absorption bands of the TlX molecules. The spectra are labeled A, B, C, and D, which identify similar spectral regions. The wavelength scale has been adjusted so that similar bands fall on top of each other. From reference (204) with permission of Elsevier Science Publishers.

predicts that transitions from the A_1 state to a B_2 state dominate over transitions to an A_1 state. Transitions to the B_1 state were found to be negligible, in agreement with the observations.

X. ACETYLENIC COMPOUNDS

Acetylene is the simplest unsaturated hydrocarbons and as such an understanding of its photochemistry is important. The reactions of ethynyl radicals (C_2H) are important in combustion as well as in the photochemistry of Jupiter and Titan atmospheres, although, unfortunately, C_2H radical has apparently only very weak and complex absorption spectra in the visible and ultraviolet region and no LIF has been found.

A. Acetylene

The photodissociation of C_2H_2 is energetically possible below 230 nm (2).

$$C_2H_2 + h\nu \longrightarrow C_2H + H, \qquad <230 \text{ nm} \tag{83}$$

Very weak fluorescence from the electronically excited $C_2H_2(A^1{}_u\text{-}X^1\Sigma)$ has been observed by Abramson et al. (206) and Stephenson et al. (207) for laser excitation near 220 nm. At this excitation energy, which is 2000 cm^{-1} above the dissociation limit, the fluorescence lifetime is 2-5 μs (206) or 0.3 μs (207). If 0.3 μs is correct, the quantum yield of fluorescence is about 0.1.

The primary photochemical process in C_2H_2 at 185 nm are process 82 and

$$C_2H_2 + h\nu \longrightarrow C_2H_2{}^* \longrightarrow \begin{cases} C_2 + H_2 & (84) \\ C_2H_2{}^{**} & (85) \end{cases}$$

where $C_2H_2{}^*$ is the A^1A_u state and $C_2H_2{}^{**}$ is a metastable (triplet) state. The quantum yields of processes 83 and 84 at 185 nm are 0.06, 0.1, and 0.84, respectively (208), and at 147 nm are 0.3, 0.1, and 0.6, respectively (209). Another primary process occurs below 136 nm (210):

$$C_2H_2{}^* \longrightarrow C_2H^* + H, \qquad <136 \text{ nm} \tag{86}$$

where C_2H^* is electronically excited C_2H (211,212). The electronically excited C_2H emits in the visible region from 400 to above 600 nm.

B. Bromoacetylene

The C_2H emission is also observed in the photolysis of C_2HBr in the vacuum ultraviolet (211,212).

$$C_2HBr + h\nu \longrightarrow C_2H^* + Br \quad (87)$$

The lifetime of the C_2H emission ranged from 3 to 10 μs. Schmieder (213) found visible emission from the photolysis of C_2H_2 at 73.6 nm (Ne emission line). The emission spectra are the C_2 Swan system ($d^3\Pi$-$a^3\Pi_u$), Deslandres-d'Azabuja system ($C^1\Pi_g$-$b^1\Pi_u$) and the CH ($A^2\Delta$-$X^2\Pi$, $B^2\Sigma$-$X^2\Pi$) system while the C_2H emission observed at 123.6 (211) and 121.6 nm (212) was absent at 73.6 nm. The quantum yield of these emissions is about 0.1%.

Kawasaki et al. (200) studied the photolysis of C_2HBr with 193 nm laser light using a time of flight mass spectrometer. Two peaks corresponding to $Br(^2P_{3/2})$ and $Br(^2P_{1/2})$ were found in the curve for Br. Only 26% of the available energy goes into translational energy.

The center of mass (CM) translational energy distribution curve ($P(E_T)$ versus E_T) derived from TOF measurements of the Br atom produced in the 193 nm photolysis of bromoacetylene has three peaks. They occur at E_T of 75, 40, and <20 kJ/mol. The first two peaks have about the energy difference associated with the spin-multiplet splitting in Br and suggest that the following primary processes occur at 193 nm:

$$HC_2Br + h\nu \longrightarrow \begin{cases} HC_2 + Br(^2P_{3/2}) & (88) \\ HC_2 + Br(^2P_{1/2}) & (89) \end{cases}$$

The low energy peak is not completely resolved in their experiment because they employed a perpendicular detection geometry. They argue, however, that this low energy peak is due to an intersystem crossing to a triplet state, followed by dissociation of this triplet state to form $Br(^2P_{3/2})$ atoms. This is represented by the reaction

$$HC_2Br + h\nu \longrightarrow HC_2Br(S,\pi^*) \longrightarrow (T) \longrightarrow HC_2 + Br \quad (90)$$

This idea is supported by the observation that the peak at low translational energies is much larger for Br containing compounds than it is for Cl containing compounds. The spin-orbit coupling in the former compounds should be larger than that in the latter compounds resulting in a higher singlet-triplet transition rate.

ACKNOWLEDGMENTS

The authors are grateful to their students and colleagues in the Laser Chemistry Division for patiently reviewing this manuscript. H. Okabe gratefully acknowledges the Department of Commerce for its support under grant No. 5430116. W.M. Jackson acknowledges support under NASA grants No. NAGW-446 and No. NSG-5071 and under the Office of Naval Research grant No. N00014-80-C-0305. These grants supported much of the research that is discussed in this review.

REFERENCES

(1) J. P. Simons in "Gas Kinetics and Energy Transfer" (P. G. Ashmore and R. J. Donovan, Eds), The Chemical Society, London; Chem. Soc. Spec. Period. Rep. 2, 56 (1977).

(2) H. Okabe, "Photochemistry of Small Molecules," Wiley, New York, 1978.

(3) M. N. R. Ashfold, M. T. Macpherson, and J. P. Simons, "Topics in Current Chemistry," Vol. 86, Springer-Verlag, Heidelberg, 1, 1979.

(4) S. R. Leone, Advances in Chemical Physics, 50, 255 (1982).

(5) A. Baronvaski, Laser Ultraviolet Photochemistry, in "Lasers as Reactants and Probes in Chemistry," (W. M. Jackson and A. Harvey, Eds), Howard University Press, Washington, D.C., 1984.

(6) R. D. Bower, W. G. Hawkins, P. L. Houston, R. W. Jones, H. R. Kim, W. J. Marinelli, and N. Sivakumar, Laser Studies of Molecular Photodissociation Dynamics, to appear in Proceedings Fourth Symposium Recent Advances in Laser Spectroscopy, May 20, 1983, Brooklyn Polytechnic Institute of New York, Wiley, New York.

(7) J. P. Simons, J. Phys. Chem., 88, 1287 (1984).

(8) G. Hancock, J. Photochem., 25, 21 (1984).

(9) M. A. West, J. Photochem., 25, 57 (1984).

(10) J. W. Hepburn, Israel J. Chem., 24, 273 (1984).

(11) P. Brewer, P. Das, G. Ondrey, and R. Bersohn, J. Chem. Phys., 79, 720 (1983).

(12) P. Brewer, N. Van Veen, and R. Bersohn, Chem. Phys. Lett., 91, 126 (1982).

(13) K. H. Welge and R. Schmiedl, Advances in Chemical Physics," Vol. 47 (J. Jortner, R. D. Levine, and S. A. Rice, Eds.), Wiley-Interscience, New York, 1981, p. 133.

(14) F. Shokoohi, S. Hay, and C. Wittig, Chem. Phys. Lett., 110, 1 (1984).

(15) D. S. Moore, D. S. Bomse, and J. Valentine, J. Chem. Phys., 79, 1745 (1983).

(16) M. Pealat, D. Debarre, J. M. Marie, J. P. E. Taran, A. Tramer, and C. B. Moore, Chem. Phys. Lett., 98, 299 (1983).

(17) H. Kawaguchi, C. Yamada, E. Hirota, and J. E. Butler, M6, XVI Informal Photochem. Conf. Harvard University, Cambridge, MA (1984).

(18) C. F. Wood, J. A. Neil, and G. W. Flynn, Chem. Phys. Lett., 109, 317 (1984).

(19) D. Imre, J. L. Kinsey, A. Sinha, and J. Krenos, J. Phys. Chem., 88, 3956 (1984).

(20) R. Bersohn, J. Phys. Chem., 88, 5145 (1984).

(21) K. H. Welge and F. Stuhl, J. Chem. Phys., 46, 2440 (1967).

(22) P. Andresen, G. S. Ondrey, and B. Titze, Phys. Rev. Lett., 50, 486 (1983).

(23) P. Andresen and E. W. Rothe, J. Chem. Phys., 78, 989 (1983).

(24) P. Andresen, and E. W. Rothe, Chem. Phys. Lett., 86, 270 (1982).

(25) P. Andresen, G. S. Ondrey, B. Titze, and E. W. Rothe, J. Chem. Phys., 80, 2548 (1984).

(26) G. A. Chamberlain and J. P. Simons, J. Chem. Soc., Faraday Trans. II, 71, 2043 (1975).

(27) J. P. Simons and A. J. Smith, Chem. Phys. Lett., 97, 1 (1983).

(28) M. T. Macpherson and J. P. Simons, Chem. Phys. Lett., 51, 261 (1977).

(29) H. Okabe, J. Chem. Phys., 72, 6642 (1980).

(30) L. C. Lee, J. Chem. Phys., 72, 4334 (1980).

(31) E. J. Stone, Rev. Sci. Instrum., 51, 677 (1980).

(32) A. Hodgson, J. P. Simons, M. N. R. Ashfold, Chem. Phys. Lett., 107, 1 (1984).

(33) G. Theodorakopoulos, C. A. Nicolaides, R. J. Buenker, and S. D. Peyerimhoff, Chem. Phys. Lett., 89(2), 164 (1982).

(34) M. Suto and L. C. Lee, Chem. Phys. Lett., 98, 152 (1983).

(35) C. L. Lin, N. K. Rohatgi, and W. B. DeMore, Geophysical Res. Lett., 5(2), 113 (1978).

(36) L. J. Stief and V. J. De Carlo, J. Chem. Phys., 50(3) 1234 (1969).

(37) G. Ondrey, N. Van Veen, and R. Bersohn, J. Chem. Phys., 78, 3732 (1983).

(38) A. Jacobs, K. Kleinermanns, H. Kuge, and J. Wolfrum, J. Chem. Phys., 79, 3162 (1983).

(39) D. J. Clouthier and D. A. Ramsay, Ann. Rev. Phys. Chem., 34, 31 (1983).

(40) C. B. Moore and J. C. Weisshaar, Ann. Rev. Phys. Chem., 34, 525 (1983).

(41) G. K. Moorgtgat, W. Seiler, and P. Warneck, J. Chem. Phys., 78, 1185 (1983).

(42) P. Ho, D. J. Bamford, R. J. Buss, Y. T. Lee, and C. B. Moore, J. Chem. Phys., 76, 3630 (1982).

(43) P. Ho and A. V. Smith, Chem. Phys. Lett., 90, 407 (1982).

(44) A. V. Smith and P. Ho, J. Molec. Spect., 100, 212 (1983).

(45) D. J. Bamford, S. V. Filseth, M. F. Foltz, J. W. Hepurn, and C. B. Moore, J. Chem. Phys., 82, 3032 (1985).

(46) C. K. Cheng, P. Ho, C. B. Moore, and M. B. Zughul, J. Phys. Chem., 88, 296 (1984).

(47) C. C. Hayden, D. M. Neumark, K. Shobatake, R. K. Sparks, and Y. T. Lee, J. Chem. Phys., 76, 3607 (1982).

(48) B. I. Sonobe and R. N. Rosenfeld, J. Am. Chem. Soc., 105, 7528 (1983).

(49) R. N. Rosenfeld and B. I. Sonobe, J. Am. Chem. Soc., 105, 1661 (1983).

(50) G. T. Fujimoto, M. E. Umstead, and M. C. Lin, Chem. Phys., 65, 197 (1982).

(51) B. I. Sonobe, T. R. Fletcher, and R. N. Rosenfeld, J. Am. Chem. Soc., 106, 4352 (1984).

(52) B. I. Sonobe, T. R. Fletcher, and R. N. Rosenfeld, Chem. Phys. Lett., 105, 322 (1984).

(53) R. N. Rosenfeld and B. R. Weiner, J. Am. Chem. Soc., 105, 6233 (1983).

(54) R. N. Rosenfeld and B. Weiner, J. Am. Chem. Soc., 105, 3485 (1983).

(55) G. W. Loge and C. S. Parameter, J. Phys. Chem., 85, 1653 (1981).

(56) J. W. Hepurn, R. J. Buss, L. J. Butler, and Y. T. Lee, J. Phys. Chem., 87, 3638 (1983).

(57) J. W. Hepurn, N. Sivakumar, and P. L. Houston, Proceedings of the AIP Conference on XUV Lasers, March 1984, Boulder, Colorado.

(58) A. Freedman, S. C. Yang, and R. Bersohn, J. Chem. Phys., 70, 5313 (1979).

(59) M. Kawasaki, K. Kasatani, H. Sato, H. Shinohara, and N. Nishi, Chem. Phys., 73, 377 (1982).

(60) M. W. Wilson, M. Rothschild, D. F. Muller, and C. K. Rhodes, J. Chem. Phys., 77, 1837 (1982).

(61) C. Fotakis, Chem. Phys. Lett., 82, 68 (1981).

(62) C. Fotakis, A. Torre, and R. J. Donovan, J. Photochem., 23, 97 (1983).

(63) T. Venkitachalam and R. Bersohn, J. Photochem., 26, 65 (1984).

(64) M. Ivanco, J. Hager, W. Sharfin, and S. C. Wallace, J. Chem. Phys., 78, 6531 (1983).

(65) W. Sharfin, M. Ivanco, and S. C. Wallace, J. Chem. Phys., 76, 2095 (1982).

(66) H. Watanabe, Y. Hyodo, S. Tsuchiya, and S. Koda, J. Phys. Chem., 86, 685 (1982); H. Watanabe, S. Tsuchiya, and S. Koda, Phys. Chem., 86, 4274 (1982).

(67) H. Watanabe, Y. Hyodo, S. Tsuchiya, and S. Koda, Chem. Phys. Lett., 81, 439 (1981).

(68) D. L. Holterman, E. K. C. Lee, and R. Nanes, J. Chem. Phys., 76, 3341 (1982).

(69) D. L. Holtermann, E. K. C. Lee, and R. Nanes, Chem. Phys. Lett., 75, 249 (1980); Chem. Phys. Lett., 75, 91 (1980).

(70) B. G. MacDonald and E. K. C. Lee, J. Phys. Chem., 86, 323 (1982).

(71) S. Kimel, D. Feldman, J. Laukemper, and K. H. Welge, J. Chem. Phys., 76, 4893 (1982).

(72) R. K. Sparks, L. R. Carlson, K. Shobatake, M. L. Kowalczyk, and Y. T. Lee, J. Chem. Phys., 72, 1401 (1980).

(73) J. C. Brock and R. T. Watson, Chem. Phys. Lett., 71, 371 (1980); Chem. Phys., 46, 477 (1980).

(74) C. E. Fairchild, E. J. Stone, and G. M. Lawrence, J. Chem. Phys., 69, 3632 (1978).

(75) G. D. Greenblatt and J. R. Wiesenfeld, J. Chem. Phys., 78, 4924 (1983).

(76) S. T. Amimoto, A. P. Force, J. R. Wiesenfeld, and R. H. Young, J. Chem. Phys., 73, 1244 (1980).

(77) P. H. Wine and A. R. Ravishanakara, Chem. Phys., 69, 365 (1982).

(78) L. C. Lee, G. Black, R. L. Sharpless, and T. G. Slanger, J. Chem. Phys., 73, 256 (1980).

(79) P. F. Zittel, and D. D. Little, J. Chem. Phys., 72, 5900 (1980).

(80) D. G. Imre, J. L. Kinsey, R. W. Field, and D. H. Katayama, J. Phys. Chem., 86, 2564 (1982).

(81) J. J. Valentini, D. S. Moore, and D. S. Bomse, Chem. Phys. Lett., 83, 217 (1981).

(82) J. J. Valentini, Chem. Phys. Lett., 96, 395 (1983).

(83) D. S. Moore, D. S. Bomse, and J. J. Valentini, J. Chem. Phys., 79, 1745 (1983).

(84) U. Platt, D. Perner, G. W. Harris, A. M. Winer, and J. N. Pitts, Jr., Nature 285, 312 (1980).

(85) R. Vasudev, R. N. Zare, and R. N. Dixon, Chem. Phys. Lett., 96, 399 (1983).

(86) R. Vasudev, R. N. Zare, and R. N. Dixon, J. Chem. Phys., 80, 4863 (1984).

(87) R. P. Mariella, Jr., B. Lantzsch, V. T. Maxson, and A. C. Luntz, J. Chem. Phys., 69, 5411 (1978).

(88) K. E. J. Hallin and A. J. Merer, Can. J. Phys., 54, 1157 (1976).

(89) A. J. Merer and K. E. J. Hallin, Can. J. Phys., 56, 1502 (1978).

(90) C. H. Chen, D. W. Clark, M. G. Payne, and S. D. Kramer, Opt. Comm., 32, 391 (1980).

(91) H. Zacharias, M. Geilhaupt, K. Meir, and K. H. Welge, J. Chem. Phys., 74, 218 (1981).

(92) T. G. Slanger, W. K. Bischel, and M. J. Dyer, J. Chem. Phys., 79, 2231 (1983).

(93) L. Bigio, R. S. Tapper, and E. R. Grant, J. Phys. Chem., 88, 1271 (1984).

(94) R. J. S. Morrison and E. R. Grant, J. Chem. Phys., 77, 5994 (1982).

(95) L. C. Lee and C. C. Chiang, J. Chem. Phys., 76, 4462 (1982).

(96) G. S. Selwyn and H. S. Johnston, J. Chem. Phys., 74, 3791 (1981).

(97) H. Lam, D. R. Hastie, B. A. Ridley, and H. I. Schiff, J. Photochem., 15, 119 (1981).

(98) W. Marx, F. Bahe, and U. Schuarth, Ber. Bunsenges. Phys. Chem., 83, 225 (1979).

(99) H. N. Volltraner, W. Felder, R. J. Pirkle, and A. Fontijn, J. Photochem., 11, 173 (1979).

(100) J. A. Davidson, C. J. Howard, H. I. Schiff, and F. E. Fehsenfeld, J. Chem. Phys., 70, 1697 (1979).

(101) N. Goldstein, G. D. Greenblatt, and J. R. Wiesenfeld, Chem. Phys. Lett., 96, 410 (1983).

(102) J. Zavelovich, M. Rotschild, W. Gornik, and C. K. Rhodes, J. Chem. Phys., 74, 6787 (1981).

(103) F. Lahmani, C. Lardeux, and D. Solgadi, Chem. Phys. Lett., 102, 523 (1983).

(104) N. Sanders, J. E. Butler, L. R. Pasternack, and J. R. McDonald, Chem. Phys., 48, 203 (1980).

(105) L. Batt, K. Christie, R. T. Miline, and A. J. Summers, Int. J. Chem. Kinet., 6, 877 (1974).

(106) F. Lahmani and C. Lardeux, J. Photochem., 15, 37 (1981).

(107) F. Lahmani, C. Lardeux, and D. Solgadi, J. Photochem., 23, 1 (1983).

(108) G. Radhakrishnan and R. C. Estler, Chem. Phys. Lett., 100, 403 (1983).

(109) T. Ebata, H. Yanagishita, K. Obi, and I. Tanaka, Chem. Phys., 69, 27 (1982).

(110) D. Schwartz-Lavi, I. Bar and S. Rosenwaks, Chem. Phys. Lett., 109, 296 (1984).

(111) M. Dubs and J. R. Huber, Chem. Phys. Lett., 108, 123 (1984).

(112) G. Geiger, H. Stafast, U. Bruhlmann, and T. R. Huber, Chem. Phys. Lett., 79, 521 (1981).

(113) M. P. Roellig and P. L. Houston, Chem. Phys. Lett., 57, 75 (1978).

(114) M. P. Roellig and P. L. Houston, J. Chem. Phys., 73, 5081 (1980).

(115) R. D. Bower, R. W. Jones, and P. L. Houston, J. Chem. Phys., 79, 2799 (1983).

(116) R. W. Jones, R. D. Bower, and P. L. Houston, J. Chem. Phys., 76, 3339 (1982).

(117) K. G. Spears and L. D. Hoffland, J. Chem. Phys., 74, 4765 (1981).

(118) K. Glanzer, M. Maier, and J. Troe, Chem. Phys. Lett., 61, 175 (1979).

(119) L. J. Butler, D. Krajnovich, Y. T. Lee, G. Ondrey, and R. Bersohn, J. Chem. Phys., 79, 1708 (1983).

(120) N. C. Blais, J. Chem. Phys., 79, 1723 (1983).

(121) M. Suto and L. C. Lee, J. Chem. Phys., 81, 1294 (1984).

(122) H. Okabe, J. Chem. Phys., 72, 6642 (1980).

(123) T. Papenbrock, H. K. Haak, and F. Stuhl, Ber. Bunsenges. Phys. Chem., 88, 675 (1984).

(124) M. Suto and L. C. Lee, J. Chem. Phys., 78, 4515 (1983).

(125) M. N. R. Ashfold, R. N. Dixon, and R. J. Stickland, J. Chem. Phys., 88, 463 (1984).

(126) T. G. Slanger and G. Black, J. Chem. Phys., 77, 2432 (1982).

(127) W. G. Hawkins and P. L. Houston, J. Phys. Chem., 86, 704 (1982).

(128) H. K. Haak and F. Stuhl, J. Phys. Chem., 88, 3627 (1984).

(129) B. M. Dekoven and A. P. Baronavski, Chem. Phys. Lett., 86, 392 (1982).

(130) A. P. Baronavski, R. G. Miller, and J. R. McDonald, J. Chem. Phys., 30, 119 (1978).

(131) R. Eng, W. Fisher, T. Carrington, C. Sandowski, and H. Dugan, SVI Informal Photochemistry Conference, Harvard University, Cambridge MA, paper M-10 (1984).

(132) G. Herzberg and K. K. Innes, Can. J. Phys., 35, 842 (1957).

(133) A. P. Baronavski and J. R. McDonald, Chem. Phys. Lett., 45, 172 (1977).

(134) G. E. Bush, J. F. Cornelius, R. T. Mahoney, R. I. Morse, D. W. Schlesser, and K. R. Wilson, Rev. Sci. Instr., 41, 1066 (1970).

(135) M. J. Sabety-Dzvonik, and R. J. Cody, J. Chem. Phys., 66, 125 (1977).

(136) J. H. Ling and K. R. Wilson, J. Chem. Phys., 63, 101 (1975).

(137) A. P. Baronavski, Ultraviolet Laser Photochemistry, in "Lasers as Reactants and Probes in Chemistry" (W. J. Jackson and A. Harvey, Eds.), Howard University Press, Washington, D.C., 1984.

(138) I. Nadler, H. Reisler, and C. Wittig, Chem. Phys. Lett., 103, 451 (1984).

(139) A. P. Baronvaski, Chem. Phys. Lett., 66, 217 (1982).

(140) H. Reisler, private communication.

(141) W. Krieger, J. Hager, and J. Pfab, Chem. Phys. Lett., 85, 69 (1982).

(142) M. D. Morse, K. F. Freed, and Y. B. Band, J. Chem. Phys., 70, 3604 (1979).

(143) W. H. Fisher, T. Carrington, S. V. Filseth, C. M. Sadowski, and C. H. Dugan, J. Chem. Phys., 82, 443 (1983).

(144) W. H. Fisher, R. Eng, T. Carrington, C. H. Dugan, S. V. Filseth, and C. M. Sadowski, J. Chem. Phys., 89, 457 (1984).

(145) M. D. Pattengill, Chem. Phys. Lett., 104, 462 (1984).

(146) W. J. Marinelli, N. Sivakumar, and P. L. Houston, J. Phys. Chem., 88, 6685 (1984).

(147) B. Waite, B. Dunlap, H. Helvajian, and A. P. Baronavski, Chem. Phys. Lett., 111, 544 (1984).

(148) S. T. Amimoto, J. R. Wiesenfeld, and R. H. Young, Chem. Phys. Lett., 65, 402 (1979).

(149) W. M. Pitts and A. P. Baronavski, Chem. Phys. Lett., 71, 395 (1980).

(150) S. R. Long and J. P. Reilly, J. Phys. Chem., 86, 56 (1982).

(151) M. N. R. Ashfold and J. P. Simons, J. Chem. Soc., Faraday Soc. II, 74, 280 (1978).

(152) M. Heaven, T. A. Miller, and V. E. Bondybey, Chem. Phys. Lett., 84, 1 (1981).

(153) J. B. Halpern and W. J. Jackson, J. Phys. Chem., 86, 3528 (1982).

(154) R. Lu, J. B. Halpern, and W. M. Jackson, J. Phys. Chem., 88, 3419 (1984).

(155) J. W. Rabalias, J. M. McDonald, V. Scheer, and S. P. McGlynn, Chem. Rev., 71, 73 (1971).

(156) X. Li, N. Sayah, and W. M. Jackson, to be published.

(157) C. Conley, J. B. Halpern, J. Woods, C. Vaughn, and W. M. Jackson, Chem. Phys. Lett., 73, 224 (1980).

(158) J. A. Guest, M. A. O'Halloran, and R. N. Zare, Chem. Phys. Lett., 103, 261 (1984).

(159) W. M. Jackson, J. Chem. Phys., 59, 960 (1973).

(160) W. M. Jackson and R. Body, J. Chem. Phys., 61, 4184 (1974).

(161) W. M. Jackson, J. Photochem., 17, 509 (1981).

(162) M. R. Taherian and T. G. Slanger, J. Chem. Phys., 81, 3814 (1984).

(163) D. Eres, M. Gurnick, and J. D. McDonald, J. Chem. Phys., 81, 5552 (1984).

(164) J. B. Halpern and W. M. Jackson, J. Phys. Chem., 86, 973 (1982).

(165) I. Nadler, J. Pfab, H. Reisler, and C. Wittig, J. Chem. Phys., 81, 653 (1984).

(166) I. Nadler, H. Reisler, M. Noble, and C. Wittig, Chem. Phys. Lett., 108, 115 (1984).

(167) M. Noble, I. Nadler, H. Reisler, and C. Wittig, J. Chem. Phys., 81, 4333 (1984).

(168) I. Nadler, M. Noble, H. Reisler, and C. Wittig, J. Chem. Phys., 82, 2608 (1985).

(169) W. G. Hawkins and P. L. Houston, J. Chem. Phys., 73, 297 (1980).

(170) M. C. Heaven, T. A. Miller, and V. E. Bondebey, Chem. Phys. Lett., 84, 1 (1981).

(171) W. G. Hawkins and P. L. Houston, J. Chem. Phys., 76, 729 (1982).

(172) G. N. A. Van Veen, K. A. Mohamed, T. Baller, and A. E. DeVries, Chem. Phys., 74, 261 (1983).

(173) K. C. Kulander, Chem. Phys. Lett., 103, 373 (1984).

(174) R. J. Hemley, D. G. Leopold, J. L. Roebler, and V. Vaida, J. Chem. Phys., 79, 5219 (1983).

(175) J. E. Butler, W. S. Drozdoski, and J. R. McDonakd, Chem. Phys., 50, 413 (1980).

(176) M. C. Addison, R. J. Donovan, and C. Fotakis, Chem. Phys. Lett., 74, 58 (1980).

(177) S. C. Yang, A. Freedman, M. Kawasaki, and R. Bersohn, J. Chem. Phys., 72, 4058 (1980).

(178) R. Lu, V. McCrary, D. Zakheim, J. Halpern, J. Russell, and W. Jackson, J. Chem. Phys., in press (1985).

(179) V. Kresin and W. Lester, Jr., Chem. Phys. Lett., 87, 392 (1982).

(180) G. Dorhofer, W. Hack, and W. Langel, J. Phys. Chem., 88, 3060 (1984).

(181) G. S. Ondrey, S. Kanfer, and R. Bersohn, J. Chem. Phys., 79, 179 (1983).

(182) G. S. Ondrey and R. Bersohn, J. Chem. Phys., 79, 157 (1983).

(183) R. Schmiedl, H. Dugan, W. Meir, and K. H. Welge, Z. Physik, A304, 137 (1982).

(184) G. N. A. Van Veen, K. A. Mohamed, T. Baller, and A. E. DeVries, J. Chem. Phys., 80, 113 (1983).

(185) R. S. Mullikan, Phys. Rev., 51, 310 (1937).

(186) H. W. Hermann and S. R. Leone, J. Chem. Phys., 76 4766

(186) H. W. Hermann and S. R. Leone, J. Chem. Phys., 76, 4766 (1982).

(187) G. N. A. Van Veen, T. Baller, A. E. DeVries, and N. J. A. Van Veen, J. Chem. Phys., 87, 405 (1984).

(188) M. D. Barry, P. A. Gorry, J. Molec. Phys., 52, 461 (1984).

(189) R. S. Mulliken, J. Chem. Phys., 3, 513 (1935).

(190) R. S. Mulliken, J. Chem. Phys., 8, 382 (1940).

(191) M. Shapiro and Ro Bersohn, J. Chem. Phys., 73, 3810 (1980).

(192) S. J. Lee and R. Bersohn, J. Phys. Chem., 86, 728 (1982).

(193) D. Krajnovich, Z. Zhang, L. Butler, and Y. T. Lee, J. Phys. Chem., 88, 4561 (1984).

(194) C. L. Sam and J. T. Yardley, Chem. Phys. Lett., 61, 509 (1979).

(195) W. H. Pence, S. L. Baughcum, and S. R. Leone, J. Phys. Chem., 85, 3844 (1981).

(196) E. Gerck, J. Chem. Phys., 79, 311 (1983).

(197) C. A. Wight and S. R. Leone, J. Phys. Chem., 87, 5299 (1983).

(198) T. K. Minton, P. Felder, R. J. Brudzynski, and Y. T. Lee, J. Chem. Phys., 81, 1759 (1984).

(199) J. E. Smedley and S. R. Leone, J. Chem. Phys., 79, 2687 (1983).

(200) M. Kawasaki, K. Kasatani, H. Sato, H. Shinohara, and N. Nishi, J. Chem. Phys., 88, 135 (1984).

(201) M. S. DeVries, N. J. A. Van Veen, M. Hutchinson, and A. E. DeVries, Chem. Phys., 51, 159 (1980).

(202) N. J. A. Van Veen, M. S. DeVries, and A. E. DeVries, Chem. Phys. Lett., 60, 184 (1979).

(203) N. J. A. Van Veen, M. S. DeVries, J. D. Sokol, T. Baller, and A. E. DeVries, Chem. Phys., 56, 81 (1981).

(204) N. J. A. Van Veen, M. S. DeVries, T. Baller and A. E. DeVries, J. Chem. Phys., 55, 371 (1981).

(205) N. J. A. Van Veen, G. N. A. van Veen, M. S. DeVries, and A. E. deVries, J. Chem. Phys., 66, 465 (1982).

(206) E. Abramson, C. Kittrell, J. L. Kinsey, and R. W. Field, J. Chem. Phys., 76, 2293 (1982).

(207) J. C. Stephenson, J. A. Blazy, and D. S. King, Chem. Phys., 85, 31 (1984).

(208) H. Okabe, J. Chem. Phys., 78, 1312 (1983).

(209) H. Okabe, J. Chem. Phys., 75, 2772 (1981).

(210) M. Suto and L. C. Lee, J. Chem. Phys., 80, 4824 (1984).

(211) H. Okabe, Can. J. Chem., 61, 850 (1983).

(212) Y. Saito, T. Hikida, T. Ichimura, and Y. Mori, J. Chem. Phys., 80, 31 (1984).

(213) R. W. Schmieder, J. Chem. Phys., 76, 2900 (1982).

(214) M. W. Wilson, M. Rothschild, D. F. Muller, and C. K. Rhodes, J. Chem. Phys., 77, 1837 (1982).

(215) R. D. Gordon and K. K. Innes, J. Chem. Phys., 71, 2824 (1979).

(216) M. S. Child and R. B. Bernstein, J. Chem. Phys., 59, 5916 (1973).

AD-A160 329 PHOTODISSOCIATION DYNAMICS OF SMALL MOLECULES(U) HOWARD 2/2
UNIV WASHINGTON DC LASER CHEMISTRY DIV
W M JACKSON ET AL. 04 OCT 85 ONR-TR-19 N00014-80-C-0305
UNCLASSIFIED F/G 7/5 NL

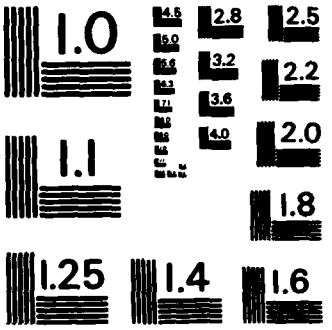

MICROCOPY RESOLUTION TEST CHART
NATIONAL BUREAU OF STANDARDS-1963-A

DL/413/83/01
GEN/413-2

TECHNICAL REPORT DISTRIBUTION LIST, GEN

	No. Copies
Office of Naval Research Attn: Code 413 800 N. Quincy Street Arlington, Virginia 22217	2
Dr. Bernard Douda Naval Weapons Support Center Code 5042 Crane, Indiana 47522	1
Commander, Naval Air Systems Command Attn: Code 310C (H. Rosenwasser) Washington, D.C. 20360	1
Naval Civil Engineering Laboratory Attn: Dr. R. W. Drisko Port Hueneme, California 93401	1
Defense Technical Information Center Building 5, Cameron Station Alexandria, Virginia 22314	12
DTNSRDC Attn: Dr. G. Bosmajian Applied Chemistry Division Annapolis, Maryland 21401	1
Dr. William Tolles Superintendent Chemistry Division, Code 6100 Naval Research Laboratory Washington, D.C. 20375	1
Dr. David Young Code 334 NORDA NSTL, Mississippi 39529	1
Naval Weapons Center Attn: Dr. Ron Atkins Chemistry Division China Lake, California 93555	1
Scientific Advisor Commandant of the Marine Corps Code RD-1 Washington, D.C. 20380	1
U.S. Army Research Office Attn: CRD-AA-IP P.O. Box 12211 Research Triangle Park, NC 27709	1
Mr. John Boyle Materials Branch Naval Ship Engineering Center Philadelphia, Pennsylvania 19112	1
Naval Ocean Systems Center Attn: Dr. S. Yamamoto Marine Sciences Division San Diego, California 91232	1

END

FILMED

11-85

DTIC